Investigation of the photoinduced dynamics of allyl systems by transient absorption spectrocopy

From the femtosecond photogeneration to the microsecond fate of the allyl photoproducts

Michael Mikhailov

Dissertation
an der Fakultät für Physik
der Ludwig-Maximilians-Universität
München

vorgelegt von
Michael Mikhailov
aus Minsk

München, im April 2014

Kurzfassung

Die moderne Anrege-Abfrage-Spektroskopie (Pump-Probe-Spektroskopie) ermöglicht es, die Mehrheit der relevanten physikalischen und chemischen Prozesse zeitaufgelöst zu messen. Die Pump-Probe-Spektroskopie wird in der fundamentalen, industriellen, biomedizinischen und Umweltforschung angewendet, um ein breites Spektrum von komplizierten Substanzen zu untersuchen. Diese Dissertation demonstriert das große Potenzial der transienten Spektroskopie für die Untersuchung von ultraschnellen chemischen Reaktionen komplizierter organischer Moleküle (Allylverbindungen). Auch einige praktische Vorschläge zur Verbesserung der spektroskopischen Messroutine werden gegeben.

Die Bestimmung des Zeit-Nullpunkts (zeitlicher Überlapp) der Anrege- und Abfragepulse ist sehr wichtige und keine triviale Aufgabe in einem Anrege-Abfrage-Experiment. Im *Kapitel 3* werden die Ergebnisse der Untersuchung von bekannten Laserfarbstoffen und anderen Substanzen, die erfolgreich zur Zeit-Nullpunkt Kalibrierung benutzt werden können, beschrieben.

In den *Kapiteln 4* und *5* werden die Ergebnisse der spektroskopischen Untersuchung von einigen interessanten Allylsystemen präsentiert. Es ist uns gelungen zu zeigen, dass die spezifische molekulare Einheit (die Styrolgruppe) als Chromophor dient, was während der UV-Anregung von Allylen mit Kurzpuls-Lasern zur Lokalisierung der Anregung auf der Styrolgruppe führt. Durch die Benutzung dieser Eigenschaft und den Wechsel von Abgangsgruppen und Substituenten haben wir detailliert den Bindungsbruch und die geminate Ionenpaar-Rekombination von unsubstituierten, symmetrisch und unsymmetrisch substituierten Allylsystemen untersucht.

Short summary

Starting from milliseconds and finishing on femtoseconds, modern pump-probe spectroscopic techniques cover the timescales of the most important physical and chemical processes. Current investigations in the field include a wide variety of complicated and complex classes of compounds that are of particular interest in fundamental research as well as in environmental studies, industrial and biomedical applications. This thesis demonstrates the great value of the transient spectroscopy in the investigation of the ultrafast chemical reactions of complicated organic substances (allyl compounds) and also gives some practical hints to improve measurement routines of transient absorption spectroscopy.

Determination of the time zero point (temporal overlap) of pump and probe pulses is a very important and sometimes not trivial task in transient absorption experiments. *Chapter 3* provides the results of the investigation of some popular laser dyes and other substances which can be successfully used as time zero determination substances.

The results of the spectroscopic investigation of the allyl systems are presented in *Chapters 4* and *5*. We managed to show that a specific molecular moiety (styrene group) serves as a chromophore, leading to the localization of excitation on styrene during the UV laser excitation of allyls. Using this feature and changing leaving groups and substituents allowed us to study in detail bond cleavage and geminate ion pair recombination dynamics of unsubstituted and symmetrically and unsymmetrically substituted allyl systems.

Publications

This thesis has led to the following paper (Appendix E):

Direct Observation of Memory Effects in SN1 Reactions by Femto- to Microsecond Spectroscopy of Allylium Ion Pairs
Michael Mikhailov, Konstantin Troshin, Herbert Mayr, Eberhard Riedle, Igor Pugliesi
In preparation.

Contents

Danksagung

If you can't explain it simply, you don't understand it well enough.

Albert Einstein

1. Introduction

Humans are visual beings because of the amount of information they process through eyes, rather than through other senses. While bats may process most of their information through their ears, we process the major part of our information through our eyes. That's why optical methods of diagnostics and control occupy the most important place in every natural science - from physics and chemistry to biology and medicine.
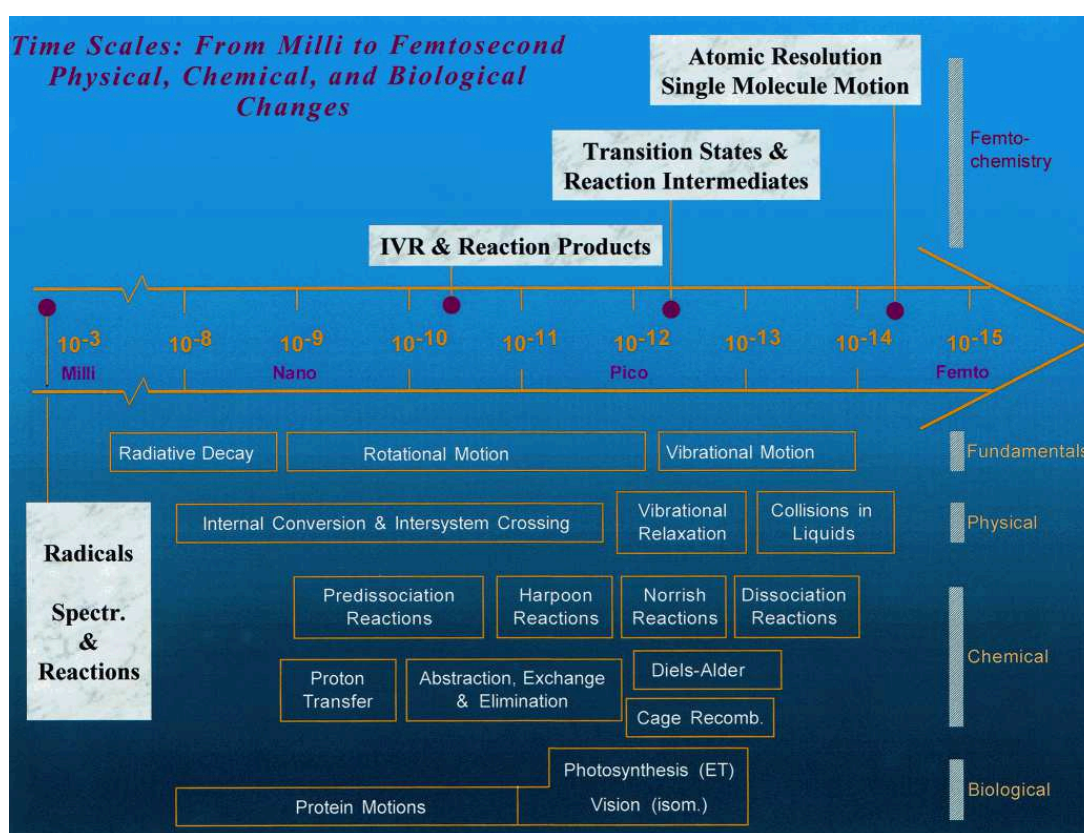

Figure 1.1: Time scales of physical, chemical and biological processes (adapted from [Zew00]). The laser systems with high (sub-50 fs) time resolution have made it possible to investigate ultrafast physical, chemical and biological processes.

For decades, optical sensors have been finding their way into an increasing number of applications. The development of semiconductors in the 1940s and 1950s led to lower-cost, com-

pact and efficient light-sensing devices. Photodetectors are used today practically everywhere: in camera light meters, street lights and traffic counters. Fiber optics allows sensitive equipment to work in electrically noisy environments. Optical sensors have improved efficiency and reliability of control systems. With the advance of analytical techniques it became possible to investigate more and more complicated processes occurring at very short times (blink of an eye that lasts approximately 100-400 ms is too slow to resolve atomic-scale dynamics – see Fig. 1.1)

The methods of visible, ultraviolet (UV) and infrared (IR) spectroscopy are undoubtedly among the most powerful methods of modern-day science. Along with nuclear magnetic resonance (NMR) spectrometry they represent all analytical techniques able to measure both quantitatively and qualitatively the interaction of electromagnetic radiation with matter.

Since 1947, when the first combined UV-visible absorption spectrometer was produced, spectrophotometers have become workhorses in every laboratory concerned with the identification and measurement of organic and inorganic compounds in a wide range of products and processes - in nucleic acids and proteins, foodstuffs, pharmaceuticals and fertilisers, in mineral oils and in paint.

Modern pico- and femtosecond laser techniques provide the possibility for many scientists investigating in various fields – from chemistry and physics to biology and medicine, to observe atomic and molecular events on a real-time scale. Many concepts that eventually evolved into present-day pump-probe and flash photolysis experiments have been established long time ago.

Thus, already in 1878, advances in photography allowed Eadweard J. Muybridge to make, in fact, the first time-resolved photographic images of creatures in motion, and among them the famous picture of the running horse (Fig. 1.2).
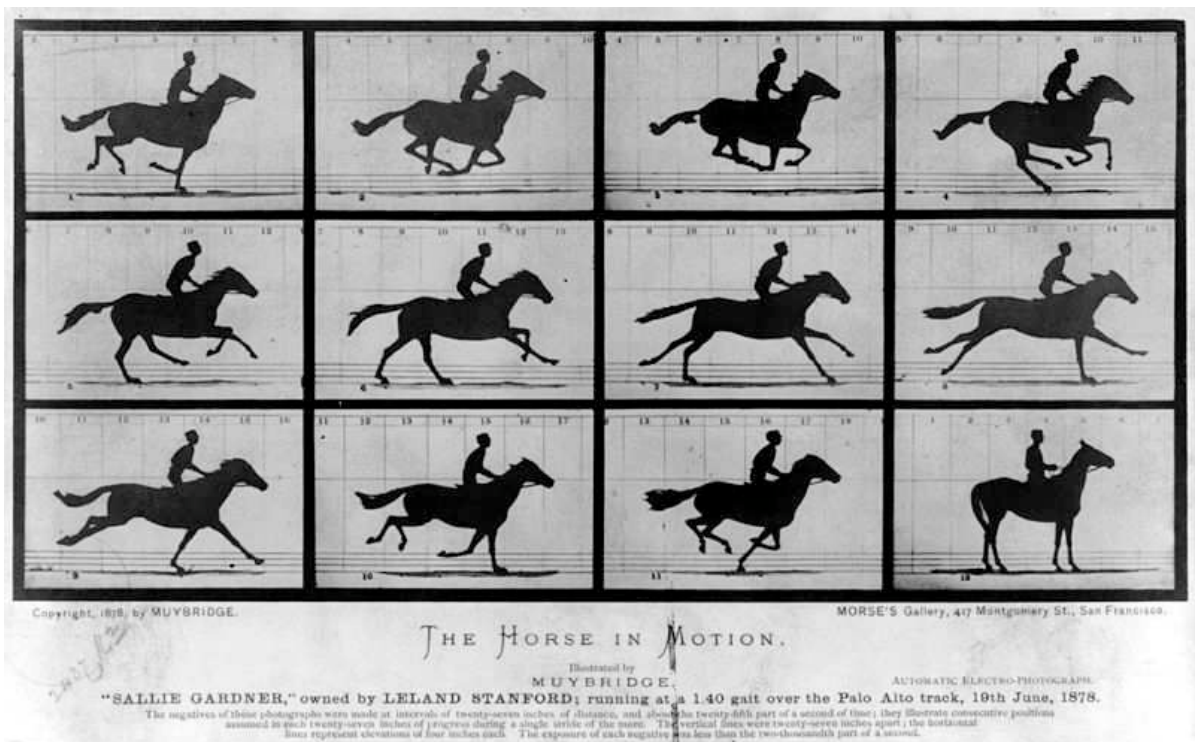
Figure 1.2: The Horse in Motion by Eadweard Muybridge. "Sallie Gardner," owned by Leland Stanford; running at a 1:40 gait over the Palo Alto track, 19th June 1878 (adapted from the Wikimedia Commons: http://en.wikipedia.org/wiki/File:The_Horse_in_Motion.jpg).

The history of modern pump-probe optical spectroscopy began in 1949 when George Porter developed new high-power flash lamps and used them for studying fast photochemical reactions. New lamps allowed him to produce a high concentration of intermediates in chemical reactions and to monitor the evolution of their spectra by means of the flash probe. Refined and improved (with lasers as the pump sources and probe beams that are generated by non-linear optical processes such as stimulated Raman scattering, high harmonic generation, stimulated emission or broad-band continuum generation), these techniques transformed into two major methods of pump-probe optical spectroscopy: laser flash photolysis (LFP) and transient absorption (TA) spectroscopy. Although predominantly home-built, there are some commercial models of transient absorption spectrometers and laser flash spectrometers on the market (Fig. 1.3).

Figure 1.3: View of a commercial laser flash spectrometer system from Edinburgh Instruments (top) (adapted from http://www.edinburghphotonics.com/spectrometers/lp920-series/) and a commercial TA spectrometer from Ultrafast Systems (bottom) (adapted from http://www.ultrafastsystems.com/helios.html).

Both methods have their positive traits and their drawbacks. To understand their origin, one should understand major differences of these two methods. Thus, in the classical LFP technique, the short intense laser pulse from a nanosecond pulsed light source creates transient species such as excited states, radicals or ions. The associated absorption changes of the sample are recorded using a spectrally continuous xenon lamp (probe source). In contrast, ultrafast TA spectrometers employ two laser pulses for pump and probe. On the one hand, because of the high intensity of the pump source, LFP spectrometers allow working with the samples of lower (approx. 100 times) concentration, which can be critical in some cases (biological samples). On the other hand, in case of TA spectroscopy the use of ultrabroad continuum as probe sources, and ultrashort femtosecond pulses for pump, much higher spectral and time resolutions are achievable. Each user, depending on his needs, should decide for one (or both) of the techniques.

Starting from milliseconds and finishing on femtoseconds, modern pump-probe spectroscopic techniques cover the timescales of the most important physical and chemical processes. Technical advances in the field enable wide broadening of the range of systems and processes investigated with TA spectroscopy and LFP. Thus, early studies were focused predominantly on relatively small molecules, including simple organic compounds and metal complexes [Orz10]. Current investigations include a wide variety of far more complicated and complex classes of compounds that are of particular interest in fundamental research as well as in environmental studies, industrial and biomedical applications.

Because of the fact that all experimental data in this thesis were obtained using the TA spectroscopy method, let us describe only some interesting experimental objects for application of this technique (because the amount of experimental scientific knowledge is growing rapidly):

- **Investigation of reaction mechanisms**. TA spectroscopy is a very convenient tool for studying light-induced photoreactions. One of the most extensively studied reaction patterns is cis-trans isomerization, with azobenzene as the most interesting and popular optical switch moiety. Different classes of azobenzene were investigated in detail [Näg97, Ban12], allowing the construction of azobenzene-based molecular machines and optically active materials [Wac11, Nor04, Rus10]. Among the other compounds for the cis-trans photoisomerization studies one can name hemithioindigo as a complex prototype for cis-trans isomerization [Nen10] and photoactive yellow protein (PYP) [Cha09]. One more typical pattern of the reaction studied with the TA spectroscopy is reversible bond cleavage. It is of vital importance of having a spectrally broad detection window in order to fully resolve the signatures of all relevant photoproducts. Modern TA methods allow to simultaneously monitor several reaction channels, as it was shown in [Meg09] for the photodissociation of diphenylmethyl chloride. It was shown, that two competing reaction channels, namely the formation of radical pairs (homolysis), and the formation of ion pairs (heterolysis), exist. Because of complexity of molecular systems of interest a combination of both theoretical and experimental methods is often necessary for a complete characterization of a system.

- **Natural and artificial photosystems**. Investigation of the natural and development of the artificial photosystems is nowadays one of the most rewarding research topics. Operation of any photosystem is based on radiation-induced electron transfer pro-

cesses. Therefore both natural and synthetic photosystems are rewarding subjects of TA spectroscopy studies. Significance of this technique is twofold: elucidation of the reaction mechanisms occurring in bacterial and plant photosystems, as well as assistance in development of artificial photosynthetic systems capable of solar energy conversion. Thus, femtosecond visible pump/mid-infrared probe and visible pump/visible probe TA spectroscopy was used by A. Stahl and coworkers to gain insight into the energy transfer in the light harvesting complex II (the most abundant membrane protein in higher plants and green algae) occurring on the femtosecond time scale [Sta09]. Honda et al. have comprehensively studied the light-harvesting mechanism in polymer:fullerene:dye ternary blends by means of TA spectroscopy. Their findings provided experimental evidence that ideal interfacial structures can be fabricated even by a simple spin-coating from blend solutions, which will help in designing efficient polymer solar cells with the ternary blend bulk heterojunction active layer [Hon11]. One interesting example of building block for supramolecular chromophoric structures is naphtalenediimides (NDIs). Efficient charge separation in the picosecond range and length-dependent charge recombination make these multi-chromophoric NDI systems potential building blocks or complex photoactive devices. Pugliesi et al. elucidated the mechanism responsible for the fluorescence quenching in a set of 2,6-sulfanyl-core-substituted NDIs [Pug10]. In the development area one of the promising concepts is hybrid solar cells, a combination of organic and inorganic nanoscale semiconductors, that allow to benefit from the advantages of both material types. Using a novel broadband (UV-Vis-NIR) TA spectroscopy with a time resolution of 40 fs, Herrmann et al. were able to directly monitor the primary photoinduced processes in hybrid P3HT polymer/silicon thin films heterojunctions [Her11]. The study of natural light harvesting systems and the development of artificial photosystems is an open field of research for both fundamental and practical purposes.

- **Study of nanoparticles and nanomaterials**. Experimental investigation and modeling of the new properties of nanoobjects and nanomaterials has become an intense field of research during the last years. This interest was motivated by the possibility of modifying these properties, playing with size, geometry, structure and composition of a nanoobject. Thus, Baida et al. investigated the properties of a single metal nanoparticle using the spatial modulation technique with a pump-probe setup [Bai11]. Since the size, shape and chemical composition of semiconductor nanocrystals con-

trol their resulting optoelectronic properties, Peng et al. used transient absorption spectroscopy to study how the changes in the chemical composition of CdS-Ag2S nanorods influence electron relaxation dynamics [Pen10]. The renewed interest in graphene composite architectures motivated Muszynski et al. to investigate the graphene-gold nanocomposites as new catalyst materials. Using TA spectroscopy, they managed to show that the optical properties of gold nanoparticles were not significantly influenced by the surrounding medium of graphene [Mus08].

- **Biological and biomedical studies**. Life on the Earth benefits from sunlight to a great extent: plants use the sun electromagnetic radiation as the main source of energy via the processes of natural photosynthesis, in various biological photoreceptors sunlight provides signals for development and movement of the organism, and vision is the main source of information for advanced organisms. On the other hand, the most energetical UV part of the sunlight, in particular when absorbed by DNA, can have deleterious effects like cell death, mutations and cancer. Therefore one of the most important topics is investigation of mechanisms of formation and repair of UV-induced lesions in DNA. Inducing certain lesions by a short laser pulse – and thus synchronizing the activity of a whole model system – opens the way to unprecedented time resolution and hence detailed understanding of mechanisms of the formation and repair of the two primary lesions, namely cyclobutane-pyrimidine dimers [Schr09] and (6-4) lesions [Har10]. One more important field of research is understanding interactions between drugs and biological macromolecules. TA spectroscopy is used here for monitoring photophysical behavior of excited drugs, that is very sensitive to medium. Data gained from such investigations enable determination of the distribution of the drug within a certain protein [Mon08]. A number of medical therapies (particularly photodynamic therapy of cancer) also profit from the power of TA spectroscopy. Thus, the molecular mechanisms of the reactions of one of the mostly used anticancer drugs cisplatin with one of the photosensitizers, as well as the effects of the molecular reaction mechanism on the resultant DNA damage in the combination therapies of cisplatin with UV/ionizing radiation and with photodynamic therapy, were investigated in [Lu07].

- **Biomimetic synthesis**. This is the attempt to follow biosynthetic pathways without the aid of enzymes. As shown by Beaudry et al. [Bea05], biomimetic electrocyclizations have proven to be very effective in the construction of structurally highly com-

plex natural products. At present time, very little is known about catalysis in electro-cyclizations. Transient absorption spectroscopy can be here a very valuable aid.

As one can see, the field of research contains a lot of topics and is still growing. Although all of them are equally important, this thesis is mainly devoted to the investigation of the complicated allyl systems by means of the TA spectroscopy. The structure of the thesis resembles the structure of a standard scientific publication and is the following: the description of the experimental methods in detail is presented in chapter 2 ("Materials and methods"). The chapter 3 ("Transient absorption spectroscopy of time zero calibration substances") deals with the investigation of a number of well-known laser dyes and organic substances in order to find the best suited time zero point determination substance. The chapter 4 ("Photoinduced dynamics of unsubstituted 1,3-Diphenylallyl chloride and its photoproducts") is devoted to the investigation of the reaction mechanism of the photoinduced generation of radicals and cations using the simplest unsubstituted model system. As a logical sequel of it, the chapter 5 ("Influence of unsymmetric substitution on the photoinduced dissociation dynamics of diphenylallyl and diarylallyl systems") presents the results of the investigation of the complicated dissociation behaviour of photogenerated products generated from unsymmetrically substituted allyl species. The last chapter 6 ("Conclusions") summarizes the obtained results and places them among other studies in the system of TA spectroscopy knowledge.

2. Materials and Methods

This part of the thesis begins with the preparation of the samples used in the experiments. Methods of steady-state optical spectroscopy that were used for the characterization of investigated compounds are also outlined here. After the brief discussion of the basic principles of TA spectroscopy the description of the home-built TA spectrometer follows.
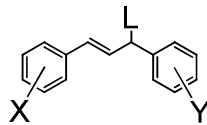
2.1 Sample preparation

2.1.1 Synthesis of the allyl compounds

All allyl species (the detailed description of the structure will be given in the chapter 4) were synthesized by Konstantin Troshin from the workgroup of Prof. Herbert Mayr (Fakultät für Chemie und Pharmazie, Ludwig-Maximilians-Universität München). The main cause for choosing these species is the unique property introduced by a double bond. Shortly, the region of the double bond plays the role of chromophore. This property influences the dissociation dynamics of the allyl compounds (see Chapter 4).

Structural formulae and abbreviations for the full names of the compounds investigated in this work are shown in Table 2.1. The compounds 1(HH)-Cl and 1(HH)-OAc were prepared as described in references [Hay89] and [Sch08]. The synthesis of the phosphonium salts was carried out according to the procedures of reference [Tro11]. The unsymmetrically substituted diarylallyl acetate 1(MeFF)-OAc was prepared according to the procedure described in reference [Sch08] from MemFF(OH) (1.000 g, 3.842 mmol), acetyl chloride (550 µL, 605 mg, 7.70 mmol), DMAP (100 mg, 0.818 mmol) and triethylamine (1.3 mL, 0.95 g, 9.4 mmol) with a yield of 0.558 g (1.85 mmol, 48%). The unsymmetrically substituted diarylallyl acetate 1(FFMe)-OAc was prepared according to the procedure described in reference [Sch08] from mFFMe(OH) (0.906 g, 3.48 mmol), acetyl chloride (500 µL, 550 mg, 7.00 mmol), DMAP (100 mg, 0.818 mmol) and triethylamine (1.2 mL, 0.87 g, 8.6 mmol) with a yield of 0.450 g (1.49 mmol, 43%). The solvents used for the spectroscopic investigation were of the highest spectroscopic grade available.

Table 2.1: Allyl compounds investigated in this work together with empirical electrophilicity parameters E of the corresponding cations and the absorption maxima of radicals and cations in CH_3CN.

					λ_{max} / nm	
X	Y	L [a]	Abbreviation	E [b]	Rad	Cat
H	H	Cl	1(HH)-Cl	2.70	356	490
H	H	OAc	1(HH)-OAc	2.70	355	487
4-Me	3,5-F$_2$	OAc	1(MeFF)-OAc	---	360	490
3,5-F$_2$	4-Me	OAc	1(FFMe)-OAc	---	360	490
H	H	PPh$_3$	1(HH)-PPh$_3$BF$_4$	2.70	c	488
4-Me	4-Me	PPh$_3$	1(MeMe)-PPh$_3$BF$_4$	1.23	c	518
3-F	3-F	PPh$_3$	1(FF)-PPh$_3$BF$_4$	4.15	c	495
4-Me	3,5-F$_2$	PPh$_2$Me	1(MeFF)-PPh$_2$MeBF$_4$	---	c	494

[a] Leaving group of the 1,3-diarylallyl compound; Cl and OAc can leave as radicals or anions, PPh$_3$ and PPh$_2$Me only as neutral molecules

[b] Electrophilicity parameter of the corresponding 1,3-diarylallyl cations from reference [Tro11]

[c] No radicals detected

2.1.2 Sample handling

If not mentioned else, all investigated compounds were used in liquid form. For the preparation they were dissolved in spectroscopic grade solvents purchased from Sigma Aldrich Chemie GmbH without further purification. As a rule, all samples were prepared shortly before each transient absorption experiment in order to minimize the possibility of changes of the sample (e. g. degradation) with time.

2.2. Experimental spectroscopic techniques

2.2.1 Steady-state spectroscopic techniques

Steady-state (stationary) absorption spectroscopy is a useful tool employed in analytical chemistry for the determination of the presence of a particular substance in a sample. In this work it was used for the following purposes:

- Investigation of purity of the synthesized sample.
- Control of needed concentration at the wavelength of interest (preparation for TA experiments).
- Checking the stability of substance after the irradiation during TA experiment.
- Control of the sample "longevity" (if the compound decays with time).

2.2.2 Principles of ultrafast transient absorption spectroscopy

In a typical TA experiment an excitation (or pump) pulse promotes a fraction of the molecules to an excited state. Depending on the type of the experiment, this fraction can range from 0.1% to tens of percent [Ber09]. The sample is probed with the subsequent weak pulse (i. e. the intensity of the pulse is low enough to avoid multiphoton processes during probing), that is sent with a time delay with respect to the pump pulse. A difference absorption spectrum (i. e. the absorption spectrum of the excited sample minus the absorption spectrum of the sample in the ground state) is then calculated in terms of the induced changes of the optical density (OD):

$$\Delta OD(\lambda, \Delta t) = -\log\left(\frac{I^*(\lambda, \Delta t)}{I_0(\lambda, \Delta t)}\right)$$

As different intermediate states of the photoinduced reaction have different absorption bands, ΔOD provides valuable information on the nature of intermediate and product states. The observed ΔOD spectrum contains contribution from various processes (see Figure 2.1):

- **Ground-state bleach (GSB)**. After the promotion of a fraction of the molecules to the excited state through the pump pulse, the number of molecules in the ground state decreases. Thus, the ground-state absorption in the excited sample is less than in the sample before excitation. As a result, a negative signal in the ΔOD spectrum is observed in the wavelength region of the ground-state absorption.

- **Stimulated emission (SE).** During the process of stimulated emission a photon of the probe pulse induces emission of the photon from the excited chromophore, which returns to the ground state. SE (that occurs only for optically allowed transitions) to the ground state will have a spectral profile that resembles the fluorescence spectrum of the excited chromophore. The photon produced by SE is emitted in the same direction as the probe photon, and hence both photons will be detected. Resulting in an increase of light intensity on the detector, SE corresponds to a negative signal in the ΔOD spectrum.

- **Excited-state absorption (ESA)**. The pump beam may induce optically allowed transitions from the lower to higher excited states of a chromophore in certain wavelength regions. The probe pulse will be absorbed at these wavelengths and a positive signal in the ΔOD spectrum is observed in the wavelength region of the ground-state absorption.

- **Product absorption**. After excitation of a photobiological or photochemical system reactions may occur that result in a transient or a long-lived molecular state (e. g. triplets, isomers, charge-separated states). The product absorption will result in a positive signal in the ΔOD spectrum. Sometimes (when irreversible) a formation of oligomers and dimers plays a negative role, depleting the amount of the investigated chromophore.
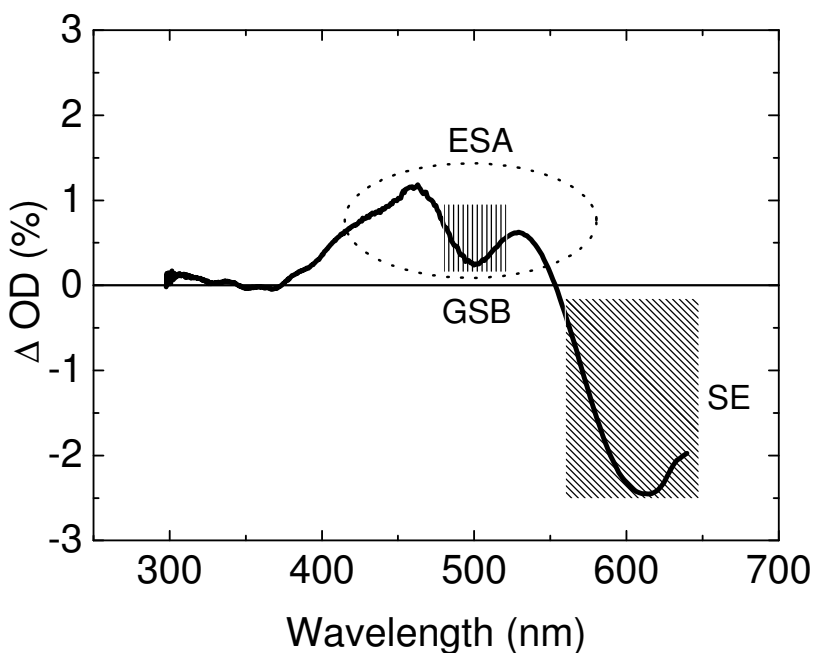
Figure 2.1: Contributions to a ΔOD spectrum (DCM laser dye in ethanol). Excitation wavelength: 278 nm.

2.2.3 Home-built TA spectrometer

A careful description of the experimental setup and the handling of samples is essential in understanding the details which allow to fully exploit the capabilities of TA spectroscopy technique [Fog01]. The TA spectrometer used in the experiments was constructed under full consideration of all technical and conceptual developments available in the last few years. Its unique features and high technical flexibility allow to use it for the investigation of a wide range of spectroscopic problems with the highest quality of the obtained data. Figure 2.2 shows a general scheme of the experimental setup, the most relevant components (photos can be found in the Appendix A) of it are:

- **Laser system used for the pump pulse generation.** As a pump source one of the two systems (depending on the required excitation pulse characteristics) is used. For the experiments with femtosecond time resolution (later: femtosecond TA experiments) we use a regenerative Ti:Sa amplifier system (CPA 2001; Clark MXR). The laser provides a train of femtosecond (150 fs) pulses at 1 kHz with 1 W of average power at the central wavelength of 775 nm. The pulse energy is about 1 mJ. For the pump pulse a fraction of fundamental pulse (200-250 µJ) is used to operate a two-stage noncollinearly phase-matched optical parametric amplifier (NOPA). The NOPA, together with a second harmonic generation (SHG) stage provides pulse tunability from the region of fundamental of about 750 nm down to about 240 nm. A fused silica prism compressor is used to achieve pulse durations below 30 fs. With such short pulses it is possible to access most of the dynamics occurring in the excited electronic states: internal conversion (IC), intramolecular vibrational relaxation and many other processes leading to reactive pathways [Fog01]. For the experiments with nanosecond time resolution (later: nanosecond TA experiments) a tunable Nd:YAG laser system is used (NT242; EKSPLA). Comprised of the pump laser, second and third harmonics generators, optical parametric generator and sum frequency generator in one device, the system provides a train of nanosecond (3 ns) pulses at 1 kHz and is continuously tunable from NUV (225 nm) to NIR (2600 nm).

- **Laser system used for probe pulse generation.** Continuum generation is utilized for the production of the probe pulse. The white pulse is obtained by tightly focus-

13

ing of approximately 1 µJ of the Ti:Sa fundamental into a 5-mm CaF_2 plate. The spectrum of the pulse extends from 290 to 720 nm [Meg09].

- **Device for the creation of time delay between pump and probe pulses.** Contrary to the simple model of TA spectroscopy, we do not change the delay of the probe pulses, but rather the pump pulses are delayed. Depending on the pump pulse system, either mechanical (femtosecond TA experiments) or electronic (nanosecond TA experiments) delay systems are utilized. The mechanic delay system utilizes a retro reflector mounted on a computer controlled linear stage. The induced absorption changes can be followed up to times given by the length of the delay line, from Δt = -50 ps to about 1.7 ns. The electronic delay system is based on the electronic delay generator and allows monitoring of the induced absorption changes from Δt = -50 ns to about 700 µs. In our standard scanning routine the delay scale is chosen to be linear between   -1 and 1 (ps / µs) and then exponential after 1 (ps / µs).

- **Flow cell.** Using flow cells instead of conventional cuvettes allows to avoid photodegradation or accumulation of photoproducts in the probed volume. In case of the femtosecond TA experiments flow cells with 200-µm windows and 110-µm spacer thickness are utilized, in order to reduce the coherent artifact [Lor02] and the group velocity mismatch [Koz05]. For the nanosecond TA experiments standard fused silica flow cells with 1 mm sample thickness (Hellma) are used. Usually the investigated sample was poured into a standard 5-mL glass flask with septum (allowing safe and stable connection with a help of a needle to a pump system). Two models of pumps were used: a micro annular gear pump (mzr-2921-M2; HNP Mikrosysteme GmbH) and a standard peristaltic pump (MCP ISM-404; Ismatec Laboratoriumstechnik GmbH). Some important improvements were introduced by the author in connection with the flow cell operation. Firstly, convenient standard catheter connectors allowing quick interchange of needles were introduced. Secondly, a convenient controller for the micro annular gear pump mzr-2921-M2, containing all controls in one small box, was built.

- **Multichannel detection.** Multichannel detection is achieved by sending the probe pulse after passing through the sample to a prism-based polychromator coupled to a CCD-based detector (Entwicklungsbüro Stresing). Chopping of the pump light allows to avoid the use of a reference channel.

In order to avoid the observation of relaxation phenomena not directly connected to excited state dynamics, measurements are made at the magic angle (excitation and probe pulses are linearly polarized at approx. 54.7 ° one respect to the other) [Lak06].

The setup provides the overall sub-50 fs (in case of femtosecond TA experiments) or 3 ns temporal resolution. Detection sensitivity of the setup is $\Delta OD = 10^{-4}$ over the whole spectral range. The use of high transmission prism-based polychromator allows to cover the complete range of the CaF_2 continuum (290-720 nm) with high efficiency.

The flexibility of the experimental setup is one of its major advantages. All components are interchangeable e. g., the probe supercontinuum can be shifted further towards the mid IR, more advanced compression techniques to obtain shorter excitation pulses can be used, different configurations of the flow cell are possible.
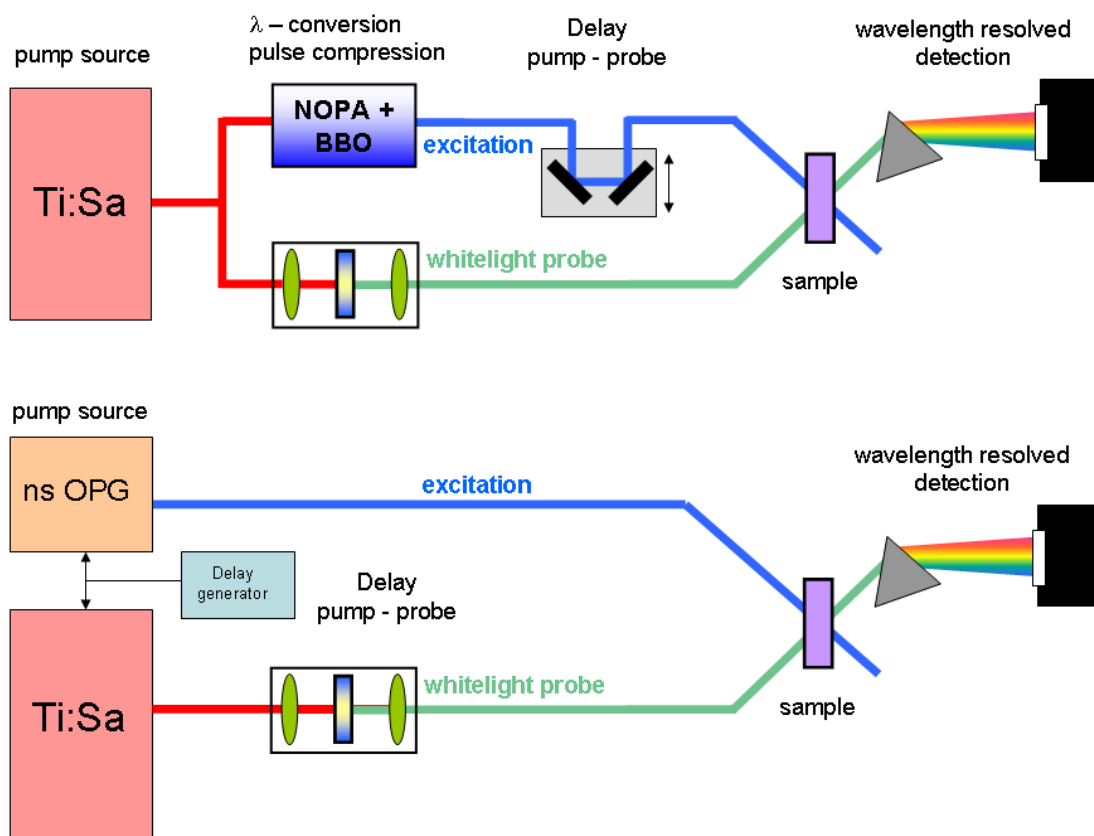
Figure 2.2: Schematic layout of the home-built broadband transient absorption spectrometer. The configuration for femtosecond TA experiments (top); the configuration for nanosecond TA experiments (bottom).

2.2.4 Data analysis

In time-resolved spectroscopy experiments normally a very large quantity of data (thousands of data points, i. e. tens to hundreds wavelengths times one to two hundred delay times) is collected. This data can be analyzed by global and target analysis techniques [Sto04], which in fact represent logical consequent steps of a time-resolved data analysis:

- **Target analysis**. Taking one wavelength and looking at its evolution in time (a so-called kinetic trace) and / or plotting the signal at different wavelengths for a given time points (a ΔOD spectrum), the experimentalist gets a glimpse of a process.

- **Global analysis**. In order to distill the overwhelming amount of data into a relatively small number of components and spectra, global analysis techniques are applied. In global analysis, the femtosecond transient data is globally analyzed using a kinetic model consisting of sequentially interconverting decay-associated difference spectra (DADS). DADS represent decay and rise of the intermediate states.

In the current thesis both target and global analysis of the femtosecond transient data were used for the interpretation of the evolution of investigated molecules. Special LabView-based routines were available for post-processing and fitting of the obtained experimental data. At first, the dynamics at the specific positions (e. g. maxima of radical and ion bands) is studied. Fit function used can be written as:

$$F(t) = IRF \otimes \left\{ \theta(t) \cdot \left[\sum_i A_i \exp\left(\frac{-t}{\tau_i} \right) + const \right] \right\} + artifact$$

The fit function consists of the instrumental response function (IRF) convoluted with the product of the step function and a sum of exponentials (where A_i and τ_i – an amplitude and a time constant, respectively). When necessary - stretched exponential functions are used [Wil70]).

The on-line calculation of the correlation matrix of all possible pairs of fit parameters is realized in the LabView routine. If one of the off-diagonal elements of the correlation matrix approaches ±1, the correlation of the two parameters is very high, that indicates that the number of free fit parameters exceeds those supported by the data. Therefore, the use of the correlation matrix helps to avoid too many exponential functions to characterize the observed dynamics and thus, over-interpretation.

Due to some technical reasons (e. g. varying contributions of the noise in the data) or as a

consequence of an incomplete rate model (standardly used models often do not include solvation, vibrational cooling, internal vibrational redistribution), the fits of the kinetic traces at single spectral positions can result in a systematic variation of the time constants. The mentioned processes can lead to spectral shifts of the band maxima and / or to narrowing and broadening of the spectral bands. If the contributions of these processes are small in comparison to the absorption changes of the signal, a global fit (global analysis technique) can be used for calculation of a set of decay time constants for the whole system.

2.2.5 Calculation of quantum yields

The time-dependent quantum yields of allyl radical and cation generation $\Phi(t)$ is given by the ratio of the radical or cation concentration to the concentration of excited molecules:

$$\Phi(t) = \frac{c_{rad/cat}(t)}{c_{exc}}$$

With the aid of the fitting amplitudes, the final (nanosecond) radical and cation quantum yields $\Phi_{rad, \infty}$ and $\Phi_{cat, \infty}$, and the quantum yields for direct homolytic and heterolytic bond cleavage Φ_{hom} and Φ_{het} can be determined:

$$\Phi_{rad, \infty} = \frac{c_{rad, \infty}}{c_{exc}} \qquad\qquad \Phi_{cat, \infty} = \frac{c_{cat, \infty}}{c_{exc}}$$

$$\Phi_{hom} = \frac{c_{rad, ET} + c_{rad, \infty}}{c_{exc}} \qquad\qquad \Phi_{het} = \frac{c_{rad, GR} + c_{catd, \infty} - c_{cat, ET}}{c_{exc}}$$

The determination of yields of specific processes (e. g. electron transfer, geminate recombination) requires fitted transient absorption amplitudes of the corresponding processes. The following relationships between the process fit amplitudes have been used:

$$Y_{GR} = \frac{c_{cat, GR}}{c_{cat, GR} + c_{cat, \infty}}$$ - fraction of the cation-anion pairs that undergoes geminate recombination.

$$Y_{ET} = \frac{c_{cat, ET}}{c_{rad, ET} + c_{rad, \infty}}$$ - fraction of radical pairs generated by homolysis that undergo electron transfer leading to ion pairs.

$$Y_{RE} = \frac{c_{rad, \infty}}{c_{rad, \infty} + c_{rad, ET}}$$ - fraction of radical pairs which are separated by diffusion to give rise to free radicals.

$$Y_{RR} = 1 - Y_{RE} - Y_{ET}$$ - fraction of radical pairs that undergo geminate recombination back to the precursor.

3. Transient absorption spectroscopy of time zero calibration substances

3.1 Organic laser dyes: applications and studies

The development of organic laser dyes – molecules, containing an extended system of conjugated bonds, started in 1960s, after the invention of the first dye laser. Phtalocyanine and rhodamine 6G were among the first laser dyes, and in the next years various other compounds were reported for this purpose [Scf90].

Laser dyes can be divided into two classes [Pav74]:

1. **Classic organic dyes**. To this category belong rhodamine 6G, fluorescein, coumarine family and others. In these molecules benzene rings or their heterocyclic derivatives are placed adjacent to each other, as in naphthalene, anthracene, acridine etc. In accordance with dyestuff theory, an organic dye is formed by the substitution of a hydrogen atom(s) in a chromophore by a so-called auxochromic group(s) like R_2N, RHN, H_2N, HO, RO. The fluorescence region (laser action region) of these compounds stretches from the violet to the near-infrared region.

2. **Organic scintillators**. To this category belongs a well-known substance p-terphenyl. These compounds are not organic dyes in the classical sense, since they contain no auxochromic groups. `The fluorescence region of these compounds extends from the near ultraviolet to the blue.

Photophysics of many laser dyes was extensively studied by means of steady-state and transient absorption spectroscopy [Hor95, Mac00, Mar95, Asi90, Lew98, Agm90, Pom95, Kov97, Pav74, Sah92, Liu11, Mrc87]. The main aims of the majority of the studies was – on the one hand the elucidation of the most efficient laser dye – with the lowest laser action threshold and the highest efficiency, and, on the other hand, the study of the processes that could decrease the laser efficiency – such as triplet states [Pav74, Asi90].

Nowadays the application of the laser dyes has shrunk since dye lasers were replaced in many cases by the optical parametric amplifiers. However, new applications are arising.

One very promising area for the application of dyes is their use as photosensitizers in nanocrystalline TiO_2 solar cells. Dyes possess the following advantages: their large absorption

coefficients lead to efficient light-harvesting properties, their structural variety provides possibilities for molecular design, last not least is their low cost [Har03].

In this thesis we will investigate one more application of the laser dyes: their use as the time zero point determination substances.

3.2 Laser dyes application for the finding of the time zero point of the transient absorption spectrometer

Finding of the time zero point (temporal overlap) of pump and probe femtosecond pulses is not a trivial task in TA experiments with broadband detection, where a broad supercontinuum (for example, CaF_2 white light) is used as a probe pulse. Even more seriously, it can be a very challenging task in case of two-color transient absorption spectroscopy, where single wavelength excitation and probe pulses are applied (in all cases when high sensitivity is required) [Loc00, Joh03]. In case of the TA experiments with a nanosecond time resolution this can be done by measuring of the time delay between both pulses with a photodiode. However, the most precise way is the application of special substances that have long-lived (nanoseconds or better microseconds) and strong and broad transient absorption signals (in the optimal case – in the whole spectral region of possible probe wavelengths). In that case the procedure of the time zero determination can be the following: if the strong transient signal is observed, it means that the pump pulse comes after the probe pulse, and absence of signal indicates that the pump pulse comes before the probe pulse. The time zero point is such a delay between pump and probe pulses, at which the transient signal becomes to be detectable. The bisection method can be applied for the quickest finding of the time zero point. The following flow chart (see Figure 3.1) illustrates a possible sequence of actions in the time zero determination procedure. Since the determination of the zero point belongs to almost everyday routine, and should be done quickly and not complicated, we made a systematical study of some available laser dyes and some other molecules in order to create a "library" containing the stationary and transient absorption spectra of compounds which can be used for the time zero determination at different pump and probe wavelengths (see Figure 3.2). Four laser dyes and three non-dye organic substances are in details discussed in this chapter, the spectral data for a number of other dyes is presented in the Appendix B.
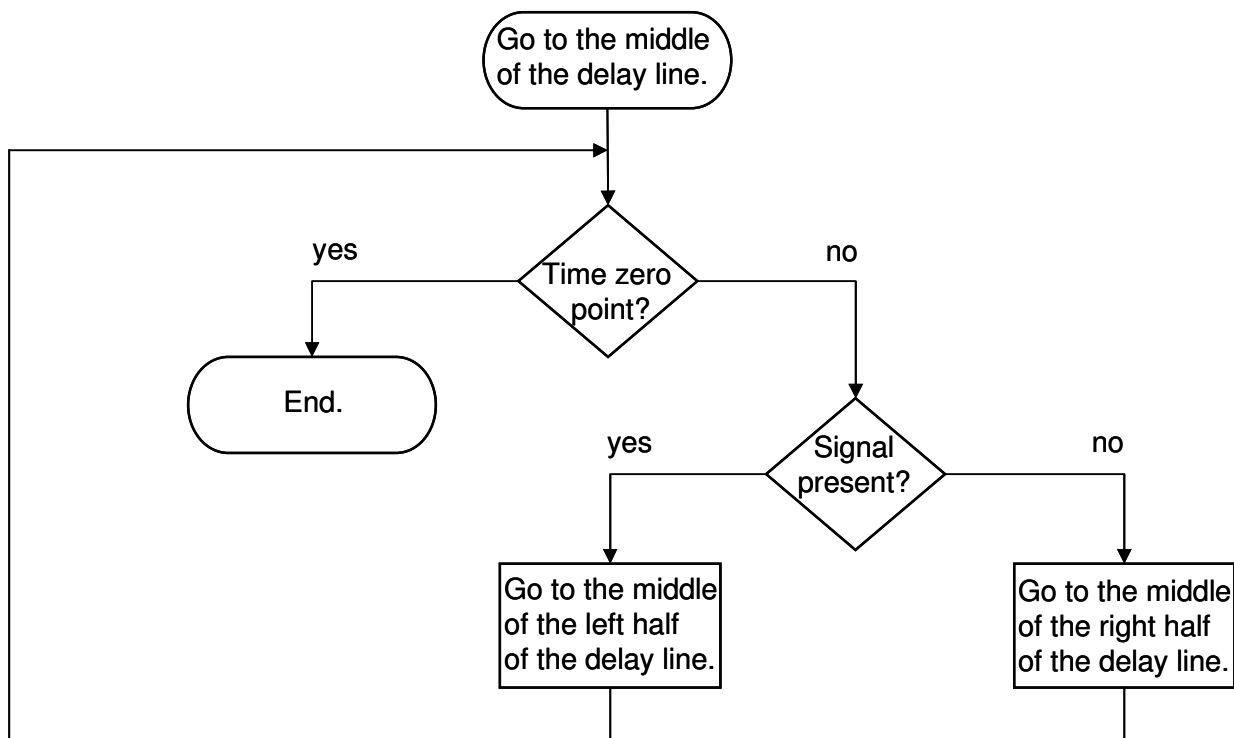
Figure 3.1: The possible sequence of actions for the time zero point determination. "Go" means changing the delay between pump and probe pulses.
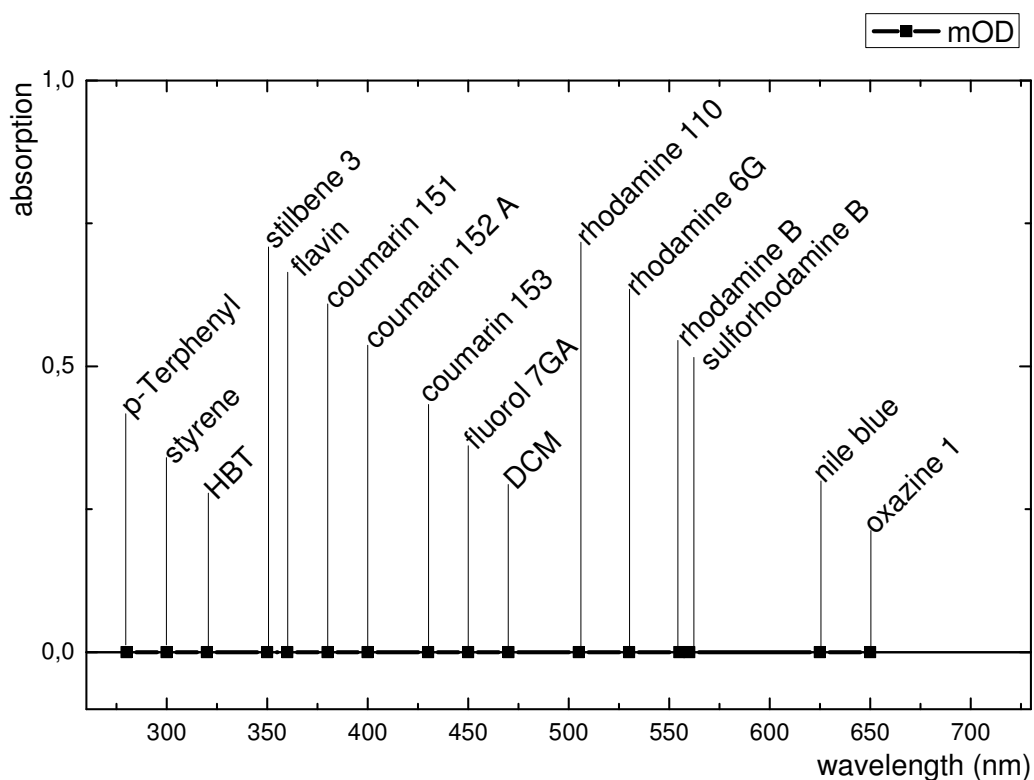

Figure 3.2: Various substances used for the time zero determination. The positions of the maxima of the absorption bands and relative values of stationary absorption signals are shown.

21

The following criteria were defined as the characteristics which an "ideal" substance for the zero point determination should possess:

- Broad absorption band covering the region of possible excitation.

- Strong transient absorption signal covering the whole spectral region of the probe continuum or selected probe wavelength.

- Robustness of the substance to laser radiation – it should be possible to use a standard absorption cell without a need to exchange the substance constantly.

Practically the tested laser dyes and some other organic molecules possessed strong absorption bands in UV region. All substances were dissolved in the solvents which were chosen on the basis of their minimal toxicity. The concentrations were set in such a way to reach an optical density of 0.5 at the excitation wavelength in a 1-mm standard absorption cell made from fused silica (Hellma). Stationary absorption spectra were recorded before and after every transient absorption measurement in order to test the substances for possible degradation induced by the pump laser beam. All substances except one showed no photodegradation or structural changes which could be noticed in the post-measurement stationary absorption spectra.

To test if the substances give strong transient absorption signals under UV excitation, each substance (after recording of the stationary absorption spectrum) in the standard absorption cell was placed in the femtosecond transient absorption spectrometer (described in detail in the Chapter 2). In order to obtain the same experiment parameters for every substance, the pump and probe parameters were set in each case to the standard (used in the majority of transient absorption experiments) values: excitation beam wavelength (frequency-doubled and compressed output of NOPA) in all cases was between 270 and 280 nm (shown in Figures 3.3a and 3.3b). The pump pulses had energy of $\approx$100 nJ and duration less than 50 fs. The beam diameter at the sample was $\approx$100 μm. The relative polarization between pump and probe beams was set to the magic angle value (54.7°). The CaF_2 - continuum ranging from 300 to 700 nm was used as a probe beam.
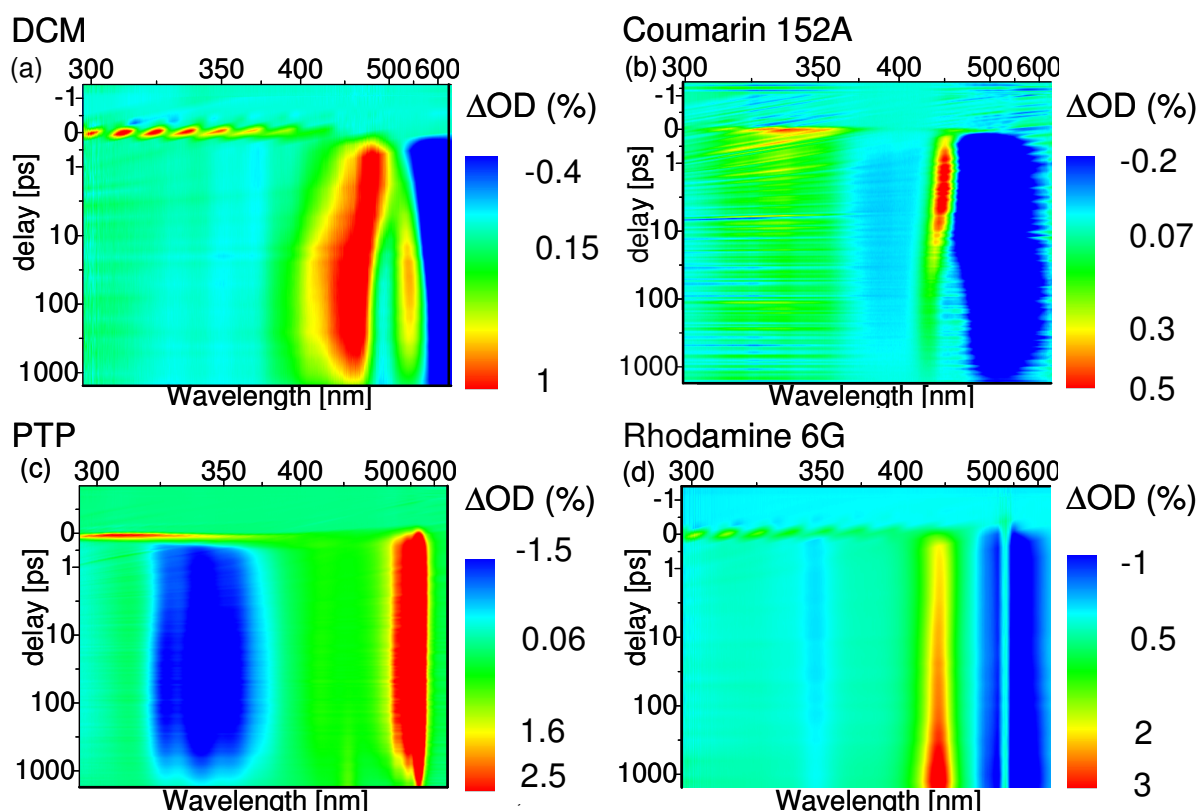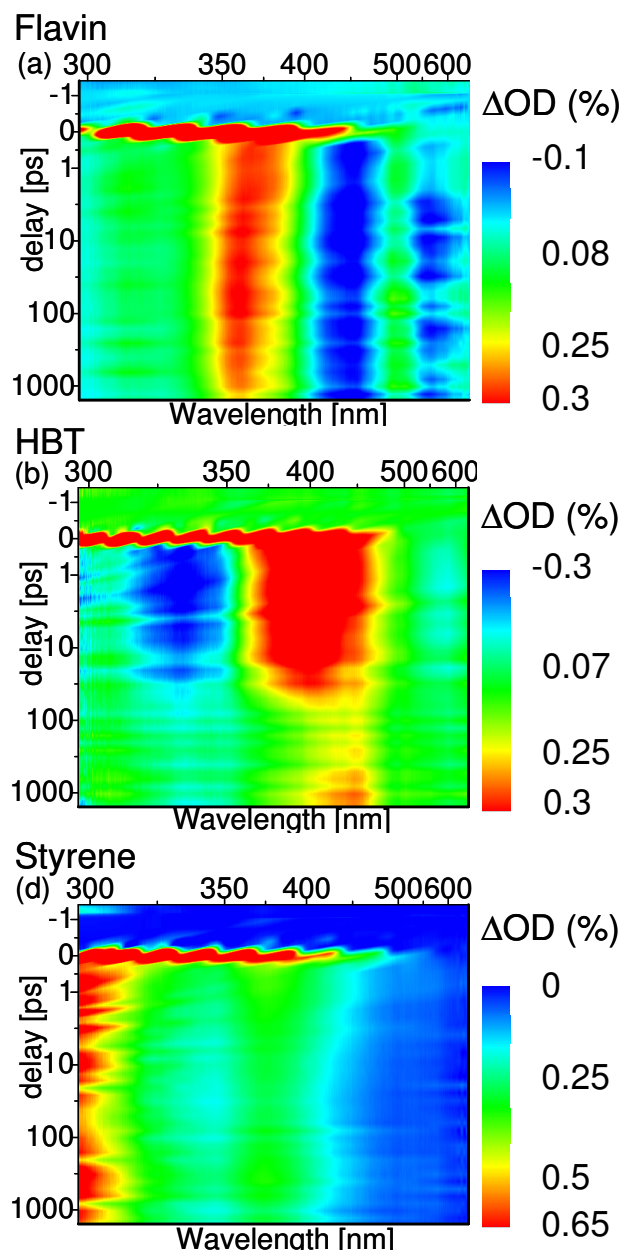
Figure 3.3: Transient absorption spectra after UV excitation of the laser dyes tested for their application for the time zero determination purposes. DCM (4-dicyanmethylene-2-methyl-6-(p-dimethylaminostyryl)-4H-pyran) in ethanol (a) (λ_{ex}=278 nm); coumarin 152A in ethanol (b) (λ_{ex}=271 nm); p-terphenyl in cyclohexane (c) (λ_{ex}=272 nm); rhodamine 6G in ethanol (d) (λ_{ex}=278 nm).

Figures 3.3 and 3.4 represent the resulting transient absorption spectra of the selected organic dyes. All tested substances were chosen because they possess strong transient absorption bands in the region of the CaF_2 continuum used as a probe beam in our transient absorption spectrometer. Since the excitation parameters were the same at every measurement, the transient absorption values are comparable without scaling.

The broadband TA spectroscopy is a very convenient tool for elucidation of the ultrafast photophysics of dyes and similar substances. Some of the tested substances (for example, DCM and coumarin 152A) showed complicated photophysical behavior, which was extensively studied by some research groups. This behavior deserves further discussion and explanation.

Figure 3.4: Transient absorption spectra after UV excitation of the organic substances tested for their application for the time zero determination purposes. Riboflavin tetraacetate in ethanol (flavin) (a) (λ_{ex}=274 nm); 2-(2-Hydroxyphenyl)benzothiazole (HBT) in ethanol (b) (λ_{ex}=278 nm); styrene in ethanol (c) (λ_{ex}=280 nm).

The widely used (because of its broad tunability and high conversion efficiency styryl laser dye DCM was extensively studied by a number of research groups, mainly because of the interesting nature of its excited fluorescent states [Mar95, Pom95, Mac00]. The steady-state absorption and emission spectra (related to $S_0 \rightarrow S_1$ and $S_1 \rightarrow S_0$ transitions) of DCM in etha-

nol shown in Figure 3.5 present a large Stokes shift of about 160 nm and a negligible overlap. The time-resolved spectrum of DCM (see Figures 3.3 (a) and 3.5 (bottom) in ethanol shows two bands which evolve in time. One band around 400-500-nm (assigned to the $S_1 \rightarrow S_N$ absorption transition) undergoes a time dependent blue shift, while the other band (gain band) around 600 nm region can be interpreted as a difference between the amplification of the white light continuum via stimulated emission and its absorption in the $S_1 \rightarrow S_N$ transition (undergoes time-dependent red shift). [Pom95].

The blue shift of the transient absorption band can be attributed to the solvation effects on the intramolecular charge transfer (ICT) absorption state, and the red shift of the gain band is due to the formation and solvation processes of the emissive ICT state [Mar95]. The shifts exhibited by both bands have roughly the same value of 20 nm in the time window of 1 to 1000 ps.

Since both bands occupy the spectral domain after 450 nm and no transient absorption signals exist in the blue spectral domain, DCM laser dye is well suited for the finding of the time zero point only in case of probe wavelengths in the region of 350-600 nm.
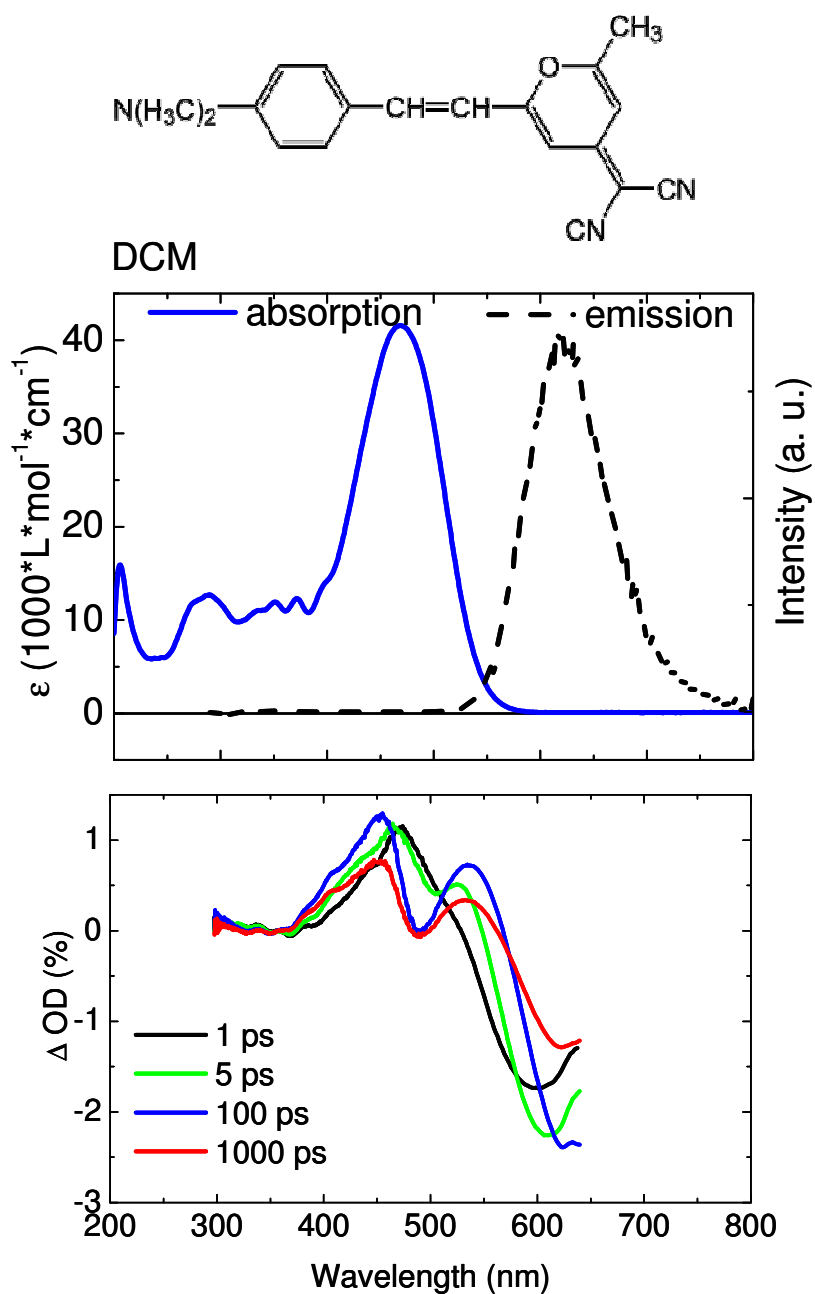
Figure 3.5: Structure (top), steady-state absorption and fluorescence spectra (middle), selected transient absorption spectra (bottom) of DCM in ethanol.

The steady-state spectra of coumarin 152A in ethanol are shown at Figure 3.6 (middle) and are pretty featureless. The transient absorption spectrum of coumarin 152A in ethanol is very similar to that of DCM dye. Both excited state absorption (around 430 nm) and gain (around 500 nm) bands can be assigned to the $S_0 \leftrightarrow S_1$ transition. The weakness of the ESA signal is due to the high concentration of the sample, which led to a strong attenuation of the probe continuum at the ESA region. The time dependent shifts exhibited by both bands (small blue shift of the ESA band and the bigger red shift of the gain band) cannot be viewed as simple probes of solvation energetics but should be rather explained with the involvement of the intramolecular processes [Kov97]. The applicability of the coumarin 152A dye as a time zero calibration substance is pretty same as for DCM dye – coumarin 152A can be considered as quite useful for the UV pump and the 350-600 probe wavelengths.

The main transient absorption fingerprints of p-terphenyl in cyclohexane (see Figure 3.7) are fluorescence band, centered at 340 nm [Liu11], and the transient absorption band (assigned to the $S_n \leftarrow S_1$.absorption [Ike88]), centered at 550 nm. Although, according to Liu et al. [Liu11] and Ikeda et al. [Ike88], both features are long-living (up to 10 nanoseconds), our single-channel fit yielded surprisingly contradictory results. Thus, both features reach their maxima within 50 ps and decay almost completely within 1000-1500 ps. Nevertheless, this dye is a good candidate for the time zero determination purposes with the probe wavelength lying in the UV. Although the spectral region from 400 to 500 nm remains uncovered, the presence of the strong transient absorption band between 500 and 600 nm makes this laser dye also applicable for the probe wavelengths laying in the visible region.

Rhodamine 6G (laser dye "per se") is the most frequently used and most widely investigated laser dye (see Figure 3.8). The species present in the transient absorption spectrum of rhodamine 6G (absorption band centered at $\approx$430 nm and fluorescence band centered at $\approx$540 nm) can be assigned to the first excited singlet state [Bmn93]. In contradiction to the expected values, both absorption and fluorescence bands are unusually narrow (FWHM 25-30 nm), which can be a significant drawback in the time zero point determination. Moreover, no transient absorption signal is present for rhodamine 6G in the spectral region below 400nm.
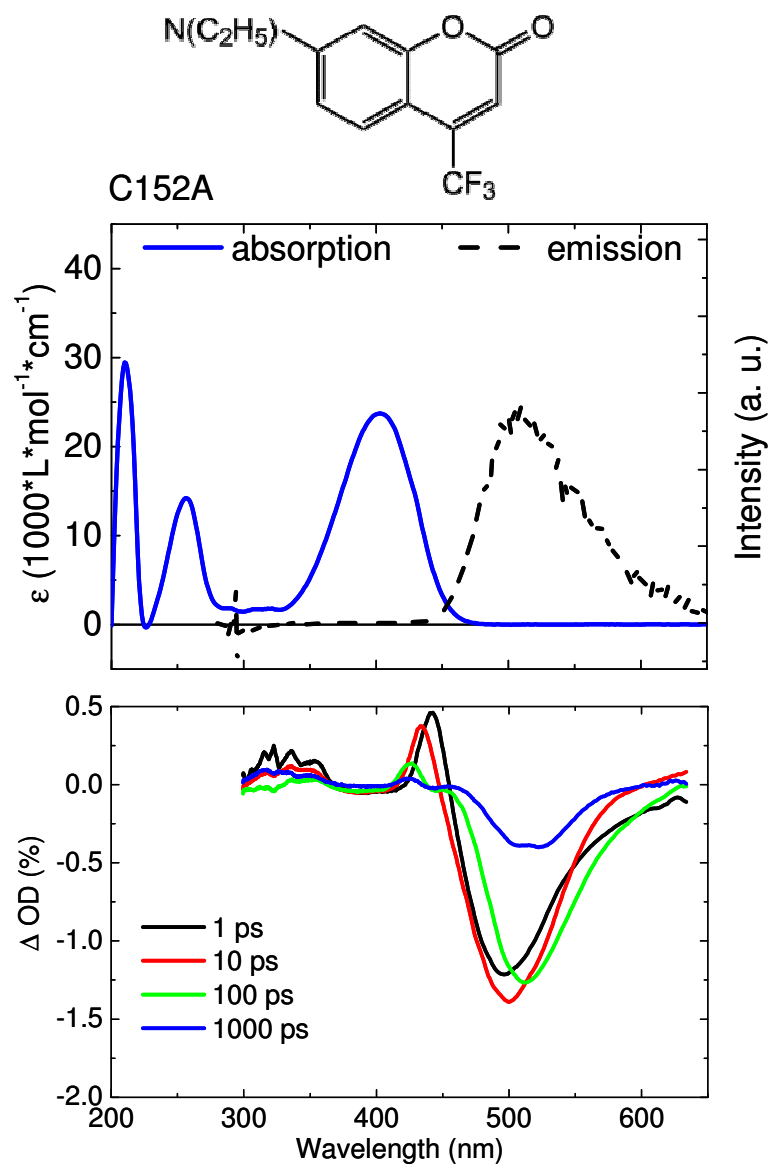
Figure 3.6: Structure (top), steady-state absorption and fluorescence spectra (middle), select-
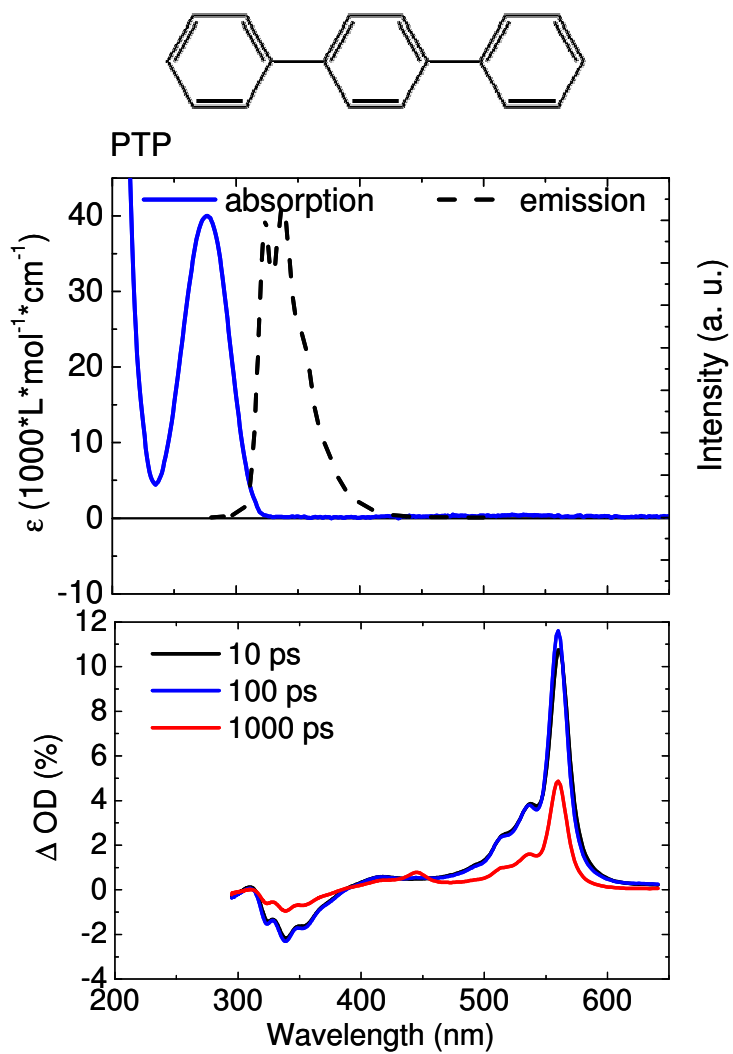ed transient absorption spectra (bottom) of coumarin 152A in ethanol.

PTP

Figure 3.7: Structure (top), steady-state absorption and fluorescence spectra (middle), select-ed transient absorption spectra (bottom) of p-terphenyl in cyclohexane.
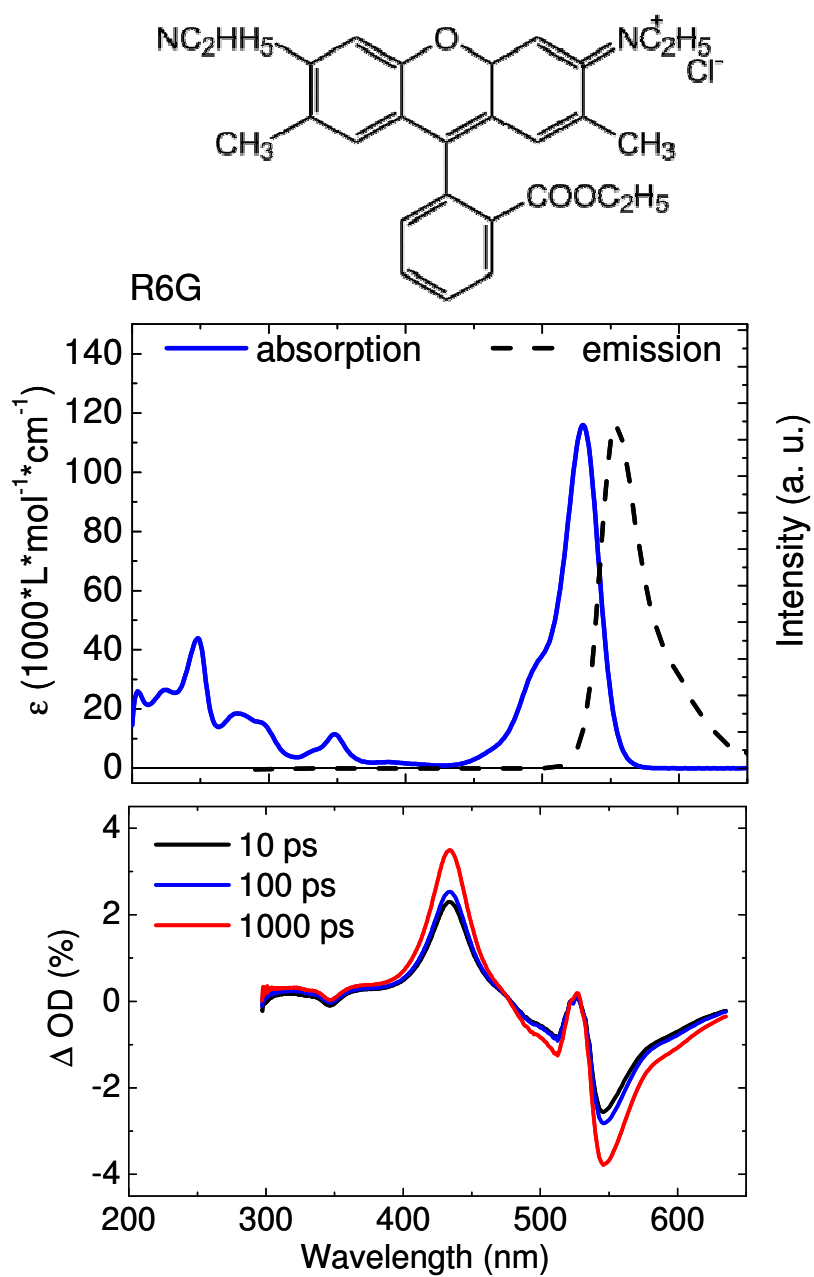
Figure 3.8: Structure (top), steady-state absorption and fluorescence spectra (middle), select-ed transient absorption spectra (bottom) of rhodamine 6G in ethanol.

Three non-dye organic substances were also tested for the time zero determination purposes and demonstrated that in comparison to laser dyes they are less suitable for their use as the time zero determination substances. However, they deserve a short discussion.

Thus, riboflavin tetraacetate (flavin), although possessing strong ESA and SE bands (centered at ≈375 nm and ≈550 nm, respectively), covering the whole 775-nm pumped CaF_2 white light spectral region, demonstrated complicated photophysics, which can be considered as a drawback for the substance used for the time zero point determination [Wei08]. Also flavin did not pass the robustness test (see below).

Since HBT was previously used in our group for the ultrafast excited-state proton transfer studies [Loc00], it was also tested for the time zero point determination purposes. The relatively short-living transient absorption signal (approximately 100 ps) makes the time zero determination procedure with HBT not very convenient (although not impossible).

Styrene (a chromophoric moiety of allyl compounds described in the chapters 4 and 5 of this thesis) exhibited broad weak ESA signal centered at ≈375 nm. Since it is practically impossible to differentiate such a signal from the background noise in the process of the time zero determination, styrene cannot be named a satisfactory time zero point determination substance.

Additionally some of the substances (DCM, coumarin 152A, flavin, HBT) were tested for their robustness – absence of substance degradation in the standard absorption cell at high pump intensities. For this test the TA spectra at selected time delays were compared for the flow cell that allowed the substance exchange (used as reference), and the standard absorption cell. Pump wavelengths were the same as in case of main measurements, pump energies were comparable to those in case of the standard TA measurements (≈100 nJ). As a result, DCM, coumarin 152A and HBT demonstrated remarkable photostability: no changes occurred in the transient absorption spectra. The only substance that failed this test, was flavin. The complete disappearance of its transient absorption spectral fingerprints can be interpreted as the complete photodegradation (see Figure 3.9).
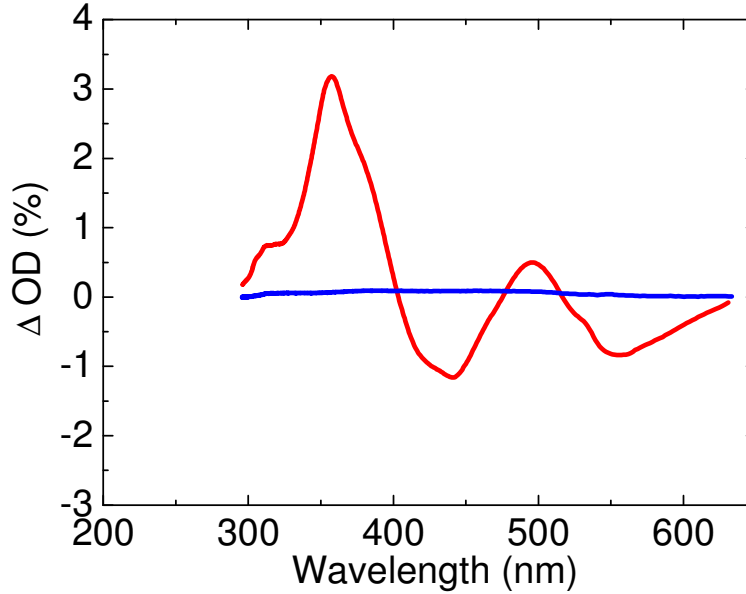
Figure 3.9: Test of robustness (photodegradation test) for flavin in ethanol. Excitation energy 400 nJ, delay time 100 ps. The spectrum for the solution in the standard absorption cell is shown in blue, for solution in the flow cell – in red.

Additionally, the linear dependence of the transient absorption spectra on the excitation energy was tested for flavin. For this test the transient absorption spectra at 100 ps delay were recorded at different values of the pump energy and then the ΔOD values of 360 nm point for flavin were plotted together, with a subsequent linear fit of the obtained curve (see Figure 3.10). The observed non-linear transient absorbance change on the excitation energy, which can be explained by significant concentration changes or saturation effects caused by the pump laser [Ujj98]. Therefore, it is practical to estimate the ratio of the amount of molecules in the excited volume to the amount of absorbed photons. At first the concentration of the sample should be calculated:

$$c = \frac{OD_{\lambda_{ex}}}{\varepsilon_{\lambda_{ex}} \times d},$$

where $OD_{\lambda_{ex}}$ is the optical density of the sample, $\varepsilon_{\lambda_{ex}}$ [L*mol^{-1}*cm^{-1}] - molar extinction coefficient at the excitation wavelength, respectively, and d [cm] – is the optical path length. Then the amount of molecules in the excited volume will be:

$$N_{mol} = V \times c \times N_A,$$

where c – the concentration of the sample,

$$V = \frac{\pi \times D^2 \times d}{4} \ - \text{the excited volume (if approximated as a cylinder),}$$

32

where D – is the pump beam diameter, N_A – the Avogadro constant. The amount of emitted photons will be: $N_{ph} = \dfrac{E_{pump}}{E_{1ph}}$, where E_{pump} – the pulse energy, and E_{1ph} - the energy of one photon at the excitation wavelength, respectively. As a next step, the ratio N_{ph}/N_{mol} should be calculated. In order to minimize saturation effects, this ratio shouldn't exceed 10%. For example, if the sample (DCM dye) has the molar extinction coefficient $\varepsilon_{\lambda_{ex}}$ of 7596.55 L*mol^{-1}*cm^{-1}, the optical density $OD_{\lambda_{ex}}$ is equal to 0.4, the optical path length is 1 mm, and the pump beam has a diameter of 130 µm, then we should set the pump energy to 930 nJ, in order to get 10% of excited molecules at the pump wavelength of 278 nm.
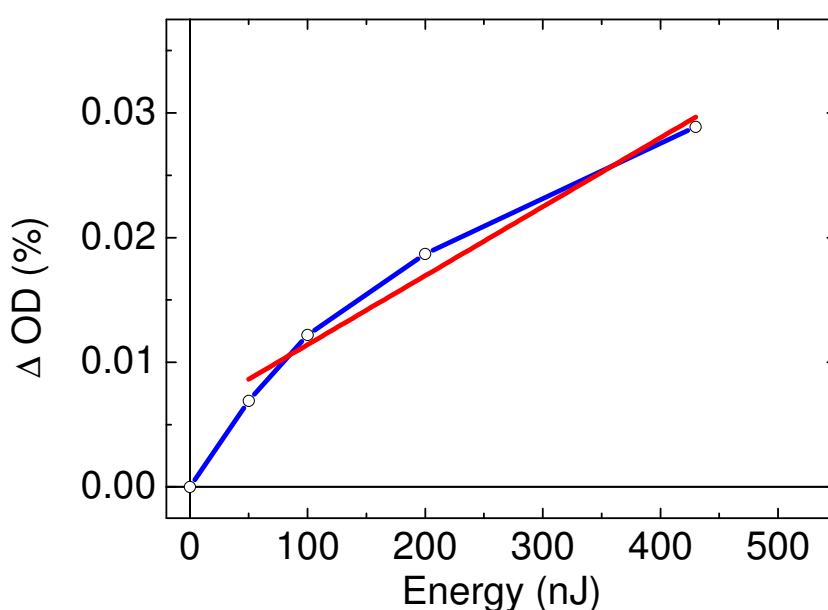
Figure 3.10: Test for the linear dependence of the transient absorption change on the excitation energy for flavin in ethanol. Experimental results are shown with circles and a blue curve. The linear fit is shown with a red curve.

3.3 Implication for spectroscopical practice

With the application of the state-of-the-art broadband transient spectrometer, a number of laser dyes and organic substances were tested for their application for the time zero determination. No tested substance exhibited a strong transient absorption signal covering the whole spectral region of the possible probe. Therefore, it is practical to have a number of substances, each used for the particular spectral region of the probe pulse. Since the non-dye organic substances (flavin, HBT, styrene), although non-expensive, lack strong and/or well-defined transient absorption signal in the 300-700 nm spectral region, it is better to use the standard

laser dyes for the time zero determination purposes. Since the transient absorption signals of DCM, coumarin 152A and rhodamine 6G cover the 400-600 nm region, they are practically equal. They can be used as a good time zero determination substance with the probe wavelength at 400-600 nm region. P-terphenyl, with its bright fluorescence band, covering the 320-370 nm spectral region, is quite well suited for the probe wavelengths lying in the UV.

The described study had some limitations, among those: different solvents were not tested, the suitability of the dyes was not tested for nanosecond time delays; only some of the substances were tested for their robustness and transient absorbance change/pump energy linearity. However, we managed to show that laser dyes are the best substances which can be used for the time zero determination purposes for the broadband and two-color transient absorption experiments. Moreover, one should take into account the facts, that laser dyes were created to suit any excitation wavelength, and some very convenient catalogues containing spectroscopic and chemical information, exist. The majority of laser dyes are extensively tested and easy to handle substances. Last not least is their comparatively low price and high availability.

4. Photoinduced dynamics of unsubstituted 1,3-Diphenylallyl chloride and its photoproducts

4.1 Stationary absorption and quantum chemical studies of the unsubstituted allyl compound with chlorine leaving group (1(HH)-Cl)

The central part of this thesis focuses on the results of the investigation of so-called allyl compounds. These compounds are very similar to the extensively investigated benzhydryl compounds [Amm12, Hee08, Bar90, Pet94], but their additional double bond moiety influences the spectroscopic properties and also the dissociation dynamics.

In contrast to benzhydryl chloride, the absorption maximum of 1,3-Diphenylallyl chloride (1(HH)-Cl) is positioned at 255 nm, and the extinction coefficient is 33 times larger (25808 $L*mol^{-1}*cm^{-1}$)(Figure 4.1b). A comparison of this absorption spectrum with the absorption spectra of the two aromatic moieties comprising diphenylallyl chloride, styrene and toluene, indicates that the strong absorption band at 255 nm almost exclusively consists of the absorption of the styrene moiety (Figure 4.1a), which has the maximum extinction coefficient of 15000 $L*mol^{-1}*cm^{-1}$ at 248 nm. This is much larger than for toluene (260 $L*mol^{-1}*cm^{-1}$ at 262 nm) but still approximately half the absorption strength of 1(HH)-Cl and also blue-shifted. If a methylchloride group is added to styrene to form cinnamyl chloride, an absorption spectrum with an extinction coefficient and band spectral position is obtained that compares very well with that of 1(HH)-Cl. This clearly shows, that the styrene moiety plays the role of the chromophore during the optical excitation of 1(HH)-Cl.

In order to additionally verify if the styrene moiety is the chief chromophore in 1(HH)-Cl, quantum chemistry calculations have been carried out on the absorption properties of 1(HH)-Cl by Dr. I. Pugliesi. The ground state geometry of 1(HH)-Cl was optimized by the RI-BP86 / SVP / T2VP level of theory and vertical transitions were computed at the SACCI / 6-31G* level (see Figure 4.2).

The vertical transition with the highest oscillator strength at 245 nm is very close to the maximum of the stationary absorption spectrum at 255 nm. This transition corresponds to an electron excitation from the HOMO to the LUMO, which are both π-orbitals, located at the styrene part of DPA(Cl).

Therefore, according to the theoretical and experimental investigation of the ground state absorption of 1(HH)-Cl, the conclusion can be drawn, that the styrene plays the role of the chromophore during the optical excitation of 1(HH)-Cl. Such interesting property of allyl

systems can be very useful for the experimental investigation of the photoinduced dissociation dynamics.
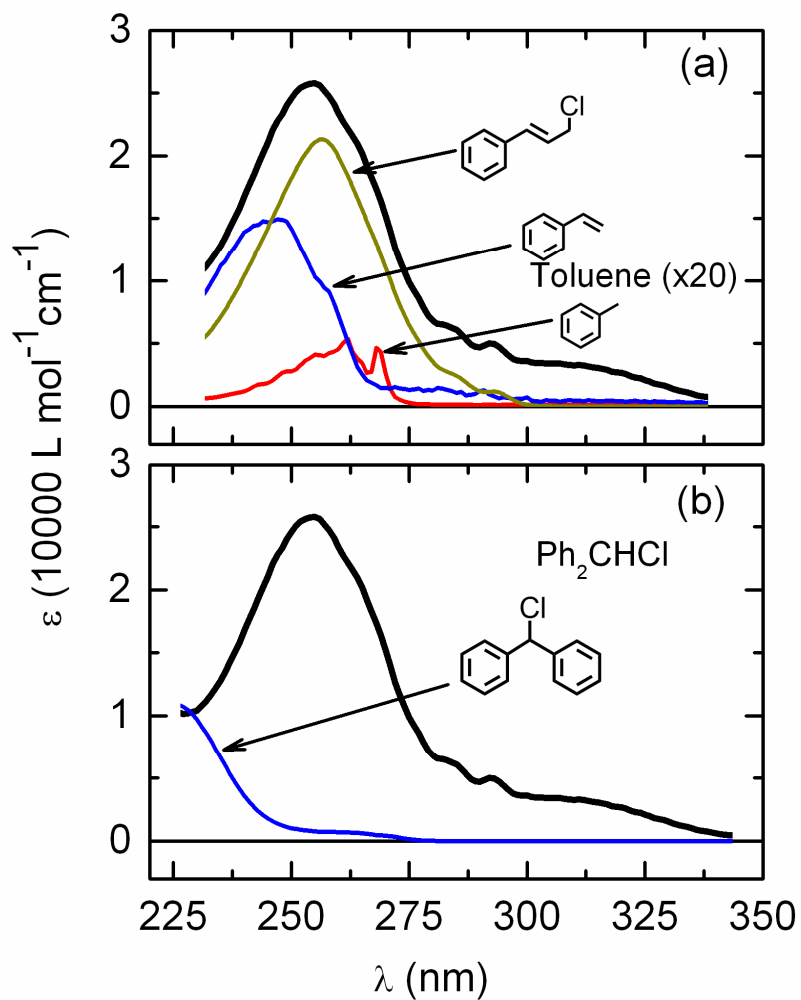

Figure 4.1: Comparison of the stationary absorption spectrum of 1(HH)-Cl (black line) in CH$_3$CN with the stationary absorption spectra of (a) toluene (red line), styrene (blue line) and cinnamyl chloride (dark yellow line) and (b) benzhydryl chloride Ph2CHCl (blue line).
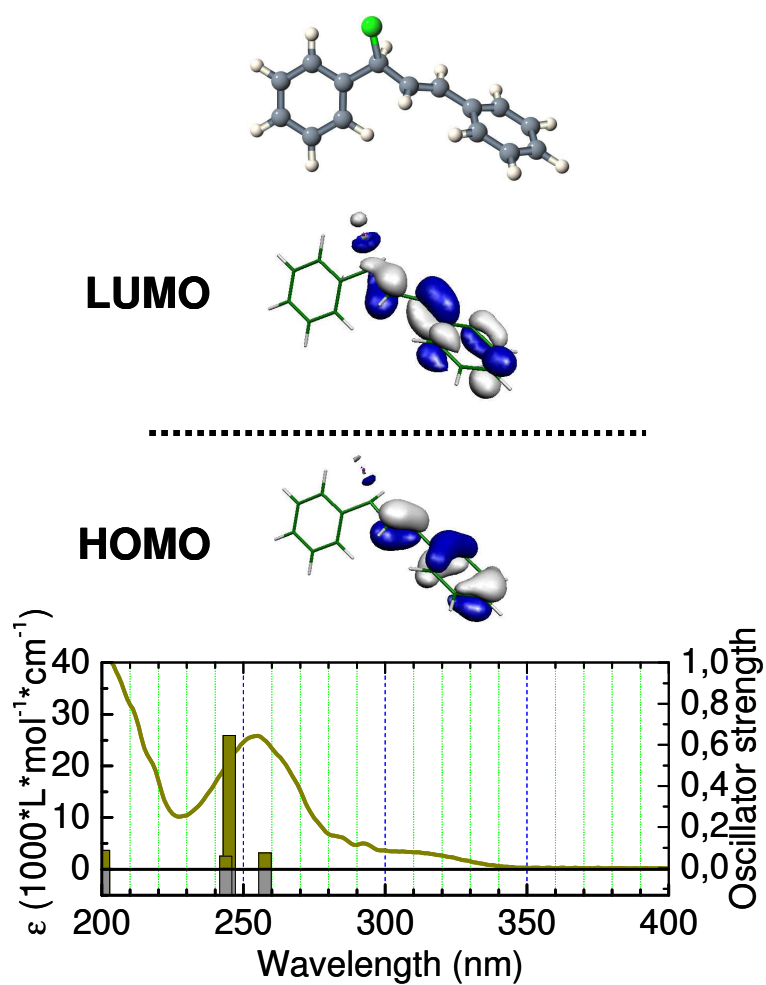
LUMO

HOMO

Figure 4.2: Quantum chemical calculations (SACCI / 6-31G*) of 1(HH)-Cl ground state (courtesy of Dr. I. Pugliesi). Optimized ground state geometry (top), lowest unoccupied and highest occupied molecular orbitals (middle) and calculated oscillator strengths superimposed with the experimental stationary absorption spectrum of 1(HH)-Cl (bottom).

4.2 Fs-ps and ns-μs UV/Vis transient absorption measurements of the unsubstituted allyl compound with chlorine leaving group (1(HH)-Cl)

As the excitation energies between the femtosecond and nanosecond UV/Vis experiments are different and the false color representations of the transient data have been chosen to clearly visualize spectral features, the false color scales are not comparable to each other.

The evolution of the transient absorption spectrum after UV-irradiation of 1,3-Diphenylallyl chloride 1(HH)-Cl in acetonitrile (CH$_3$CN) is shown in Figure 4.3b. The probe wavelength is plotted on the horizontal axis and the pump-probe delay on the vertical axis. Blue color indicates low absorbance and red color high absorbance. The delay on the vertical axis is shown in a linear scale for the first ps and in a logarithmic scale afterwards.
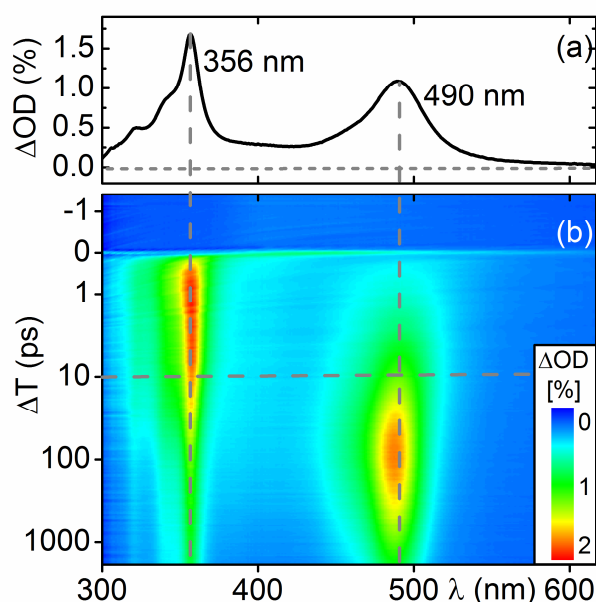
Figure 4.3: (a) Transient spectrum at a pump-probe delay of 10 ps and (b) false color representation of the transient data on the femto- to picosecond timescale of 1(HH)-Cl in CH$_3$CN after 261 nm UV excitation.

Under UV irradiation at 261 nm two bands at 356 nm and 490 nm are generated (see Figure 4.3a for the spectrum observed after 10 ps). The band at 490 nm coincides with the product bands observed in nanosecond laser flash photolysis experiments on allyl phosphonium ions and chemically generated cations from allyltrimethylsilanes [Tro11]. Therefore, we assign the band at 490 nm to the diphenylallyl cation. The second band at 356 nm belongs to the

diphenylallyl radical analogous to the observations made on the related benzhydryl chloride [Sai13a, Bar90] and 1,3-dichloro-1,3-diphenylpropane systems [Mir01]. The radical band reaches its maximum shortly before 1 ps and subsequently decays within a few 100 ps to about half of its initial intensity (Figure 4.5b). In contrast, the cation band reaches its maximum within 100 ps and subsequently decays within a few hundred picoseconds. The transient measurements on the nano- microsecond timescale in Figure 4.4 show that after the dynamics on the picosecond timescale the cation signal lives for up to a few microseconds and the radical signal even up to several hundred microseconds.
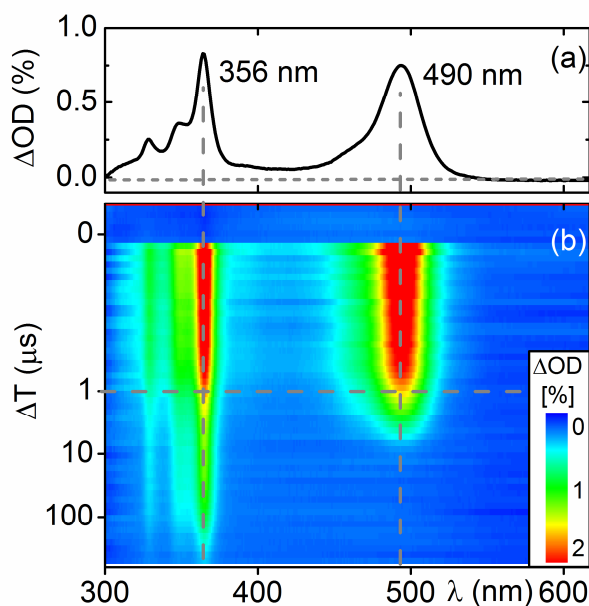
Figure 4.4: (a) Transient spectrum at a pump-probe delay of 1 μs and (b) false color representation of the transient data on the nano- to microsecond timescale of 1(HH)-Cl in CH_3CN after 261 nm UV excitation.

The temporal evolution of the both signals attributed to the cation and radical population in CH_3CN along the vertical lines in Figure 4.3b is shown in Figure 4.5 (black lines). The product dynamics is quantified by exponential fits on the band maxima of cation and radical. The results are shown in Table 6.2. The radical demonstrates a fast initial rise of a $\tau_{Ho} = 300$ fs, which is very similar to the time reported for the related benzhydryl system [Sai13a, Fin12].

In difference to the benzhydryl system no fast femtosecond rise is observed for the cation band of the diphenylallyl system. The subsequent picosecond decay of the radical and the

rise of the cation can be satisfactorily fitted only with a stretched-exponential function $A(t) = A_{SE} \exp\left(-(t/\tau_{SE})^{\beta_{SE}}\right)$ with $\beta_{SE} = 0.5$. For the decay of the radical and the rise of the cation we obtain a $\tau_{SE} = 18$ ps. At later delay times the cation absorption shows a substantial decay and then reaches a constant level after 3 ns. This decay has also to be fitted with a stretched exponential function with a $\tau_{SE} = 324$ ps. The need to use a stretched exponential for the ion pair decay is explained and rationalized in Chapter 5.
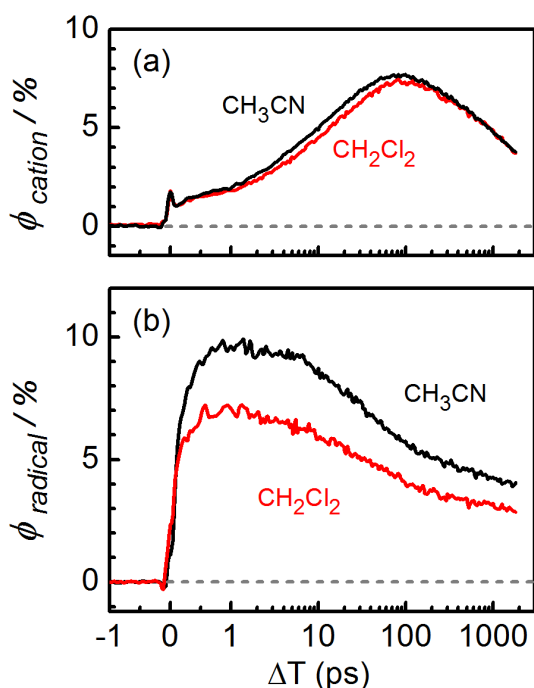
Figure 4.5: Temporal evolution of (a) the cation quantum yield and (b) the radical quantum yield of 1(HH)-Cl in CH_3CN and CH_2Cl_2.

Based on the presented experimental data and fits, we developed a kinetic reaction scheme for the population dynamics of the photoproducts which is shown in Chart 6.1 (Conlusions chapter). The $\tau_{Ho} = 300$ fs time constant is assigned to the photoinduced homolytic C–Cl bond cleavage and subsequent solvent and geometric relaxation of the diphenylallyl radical. Details of this complex evolution of the earliest signals are discussed for the related benzhydryl system in reference [Fin12]. The quantum yield for the initially photogenerated radicals is 10%, which is approximately four times lower than for benzhydryl chloride. This differ-

ence can be attributed to a larger potential energy barrier the wavepacket has to cross in order to reach the conical intersection leading to the radical pair.

The stretched exponential time constant τ_{SE} = 18 ps is associated with a dramatic rise of the cation signal and a substantial decrease of the radical signal. This coordinated behaviour indicates that the cations are formed from the radicals via an electron transfer from the diphenylallyl radical to the chlorine radical in close vicinity. Ab initio calculations (M062X/6-311+G(d) level of theory) on the radical and cation optimized in the solvent model IEFPCM give an exergonic change in Gibbs free reaction energy for the electron transfer of ΔG_{ET} = -1.74 eV [Gau09]. This clearly shows that electron transfer is energetically allowed. The fact that the electron transfer has to be fitted with a non-exponential function indicates that the observed ensemble kinetics is actually a superposition of dynamics in sub-ensembles (as it was shown by Sailer et al. [Sai13a]). These sub-ensembles are represented by a distribution of fragment distances created by the homolytic bond cleavage leading to a time-dependent electron transfer rate, seen in the experiment as stretched exponential decay. The mean electron transfer time can be calculated by duplication of τ_{SE} [San05], i.e. $<\tau_{ET}>$ = $2\tau_{SE}$ = 36 ps.

The main process depleting the radical population by nearly 50% is the electron transfer. The remaining radical pairs can avoid electron transfer or recombination and separate by diffusion to free radicals. More than half of the formed cations decay via geminate recombination albeit here with a stretched exponential time constant of τ_{SE} = 324 ps, similarly to the benzhydryl system. The remaining cations live for up to a microsecond. As in the case of benzhydryl chloride a competition between geminate recombination of the ion pair and diffusional separation of the ions is observed. After the photoinduced C–Cl bond cleavage the ion pairs generated by electron transfer can either separate to give rise to long-lived free ions or recombine to precursor molecule 1(HH)-Cl. The geminate recombination process can occur as long as the fragments are in close vicinity and is terminated by diffusional separation. Therefore, the observed mean cation decay time of a $<\tau_{Rec+Diff}>$ = 648 ps is determined jointly by the geminate recombination and the cation separation. Characteristic times for the individual processes can be calculated from the data and turn out to be a $<\tau_{IPrec}>$ = 1.0 ns for the recombination and a $<\tau_{IPsep}>$ = 1.8 ns for the separation.

The dynamics of the diphenylallyl radicals and cations in the femtosecond measurements matches qualitatively the dynamics of the related benzhydryl system, although all steps are slower. This can be related to a significantly lower reactivity of the allyls, compared to the benzhydryls [Tro11]. However, an interesting difference is observed in the solvent depend-

41

ent behaviour of both systems: in the case of benzhydryl chloride a significant fraction of the ion pairs separates diffusionally to free ions only in highly polar solvents such as CH_3CN, and in the case of 1,3-Diphenylallyl chloride long-lived free radicals and cations are observed in less polar solvents such as dichloromethane (CH_2Cl_2) (see Figure 4.5, red lines). This can be explained in the following way: as in the case of 1,3-Diphenylallyl chloride the positive charge is distributed over the allyl moiety, the lower permittivity of CH_2Cl_2 affords a shielding of the coulomb attraction that is large enough for the generation of free ions.

The nano- to microsecond photoinduced evolution of the transient absorption spectrum of 1(HH)-Cl in CH_3CN is shown in Figure 4.4b. Both the diphenylallyl radical and cation are present at the same spectral position as in the femto- to nanosecond measurement (Figure 4.3b). Time traces of the radical and cation bands are shown in Figure D2 (Appendix D) and the fit results are presented in Table 6.3 (Conclusions chapter). The processes associated with these time constants are not shown in Scheme 1. The cation signal decays within the first two microseconds, the decay of the radical signal is much slower - within several hundred microseconds. At the end of the measurement no residual signal is found throughout the spectrum. Compared to the benzhydryl radical and cation, the allyl radical and cation live nearly an order of magnitude longer. This is related to the delocalization of the radical / charge character over the allyl moiety which reduces their reactivity [Tro11]. The absorption signal evolution of the cation shows monoexponential decay with a time constant of a $\tau_{encount} = 2.4 \, \mu s$. This is well in agreement with the first order decay rates found by Troshin et al. [Tro11]. This process can be assigned to diffusion controlled re-encounter of the free diphenylallyl cation and chlorine anion.

The absorption signal evolution of the radical has a more complex temporal behaviour and is to be fitted with the sum of three exponential functions. About 50% of the radicals decay with a time constant of a $\tau_{react \, GP} = 0.8 \, \mu s$. A further 23% decay with a longer time constant of a $\tau_{olig} = 98 \, \mu s$ while the remaining 27% are very long lived with a time constant of a $\tau_{encount} = 585 \, \mu s$. This behaviour is significantly different compared to the behaviour of the benzhydryl radicals, which decay with only two time constants [Sai13b]. The $\tau_{react \, GP} = 0.8 \, \mu s$ time constant describes most likely those radicals that are still geminate pairs that have not separated far enough or statistically re-encounter. In order to clarify the processes behind the two longer time constants illumination experiments on 1,3-Diphenylallyl chloride in CH_3CN have been performed and the photoproducts analyzed with standard chemical methods. The details are described in the Appendix C. In short, we find that light

exposure induces oligomerization processes of the diphenylallyl unit yielding a product whose NMR spectrum is comparable to polystyrene. Based on these results we believe that the process behind the time constant of $\tau_{olig} = 98\,\mu s$ is oligomerization while the time constant of $\tau_{encount} = 585\,\mu s$ is due to the radicals that have distributed equally in solution and slowly find a reaction partner by diffusion.

5. Influence of unsymmetric substitution on the photoinduced dissociation dynamics of diphenylallyl and diarylallyl systems

5.1 Investigation of the photoinduced dissociation dynamics of unsymmetrically substituted 1,3-Diphenylallyl acetate

Figure 5.1 shows the stationary absorption spectra of three species with oxyacetate leaving group: unsubstituted diphenylallyl acetate (1(HH)-OAc) and two unsymmetrically substituted diarylallyl species (1(MeFF)-OAc and 1(FFMe)-OAc) in acetonitrile (CH_3CN).
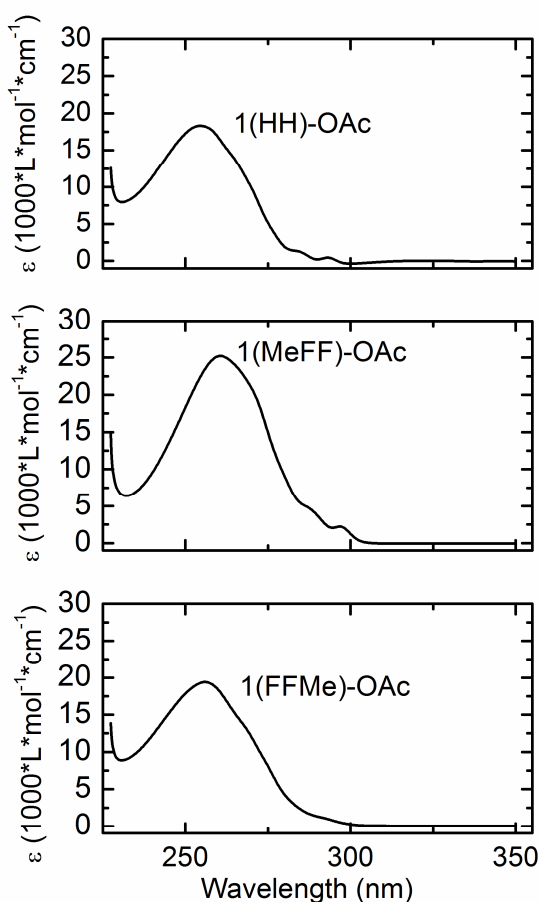
Figure 5.1: Stationary absorption spectra of three diphenylallyl acetate compounds in CH_3CN investigated in this work.

If we compare the positions of the band maxima of species with oxyacetate leaving group with those of 1,3-Diphenylallyl chloride, we will see that exchanging the chlorine leaving group with an acetate leaving group has no major effect on the position of the band maxi-

44

mum (compare Figures 4.1a and 5.1), we conclude that the the styrene moiety plays the role of the chromophore also during the optical excitation of species with oxyacetate leaving group.

The evolution of the transient absorption spectrum of 1(HH)-OAc in CH_3CN is shown in Figure 5.2b. As the excitation energies between the femtosecond and nanosecond UV/Vis experiments are different and the false color representations of the transient data have been chosen to clearly visualize spectral features, the false color scales are not comparable to each other. After UV excitation at 261 nm, the appearance of an instantaneous long-lived broad and featureless absorption band ranging from the visible region into the UV-region is observed, which decays within 500 ps. This spectral feature is very similar to the broad and long-lived excited state absorption (ESA) of styrene and diphenylpropene (Figure 5.3). It allows us to assign this spectral feature to the absorption of the optically excited 1(HH)-OAc precursor. At delays after 500 ps two product bands around 355 nm and 487 nm appear. They can be ascribed to the diphenylallyl radical and cation by the same line of argumentation as in the case of the diphenylallyl chloride.

As the transient spectra of 1(HH)-OAc are quite complicated to interpret, we quantify the photoinduced dynamics with a global fit procedure [Fit06] based on a rate model. The results are listed in Table 6.2. The decay associated difference spectra (DADS) can be found in Figure 5.4. The best fit is obtained with a time constant of $\tau_{Ho/Het} = 401$ ps and an offset. The DADS associated with the $\tau_{Ho/Het} = 401$ ps time constant describes the decay of the broad featureless ESA of the excited precursor and the simultaneous rise of the radical and cation band which live for several microseconds as shown by the transient measurements on the nano- microsecond timescale in Figure D4 (Appendix D). The characteristic concerted behaviour of the radical and cation bands due to electron transfer cannot be observed. The same trend is observed in the temporal evolution of the unsymmetrically substituted 1(MeFF)-OAc shown in Figure 5.5. One can clearly see that the radical (red line) and cation traces (blue line) rise with the similar rate the ESA (black line) decays.
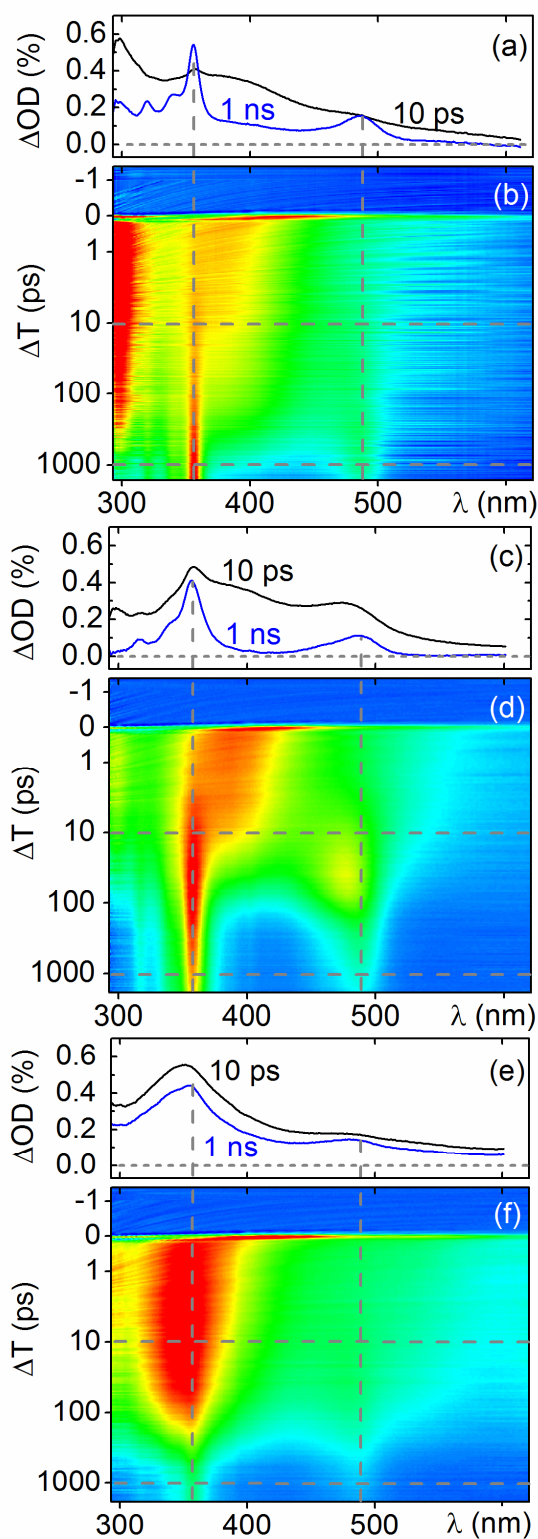
Figure 5.2: Transient spectrum at pump-probe delays of 10 ps and 1 ns (a) of 1(HH)-OAc, (c) 1(MeFF)-OAc and (e) 1(FFMe)-OAc in CH_3CN after 261 nm UV excitation. (b), (d) and (f) are false color representations of the transient data of 1(HH)-OAc, 1(MeFF)-OAc and 1(FFMe)-OAc.

46

Direct heterolysis has already been observed in benzhydryl chloride [Sai13a] although it does not represent the major channel for cation generation. Analogous to the lone pairs of the chlorine leaving group in benzhydryl chloride it is conceivable that the lone pairs of the acetate open up both the homolytic and heterolytic channels [Sai13c]. Radicals and cations are observed to be generated in comparable amounts, which indicates that the conical intersections for radical and ion pair formation are closer to each other on the potential energy surface than in the case of benzhydryl chloride [Fin12, Sai13c].

Although the calculated change in Gibbs free reaction energy for the electron transfer of the radical pair to the cation pair is exergonic (ΔG_{ET} = -1.10 eV) we observe no electron transfer in the temporal evolution of the absorption changes. The ΔG_{ET} value for 1(HH)-OAc suggests a mean electron transfer rate comparable to 1(HH)-Cl, where the ΔG_{ET} =-1.74 eV, in the region of 30 ps. In the case of 1(HH)-OAc, where the rise of the radical and cation band occurs with 401 ps, the electron transfer being much faster would not be detectable. However, for 1(MeFF)-OAc, where the radical and cation rise is completed well within 100 ps, the effects of electron transfer should become observable in the temporal evolution. Since the timescales for heterolysis and the electron transfer are very similar, we carried out a Maximum Entropy analysis [Kut13]. This model free analysis yields a direct visual evaluation of the distribution of lifetimes present in the experimental data, allowing to see if the small differences between the rise of the radical and the cation signal, that cannot be modeled any longer with a global fit procedure, exist. If electron transfer is present, the radical signal would have a slightly faster rise compared to the cation signal. As can be seen from the results of the analysis (see Figure D17 in Appendix D), this is indeed the case. The resulting matrix of the lifetime distribution $p(\tau,\lambda)$ is visualized as a false colour plot, the blue regions are representing lifetimes contributing to signal rises, while red regions are representing lifetimes contributing to signal falls. After 1 ps an extended lifetime distribution from 5 ps to 30 ps is observed for the rise of the radical, while for the rise of the cation we observe a more localized lifetime distribution around 20 ps. We can assign the fall around 5 ps at the spectral position of cation to the decay of the excited state precursor ESA. Based on these results we suggest that after excitation and radical generation, the equilibration of the system in both the hemolytic and heterolytic channels is reached and the processes of direct generation of cations via heterolysis and indirect generation via electron transfer in the radical pairs become equally probable.

A more interesting result is obtained when comparing the evolution of the transient absorp-

tion spectrum of the two unsymmetrically substituted diarylallyl acetates 1(MeFF)-OAc and 1(FFMe)-OAc presented in Figure 5.2d and 5.2f. Unlike in the case of the related benzhydryl systems, exchanging the substituents between the styrene and toluene moiety has a dramatic effect on both the dissociation dynamics and the yield of cation and radical. In the case of 1(MeFF)-OAc the global fit yields a time constant of $\tau_{Ho/Het} = 18$ ps for the generation of cation and radical, while for 1(FFMe)-OAc the same process occurs with $\tau_{Ho/Het} = 190$ ps. Furthermore, the yield is 5 times higher for 1(MeFF)-OAc than for 1(FFMe)-OAc.

As it was already mentioned in the beginning of this chapter, the styrene moiety plays the role of the chromophore during the optical excitation of allyl compounds. In contrast to the benzhydryl system [Fin08], the excitation in case of allyl species is localized on the styrene moiety. Thus only substituents on the styrene moiety can affect the dissociation dynamics and yield of cations and radicals. The sp^3 hybridised carbon centre on which the leaving group is attached prevents any communication between the p-system of the styrene moiety and the toluene moiety. Substituents on the toluene moiety therefore cannot influence the photoinduced dissociation dynamics.
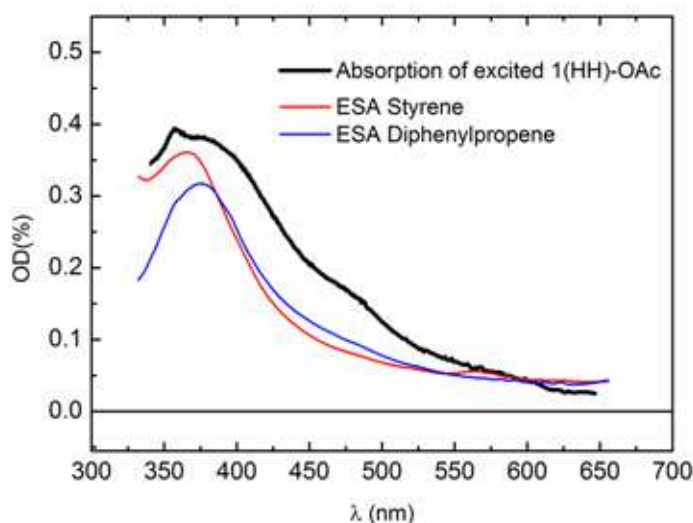
Figure 5.3: Species-associated spectra of 1(HH)-OAc.

As it can be seen from the fit results from the femtosecond transient measurements, electron donating substituents on the styrene side lead to faster dissociation dynamics and increase

the yield of cation and radical compared to electron withdrawing substituents. As ab initio studies on the benzhydryl system show, heterolysis and homolysis occur at conical intersections between the excited state precursor and the ground state product potential energy surface [Fin08, Fin12, Sai13c]. Recent theoretical investigations have demonstrated that the position and topology of conical intersections are strongly affected by substituent effects [Nen12]. There is however no general method that allows to determine in which direction the electron donating / withdrawing character shifts the dissociation dynamics and product yield. This requires the knowledge of the orbitals involved in the conical intersections as well as the topology of the nearby energy landscape. Such an extended theoretical investigation is beyond the scope of this work, but we envision that unsymmetrically substituted diarylallyl systems are very good model systems for theoretical investigation of the effects of substitution on conical intersections.

The TA experiments on the nano- microsecond time scale have shown that the unsymmetric substitution has no effects on the dynamics of the cations and radicals (see Figures D5 and D7, Appendix D). For both diarylallyl acetates (1(MeFF)-OAc and 1(FFMe)-OAc) we obtain comparable time constants (see Table 6.3, Conclusions chapter). The cation decays with a time constant of $\tau_{encount} = 6\,\mu s$. The radical traces can be modelled with a triple exponential decay of $\tau_{react\,GP} = 0.8\,\mu s$, $\tau_{olig} = 63\,\mu s$ and $\tau_{encount} = 501\,\mu s$. Analogous to diphenylallyl chloride, we assign these time constants to recombination of diphenylallyl radical and acetate radical in close proximity, the oligomerization of diphenylallyl radicals and the diffusive encounter of diphenylallyl and acetate radicals.

After photoinduced bond cleavage the diphenylallyl cation and radical undergo ultrafast planarization, just like the benzhydryl system [Fin12]. Due to this planarization, the radicals and cations originating from the unsymmetrically substituted 1(MeFF)-OAc and 1(FFMe)-OAc become chemically indistinguishable and thus give rise to the same recombination dynamics.
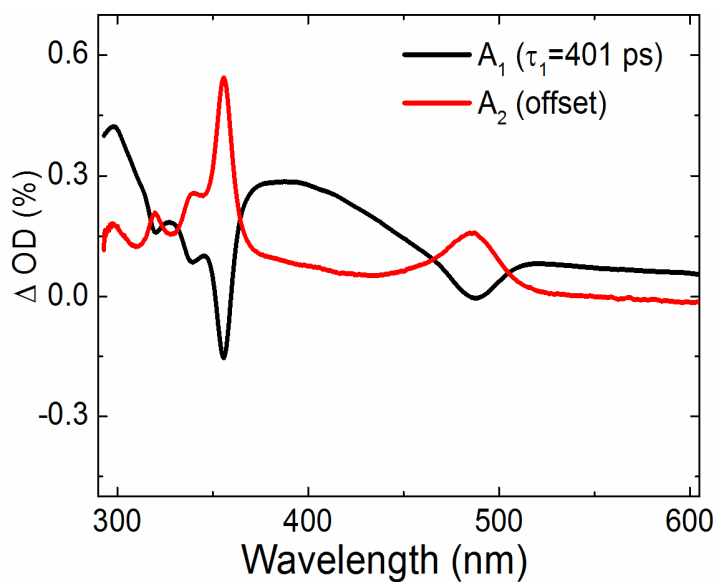
Figure 5.4: Global fit of radical and cation bands of 1(HH)-OAc in CH_3CN, fs-ps experiment (261 nm excitation).
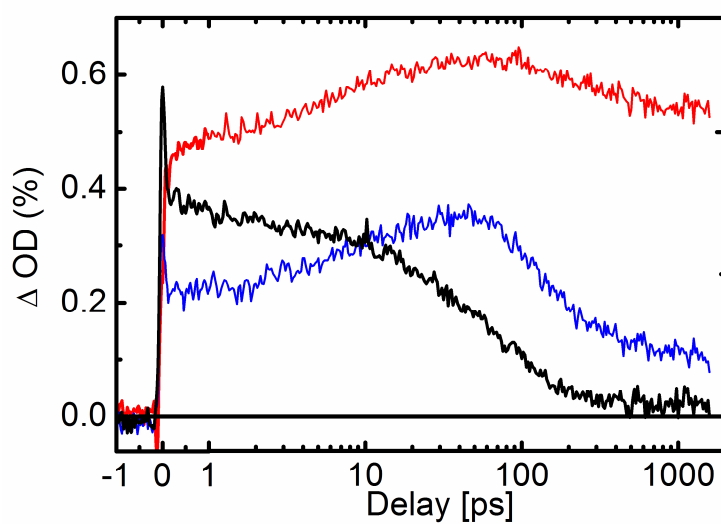
Figure 5.5: Temporal evolution of the absorption changes of the cation band (blue line), the radical band (red line) and the precursor ESA band (black line) of 1(MeFF)-OAc in CH_3CN after 261 nm UV excitation.

5.2 Investigation of non-exponential dynamics of photogenerated ion pairs in 1,3-diarylallyl phosphonium salts

During the photolysis of 1,3-diarylallyl phosphonium salts only cations [Tro11] and no radicals are generated. There are no competing channels that can interfere with the ion pair dynamics.

The stationary absorption spectra of all investigated diphenylallyl phosphonium salts are shown in Figure 5.6. The characteristic form and position of absorption bands maxima indicate clearly that the styrene moiety also plays the role of chromophore in diphenylallyl phosphonium salts.

Figure 5.7b shows the evolution of the transient absorption spectrum of the unsubstituted diparylallyl phosphonium salt 1(HH)-PPh$_3$BF$_4$ in CH$_3$CN. As in the related benzhydryl phosphonium system UV excitation at 270 nm generates two types of bands: (i) a broad absorption band below 400 nm, which decays within the first picoseconds, which is assigned to the excited state absorption of the phosphonium salt precursor; (ii) a long-lived product band around 488 nm, which is due to the 1,3-diarylallyl cation [Tro11].

The temporal evolution of the signal attributed to the diarylallyl cation along the vertical line at 488 nm in Figure 5.7b is shown in Figure 5.8a and b (black line). The dynamics is quantified by an exponential fit, the results of which are listed in Table 6.2 (Conclusions chapter). The major part of the cation band is formed with an initial fast rise of τ_{Het} = 200 fs, which is much faster than 10 ps time reported for the benzhydryl phosphonium salts in references [Sai11, Amm12].
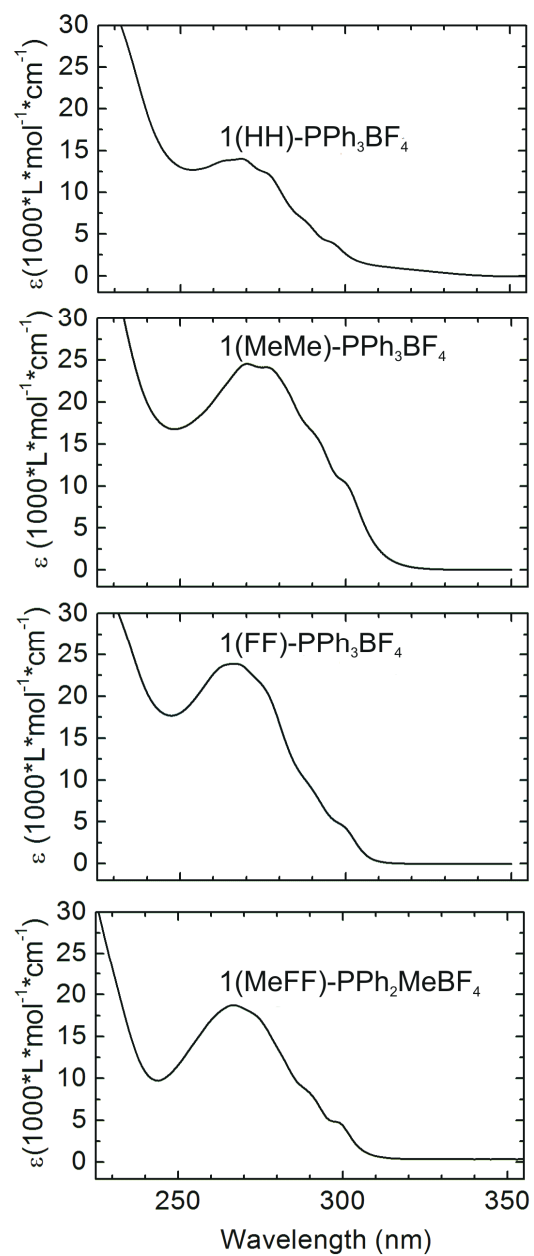
Figure 5.6: Stationary absorption spectra of all diphenylallyl phosphonium salts in CH_3CN investigated in this work.
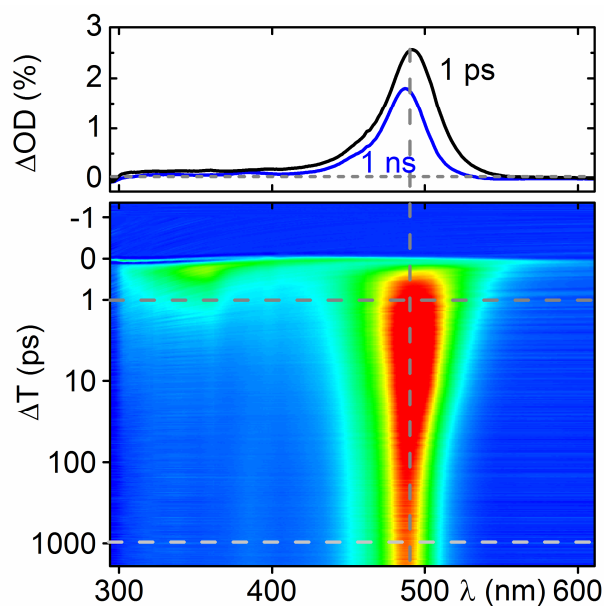
Figure 5.7: (a) Transient spectrum at a pump-probe delay of 1 ps and 1 ns and (b) false color representation of the transient data of 1(HH)-PPh$_3$BF$_4$ in CH$_3$CN after 270 nm UV excitation.

The $\tau_{\text{Het}} = 200$ fs time constant is assigned to the photoinduced C–P bond cleavage and subsequent solvent rearrangement and geometric planarization of the cation. A further rise of $\tau_{\text{cool}} = 0.9$ ps brings the cation band to its maximum. This time constant is attributed to vibrational cooling as in the fit of the band integral over the cation band this time constant disappears entirely (black and violet lines in Figure 5.8b). A subsequent picosecond decay due to diffusion terminated geminate recombination decreases the cation population by about 30% before a population, that is stable on the microsecond time scale, is reached. The picosecond decay can only be satisfactorily fitted with a stretched exponential function just as in the case of 1(HH)-Cl and 1(MeFF)-OAc. A comparative monoexponential fit for this decay is shown in Figure D16 (Appendix D). In order to confine the number of free fit parameters β_{SE} was set to 0.5, as the dynamics of all the phosphonium salts reported below can be well fitted with $\beta_{\text{SE}} = 0.5$. For the decay of the cation we obtain a $\tau_{\text{SE}} = 55$ ps. In order to exclude that the need for a stretched exponential function is due to a spectral shift of the cation band, we evaluated the spectral position of the cation band maximum and compared the temporal evolution of the band maximum with the time slice at 488 nm. We used the same procedure outlined in detail in reference [Sai13a].
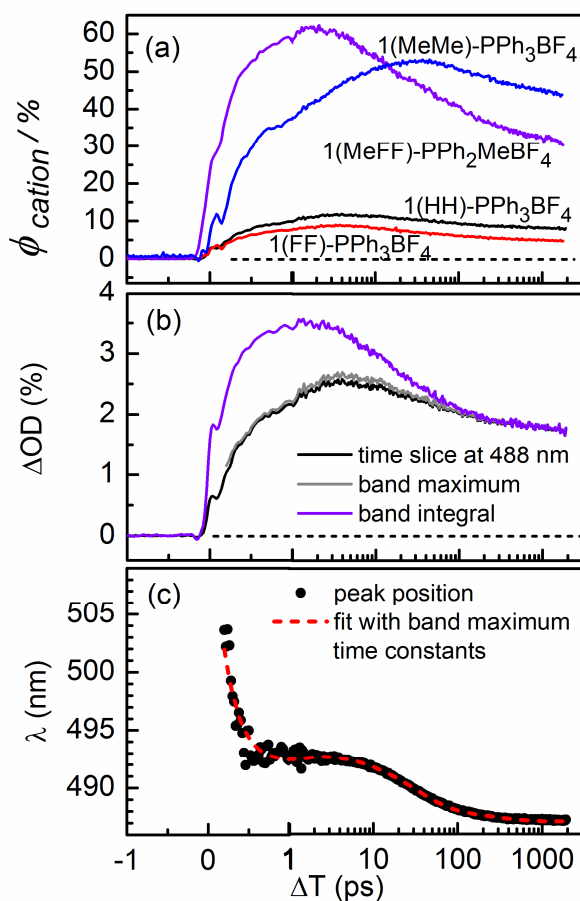
Figure 5.8: (a) Temporal evolution of the cation quantum yield originating from the precursors with the phosphonium leaving group in CH_3CN, (b) the comparison of time slice, band maximum and band integral of the cation band at 488 nm and (c) measured (dots) and fitted (red dashed line) temporal evolution of the cation peak position after photolysis of 1(HH)-PPh3BF4.

Also the spectral shift of the band maximum was analyzed. The results are shown in Figure 5.8c. The following behaviour is observed: a large blue shift of 10 nm within the first 200 fs time constant is accompanied by a small red shift of 2 nm within the first picoseconds before the final blue shift of 5 nm on the time range of 100 ps. The time scale of this last blue shift coincides with the picosecond decay of the diffusion terminated geminate recombination. The spectral band shift is not large enough to alter the temporal evolution of the 488 nm time slice in such a way that a stretched exponential function would be needed. This becomes clear by the nearly perfect match between the time slice at 488 nm (black line in Figure 5.8b) and the temporal evolution of the band maximum (grey line in Figure 5.8b). Therefore we

can conclude that the stretched exponential behaviour of the geminate recombination is due to a characteristic of the process itself, and not a spectral artifact.

Analogous to the electron transfer in benzhydryl chloride, the fact that the geminate recombination has to be fitted with a non-exponential function indicates that the observed ensemble kinetics is again a superposition of dynamics in sub-ensembles. In the case of the geminate recombination these sub-ensembles are represented by a distribution of geminate ion pair distances. As has been shown in reference [Sai13a] the geminate recombination is distance dependent. Geminate pairs at shorter interionic distances recombine faster than those at larger interionic distances. Therefore a time-dependent rate for geminate recombination is obtained, which is seen in the experiment as stretched exponential decay. The mean recombination time is given by twice τ_{SE} [San05], i.e. $<\tau_{rec+diff}> = 2\tau_{rec+diff} = 110$ ps. As the geminate recombination is terminated by diffusional separation, the observed mean recombination time of $<\tau_{rec+diff}> = 110$ ps is a sum of geminate recombination and ion pair separation. The characteristic times for the individual are $<\tau_{IPrec}> = 325$ ps for the recombination and $<\tau_{IPsep}> = 166$ ps for the separation.

The distribution of interionic distances is created not due to the photoinduced bond cleavage as in the case of the benzhydryl system, but rather due to the suprafacial migration of the phosphonium leaving group along the allylic chain. This motion has already been observed by Goering and coworkers [Goe54 - Goe78] in cyclic allyl cations. Troshin et al. [Tro13b] have shown that in the case of the geminate pair formed between the 1-(4-chlorophenyl)-3-phenylallyl cation and the paranitrobenzoate anion, suprafacial migration leads to partial stereoselectivity in the geminate recombination. From their data they extracted the rate of the suprafacial migration to be $(10 \, ps)^{-1}$. The *E* parameter of 2.67 for the 1-(4-chlorophenyl)-3-phenylallyl cation is almost identical to that of the diphenylallyl cation and the *N* parameter of the paranitrobenzoate anion of 9.94 is not significantly lower than that of the triphenylphosphonium leaving group (*N* = 14.33). Therefore the rate of suprafacial migration cannot be substantially different in the geminate pair between the diphenylallyl cation and the triphenylphosphonium. The suprafacial migration is about 30 times faster than the rate of geminate recombination of $<\tau_{IPrec}> = 325$ ps. Therefore, this motion is fast enough for the geminate pairs to form a significant distribution of interionic distances before geminate recombination occurs.

The attachment of substituents on the phenyl rings does not have any substantial effects on the photoinduced bond cleavage and subsequent solvent rearrangement and geometric pla-

narization of the cation (300 – 500 fs). This is also true for the low picosecond cooling. However, a significant difference in the rate for geminate recombination is observed. While for 1(MeMe)-PPh$_3$BF$_4$ it occurs with much slower rate ($<\tau_{IPrec}>$ = 6.7 ns) than in the case of the unsubstituted diphenylallyl cation, generated from 1(HH)-PPh$_3$BF$_4$, a significant speed up is observed in the case of 1(FF)-PPh$_3$BF$_4$ ($<\tau_{IPrec}>$ = 182 ps). This difference is directly related to the electrophilicity E parameter of the cations, which is modulated by the phenyl substitution. Electron withdrawing groups yield a larger E parameter and thus a more reactive allyl cation, while electron donating substituents decrease the E parameter and reactivity with the nucleophilic leaving group. For the unsymmetrically substituted diphenylallyl phosphonium salt 1(MeFF)-PPh$_2$MeBF$_4$ we observe a rate for geminate recombination of $<\tau_{IPrec}>$ = 177 ps that is very similar to that of 1(FF)-PPh$_3$BF$_4$. Therefore, the influence of the two fluorine substituents on the one phenyl ring outweighs the electron donating effects of the methyl group on the other phenyl ring.

6. Conclusions

The current thesis demonstrates the great value of the TA spectroscopy in the investigation of the ultrafast chemical reactions of complicated organic substances (allyl compounds).

Chapter 3 of this thesis is devoted to the improvement of the measurement routine – namely, to the creation of the library of standard laser dyes for the time zero determination purposes of the TA spectrometer.

Chapters 4 and 5 contain the results of the experimental investigation of photoinduced dynamics of the allyl systems. It was shown in the thesis that the allyl systems offer a wealth of interesting properties that can be exploited for the synthesis of suitable precursors of carbocations. In the case of allyl halides (Chapter 4) the time resolved experiments show that the picosecond dynamics is somewhat slower than in the related benzhydryl halides. The photoinduced reaction mechanism and the yields of cations and radicals are however well comparable with the benzhydryl halides. As the reactivity range of the diphenylallyl cations spans 16 orders of magnitude, allyl halides are as versatile as benzhydryl halides for the photogeneration of carbocations and their applications in physical chemistry and organic synthesis.

In the case of allyl acetates (Chapter 5) no electron transfer from radical pair to cation pair was observed. As the excitation is localized on the styrene moiety, unsymmetric substitution has a dramatic effect on the picosecond dissociation dynamics and the yield of the cation. Electron withdrawing substituents on the styrene side lead to slower dissociation dynamics and decrease the yield of the cation compared to electron donating substituents. The asymmetric substitution has no influence on the diffusion controlled re-encounter of the free diarylallyl cation and acetate anion due to the planarization of the cation after the heterolysis.

The diarylallyl phosphonium salts (Chapter 5) allowed for a detailed investigation of the dynamics of the geminate ion pairs as the photoinduced bond cleavage exclusively generates carbocations. The partial stereoselectivity of internal ion return in the solvolysis of optically active allyl compounds observed by Goering et al. [Goe78] and Troshin et al. [Tro13b] could only be explained by a suprafacial migration of the leaving group that is substantially faster than the racemising migration of the leaving group to the other face of the cation. The suprafacial motion was estimated to be as fast as 10 ps. In our time resolved experiments we observed a stretched exponential dynamics of the geminate recombination. As this recombination depending on the substitution occurs on a time scale of a few hundred picoseconds, the

stretched exponential dynamics is a direct proof of the suprafacial migration of the photoleaving group along the allylic chain generating a distribution of interionic distances on the low picosecond timescale.

An unexpected but still valuable information was obtained during the long time light exposure experiment of 1,3-Diphenylallyl chloride. It was found that the UV-light exposure induced oligomerization of the diphenylallyl unit, resulting in a formation of a polymer whose NMR spectrum resembles polystyrene. Thus, the competing parasitic reaction channel was discovered. We believe that such parasitic photoreactions induced by excitation pulses can make pump-probe experiments more complicated, producing signals which overlap with signals of interest.

Chart 6.1: Reaction mechanism (not to scale) generalized to all investigated compounds for the processes investigated with the femtosecond UV/Vis transient absorption. DPA= diarylallyl; L = Leaving group;
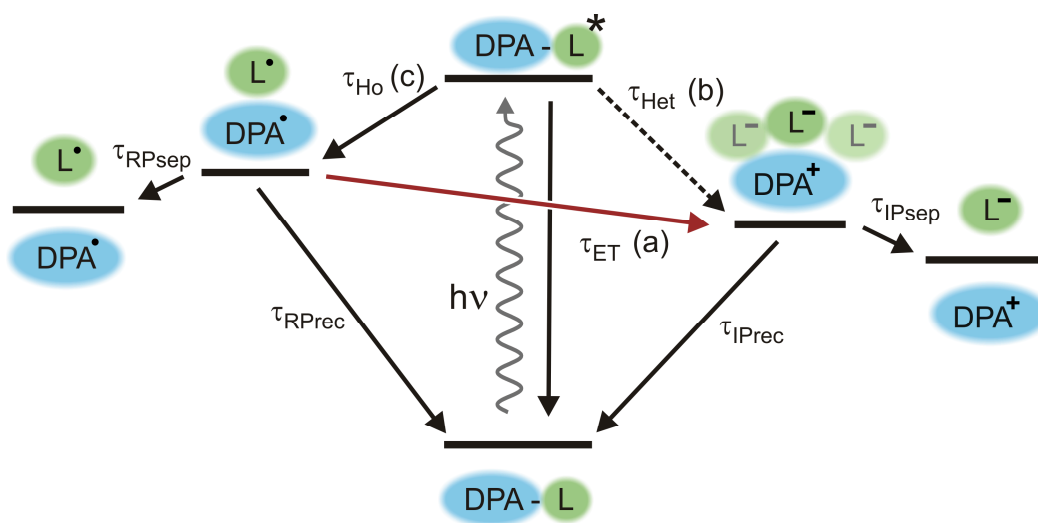
(a) The electron transfer channel exists only for allyl compounds with the leaving group L = Cl

(b) The heterolysis channel exists only for allyl compounds with the leaving group L = OAc and PPh$_3$

(c) The homolysis channel exists only for allyl compounds with the leaving group L = Cl and OAc

Table 6.2: List of all time constants obtained from femtosecond UV/Vis transient absorption measurements for the diarylallyl compounds in CH_3CN investigated in this work listed with decreasing electrophilicity parameter E and decreasing nucleophilicity parameter N of the leaving group. E n.d. = Electrophilicity parameter has not been determined. L = Leaving group.

		Cl^- (N = 17.20)		OAc^- (N = 16.90)		PPh_3 (N = 14.33)	
		Rad.	Cat.	Rad.	Cat.	Rad.	Cat.
FF(L) E = 4.15	$\tau_{Ho/Het}$ (ps)					---	0.5
	τ_{cool} (ps)					---	1.7
	$\tau_{Rec+Diff}$ (ps)					---	82 [d]
HH(L) E = 2.70	$\tau_{Ho/Het}$ (ps)	0.3	---	401	401	---	0.2
	τ_{ET} (ps)	36 [a]	36 [a]	---	---	---	---
	τ_{cool} (ps)	---	---	---	---	---	0.9
	$\tau_{Rec+Diff}$ (ps)	---	648 [b]	---	---	---	110 [e]
MeMe(L) E = 1.23	$\tau_{Ho/Het}$ (ps)					---	0.3
	τ_{cool} (ps)					---	4.6
	$\tau_{Rec+Diff}$ (ps)					---	1094 [f]
MemFF(L) E n.d.	$\tau_{Ho/Het}$ (ps)			18	18	---	0.4
	τ_{cool} (ps)			---	---	---	2.0
	$\tau_{Rec+Diff}$ (ps)			---	206 [c]	---	84 [g]
mFFMe(L) E n.d.	$\tau_{Ho/Het}$ (ps)			190	190		
	τ_{cool} (ps)			---	---		
	$\tau_{Rec+Diff}$ (ps)			---	---		

[a] mean electron transfer time $<\tau_{ET}>$ obtained from the stretched exponential

[b] mean recombination time $<\tau_{Rec+Diff}>$ composed of $<\tau_{IPrec}>$ = 1.0 ns and $<\tau_{IPsep}>$ = 1806 ps

[c] mean recombination time $<\tau_{Rec+Diff}>$ obtained from stretched exponential

[d] $<\tau_{Rec+Diff}>$ composed of $<\tau_{IPrec}>$ = 182 ps and $<\tau_{IPsep}>$ = 149 ps

[e] $<\tau_{Rec+Diff}>$ composed of $<\tau_{IPrec}>$ = 325 ps and $<\tau_{IPsep}>$ = 166 ps

[f] $<\tau_{Rec+Diff}>$ composed of $<\tau_{IPrec}>$ = 6.7 ns and $<\tau_{IPsep}>$ = 1.3 ns

[g] $<\tau_{Rec+Diff}>$ composed of $<\tau_{IPrec}>$ = 177 ps and $<\tau_{IPsep}>$ = 160 ps

Table 6.3: List of all time constants in CH_3CN obtained from nanosecond UV/Vis transient absorption measurements for the allyl compounds investigated in this work listed with decreasing electrophilicity parameter E and decreasing nucleophilicity parameter N of the leaving group. E n.d. = Electrophilicity parameter has not been determined. L = Leaving group.

		Cl^- (N = 17.20)		OAc^- (N = 16.90)		PPh_3 (N = 14.33)	
		Rad.	Cat.	Rad.	Cat.	Rad.	Cat.
FF(L) E = 4.15	$\tau_{react\ GP}$ (μs)					---	---
	τ_{olig} (μs)					---	---
	$\tau_{encount}$ (μs)					---	4.3
HH(L) E = 2.70	$\tau_{react\ GP}$ (μs)	0.8	---	0.7	---		
	τ_{olig} (μs)	98	---	88	---		
	$\tau_{encount}$ (μs)	585	2.4	577	1.6		
MeMe(L) E = 1.23	$\tau_{react\ GP}$ (μs)					---	---
	τ_{olig} (μs)					---	---
	$\tau_{encount}$ (μs)					---	39
MemFF(L) E n.d.	$\tau_{react\ GP}$ (μs)			0.8	---	---	---
	τ_{olig} (μs)			63	---	---	---
	$\tau_{encount}$ (μs)			501	6.0	---	7.0
mFFMe(L) E n.d.	$\tau_{react\ GP}$ (μs)			0.8	---		
	τ_{olig} (μs)			63	---		
	$\tau_{encount}$ (μs)			501	6.0		

7. References

[Acc10]   G. Accorsi, N. Amaroli, *J. Phys. Chem.* C, **2010**, *114*, 1385-1403.

[Agm90]   N. Agmon, *J. Phys. Chem. C*, **2010**, *94*, 2959-2963.

[Alf72]   R. R. Alfano, S. L. Shapiro, *Opt. Commun.* **1972**, 6, 98-100.

[Alf97]   Z. B. Alfassi, P. Neta, *J. Phys. Chem. A*, **1997**, *101*, 2153-2158.

[Amm12]   J. Ammer, C. F. Sailer, E.Riedle, H. Mayr, *JACS.* **2012**, *134*, 11481-11494.

[Asi90]   M. M. Asimov, V. N. Gavrilenko, A. N. Rubinov, *J. Lumin.* **1990**, *46*, 243-249.

[Bai11]   H. Baida, A. Crut, P. Maioli, T. B. Nguyen, D. H. Nguyen, N. D. Fatti et al. *Adv. Nat. Sci. Nanosci. Nanotechnol.* **2011**, *2*, 035011.

[Ban12]   H. M. Bandara, S. C. Burdette, *Chem. Soc. Rev.* **2012**, *41*, 1809-1825.

[Bar90]   J. Bartl, S. Steenken, H. Mayr, R. A. McClelland, *JACS.* **1990**, *112*, 6918-6928.

[Bea05]   C. M. Beaudry, J. P. Malerich, D. Trauner, *Chem. Rev.* **2005**, *105*, 4757-4778.

[Bmn93]   P. C. Beaumont, D. G. Johnson, B. J. Parsons, *J. Chem Soc. Faraday Trans.* **1993**, *89*, 4185-4191.

[Ben03]   S. J. Benkovic, S. Hammes-Schiffer, *Science* **2003**, *301*, 1196-1202.

[Ber09]   R. Berera, I. H. M. van Stokkum, S. d´Haene, J. T. M. Kennis, R. van Grondelle, *Photosynth. Res.* **2009**, *101*, 105-118.

[Ber09]   R. Berera, R. van Grondelle, J. T. M. Kennis, *Photosynth. Res.* **2009**, *101*, 105-118.

[Bov65]   F. A. Bovey, F. P. Hood III, E. W. Anderson, L. C. Snyder, *J. Chem. Phys.* **1965**, *42*, 3900-3910.

[Bra00]   U. Brackmann, Lambdachrome ® *Laser Dyes*, 3rd edition, Lambda Physik AG, Göttingen, **2000**.

[Cem04]   A. Cembran, F. Bernardi, M. Garavelli, L. Gagliardi, G. Orlandi, *JACS*, **2004**, *126*, 3234-3243.

[Cha09]   P. Changenet-Barret, P. Plaza, M. M. Martin, H. Chosrowjan, S. Taniguchi, N. Mataga et al. *J. Phys. Chem. C* **2009**, *113*, 11605-11613.

[Che97]   E. Chen, R. A. Goldbeck, D. S. Kliger, *Annu. Rev. Biophys. Biomol. Struct.*

1997, *26*, 327-355.

[Cor08]   T. Cordes, C. Elsner, T. T. Herzog, C. Hoppmann, T. Schadendorf, W. Summerer et al. *Chem. Phys.* **2009**, *358*, 103-110.

[Dua95]   F. J. Duarte, *Tunable lasers handbook*, Academic Press, San Diego, **1995**.

[Egg97]   C. Eggeling, L. Brand, C. A: M. Seidel, *Bioimaging*, **1997**, *5*, 105-115.

[Fin08]   B. P. Fingerhut, D. Geppert, R. de Vivie-Riedle, *Chem. Phys.* **2008**, *343*, 329-339.

[Fin12]   B. P. Fingerhut, C. F. Sailer, J. Ammer, E. Riedle, R. de Vivie-Riedle, *J. Phys. Chem.* A **2012**, *116*, 11064-11074.

[Fit06]   P. Fita, P. Luzina, T. Dziembowska, Cz. Radzewicz, A. Grabowska, *J. Chem. Phys.* **2006**, *125*, 184508.

[Fog01]   P. Foggi, L. Bussotti, F. V. R. Neuwahl, *Int. J. Photoenergy* **2001**, *3*, 103-109.

[Gau09]   For all ab initio calculations the Gaussian 09 ab initio suite was employed: Gaussian 09, Revision A.02, M. J. Frisch, G. W. Trucks, H. B. Schlegel, G. E. Scuseria, M. A. Robb, J. R. Cheeseman, G. Scalmani, V. Barone, B. Mennucci, G. A. Petersson, H. Nakatsuji, M. Caricato, X. Li, H. P. Hratchian, A. F. Izmaylov, J. Bloino, G. Zheng, J. L. Sonnenberg, M. Hada, M. Ehara, K. Toyota, R. Fukuda, J. Hasegawa, M. Ishida, T. Nakajima, Y. Honda, O. Kitao, H. Nakai, T. Vreven, J. A. Montgomery, Jr., J. E. Peralta, F. Ogliaro, M. Bearpark, J. J. Heyd, E. Brothers, K. N. Kudin, V. N. Staroverov, R. Kobayashi, J. Normand, K. Raghavachari, A. Rendell, J. C. Burant, S. S. Iyengar, J. Tomasi, M. Cossi, N. Rega, J. M. Millam, M. Klene, J. E. Knox, J. B. Cross, V. Bakken, C. Adamo, J. Jaramillo, R. Gomperts, R. E. Stratmann, O. Yazyev, A. J. Austin, R. Cammi, C. Pomelli, J. W. Ochterski, R. L. Martin, K. Morokuma, V. G. Zakrzewski, G. A. Voth, P. Salvador, J. J. Dannenberg, S. Dapprich, A. D. Daniels, O. Farkas, J. B. Foresman, J. V. Ortiz, J. Cioslowski, and D. J. Fox, Gaussian, Inc., Wallingford CT, 2009.

[Goe54]   H. L. Goering, J. P. Blanchard, E. F. Silversmith, *J. Am. Chem. Soc.* **1954**, *76*, 5409−5418.

[Goe55]   (a) H. L. Goering, E. F. Silversmith, *J. Am. Chem. Soc.* **1955**, *77*, 1129−1133.

               (b) H. L. Goering, E. F. Silversmith, *J. Am. Chem. Soc.* **1955**, *77*, 6249−6253.

(c) H. L. Goering, T. D. Nevitt, E. F. Silversmith, *J. Am. Chem. Soc.* **1955**, *77*, 5026−5032.

[Goe60]   H. L. Goering, J. Takahashi Doi, *J. Am. Chem. Soc.* **1960**, *82*, 5850−5854.

[Goe62]   H. L. Goering, R. R. Josephson, *J. Am. Chem. Soc.* **1962**, *84*, 2779−2785.

[Goe71]   H. L. Goering, G. S. Koermer, E. C. Linsay, *J. Am. Chem. Soc.* **1971**, *93*, 1230−1234

[Goe78]   H. L. Goering, R. P. Anderson, *J. Am. Chem. Soc.* **1978**, *100*, 6469-6474

[Har03]   K. Hara, T. Sato, R. Katoh, A. Furube, Y. Ohga, A. Skinpo et al. *J. Phys. B* **2003**, *107*, 597-606.

[Har10]   P. H. P. Harbach, J. Borowka, M.-V. Bohnwagner, A. Dreuw, *J. Phys. Chem. Lett.* **2010**, *1*, 2556-2560.

[Hay89]   T. Hayashi, A. Yamamoto, Y. Oto, E. Nishioka, H. Miura, K. Yanagi, *JACS* **1989**, *111*, 6301-6311.

[Hee08]   L. R. Heeb, K. S. Peters, *JACS* **2008**, *130*, 1711-1717.

[Hen02]   N. E. Henriksen, *Chem. Soc. Rev.* **2002**, *31*, 37-42.

[Her11]   D. Herrmann, S. Niesar, C. Scharsich, A. Köhler, M. Stutzmann, E. Riedle, *JACS*, **2011**, *133*, 18220-18233.

[Hon11]   S. Honda, S. Yokoya, H. Ohkita, H. Benten, S. Ito, *J. Phys. Chem. C* **2011**, *115*, 11306-11317.

[Hor95]   M. L. Horng, J. A. Gardecki, A. Papazyan, M. Maroncelli, *J. Phys. Chem.* **1995**, *99*, 17311-17337.

[Hua05]   Z. Huang, *Technol. Cancer Res. Treat.* **2005**, *4*, 283-293.

[Hub01]   R. Huber, H. Satzger, W. Zinth, J. Wachtveitl, *Opt. Commun.* **2001**, *194*, 443-448.

[Ike88]   N. Ikeda, M. Koshioks, H. Masunara, *Chem. Phys. Lett.* **1988**, *150*, 452-456.

[Imr93]   C. Imrie, T. A. Modro, E. R. Rohwer, C. C. P. Wagener, *J. Org. Chem.* **1993**, *58*, 5643-5649.

[Jhn93]   L. J. Johnston, *Chem. Rev.* **1993**, *93*, 251-266.

[Joh03]   A. Johansson, M. K. Raarup, Z. S. Li, V. Lokhnygin, D. Descamps, C. Lynga et

al. *Eur. Phys. J. D*, **2003**, *22*, 3-11.

[Kao12]   Y.-T. Kao, X. Guo, Y. Yang, Z. Liu, A. Hassanali, Q.-H. Song, L. Wang, D.Zhong, *J. Phys. Chem. B*, **2012**, *116*, 9130-9140.

[Koh54]   R. Kohlrausch, *Annalen der Physik und Chemie* (Poggendorf). **1854**, *91*, 56-82, 179-213.

[Kov97]   S. A. Kovalenko, J. Ruthmann, N. P. Ernsting, *Chem. Phys. Lett.* **1997**, *271*, 40-50.

[Koz05]   I. Z. Kozma, P. Krok, E. Riedle*, J. Opt. Soc. Am. B* **2005**, *22*, 1479-1485.

[Koh95]   B. Kohler, J. L. Krause, F. Raksi, K. R. Wilson, V. V. Yakovlev, R. M. Whitnell et al. *Acc. Chem. Res*. **1995**, *28*, 133-140.

[Kut13]   Kutta, R.-J.; Langenbacher, T.; Kensy, U.; Dick, B. *Appl.Phys. B* **2013**, 111, 203.

[Kum08]   A. S. Kumar, T. Ye, T. Takami, B.-C. Yu, A. K. Flatt, J. M. Tour, P. S. Weiss, *Nano Lett.* **2008**, *8*, 1644-1648.

[Lak06]   J. R. Lakowicz, *Principles of Fluorescence Spectroscopy*, 3rd edition, Springer, Berlin, **2006**.

[Lei11]   A. M. Leifer, C. Fang-Yen, M. Gershow, M. J. Alkema, A. D. T. Samuel, *Nature Meth.*, **2011**, *1554*, 1-8.

[Let72]   V. S. Letokhov, *Chem.Phys. Lett* **1972**, *15*, 221-222.

[Lew98]   J. E. Lewis, M. Maroncelli, *Chem.Phys. Lett*, **1998**, *282*, 197-203.

[Li10]   J. Li, Z. Liu, C. Tan, X. Guo, L. Wang, A. Sancar, D. Zhong, **Nature**, **2010**, *466*, 887-891.

[Liu11]   K.-L. Liu, Y.-T. Chen, H.-H. Lin, C.-S. Hsu, H.-W. Chang, I-C. Chen, *J. Phys. Chem. C*, **2011**, *115*, 22578-22586.

[Loc00]   S. Lochbrunner, A. J. Wurzer, E. Riedle, *J. Chem. Phys.*, **2000**, *112*, 10699-10702.

[Lor02]   M. Lorenc, M. Ziolek, R. Naskrecki, J. Karolczak, J. Kubicki, A. Maciejewski, *Appl. Phys. B*, **2002**, *74*, 19-27.

[Lu07]   Q.-B. Lu, *J. Med. Chem.*, **2007**, *50*, 2601-2604.

[Mac00]   A .Maciejewski, R. Naskrecki, M. Lorenc, M. Ziolek, J. Karolczak, J. Kubicki et al. J. *Mol. Struct.* **2000**, *555*, 1-13.

[Mrc87]   M. Maroncelli, G. R. Fleming, *J. Chem. Phys.* **1987**, *86*, 6221-6239.

[Mar95]   M. M. Martin, P. Plaza, Y. H. Meyer, *Chem. Phys.*, **1995**, *192*, 367-377.

[Mat08]   J. M. Mativetsky, G. Pace, M. Elbing, M. A. Rampi, M. Mayor, P. Samori, *JACS*, **2008**, *130*, 9192-9193.

[May03]   H. Mayr, B. Kempf, A. R. Ofial, *Acc. Chem. Res.* **2003,** *36*, 66-77.

[Meg09]   U. Megerle, I. Pugliesi, C. Schriever, C. F. Sailer, E. Riedle, *Appl. Phys. B* **2009**, *96*, 215-231.

[Mey90]   M. Meyer, J.-C. Mialocq, B. Perly, *J. Phys. Chem.*, **1990**, *94*, 98-104.

[Mir98]   M. A. Miranda, J. Perez-Prieto, E. Font-Sanchis, K. Konya, J. C. Scaiano, *J. Phys. Chem. A*, **1998**, *102*, 5724-5727.

[Mir01]   M. A. Miranda, J. Perez-Prieto, E. Font-Sanchis, J. C. Scaiano, *Acc. Chem. Res.*, **2000**, *34*, 717-726.

[Mon08]   S. Monti, I. Manet, F. Manoli, G. Marconi, Phys. *Chem. Phys.*, **2008**, *10*, 6597-6606.

[Mus08]   R. Muszynski, B. Seger, P. V. Kamat*, J. Phys. Chem. C*, **2008,** *112*, 5263-5266.

[Näg97]   T. Nägele, R. Hoche, W. Zinth, J. Wachtveitl, *Chem. Phys. Lett.*, **1997**, *272*, 489-495.

[Nen10]   A. Nenov, T. Cordes, T. Herzog, W. Zinth, R. de Vivie-Riedle, *J. Phys. Chem.* **2010**, *114*, 13016-13030.

[Nen12]   A. Nenov, R. de Vivie-Riedle, *J. Chem. Phys.* **2012**, *137*, 074101.

[Nor04]   Y. Norikane, N. Tamaoki, *Org. Lett.*, **2004**, *6*, 2595-2598.

[OLS09]   S. Ombinda-Lemboumba, A. du Plessis, R. W. Sparrow, P. Molukanele, L. R. Botha, E. G. Rohwer et al. *S. Afr. J. Sci.*, **2009**, *105*, 376-386.

[Orz10]   Ł. Orzeł, A. Jańczyk, M. Brindell, G. Stopa, G. Stochel, *J. Coord. Chem.*, **2010**, *63*, 2695-2714.

[Pav74]   T. G. Pavlopoulos, P. R. Hammond, *JACS*, **1974**, *96*, 1974.

[Pen10]   P. Peng, B. Sadtler, A. P. Alivisatos, R. S. Saykally, *J. Phys. Chem. C*, **2010**,

114, 5879-5885.

[Pet94]   K. S. Peters, B. Li, *J. Phys. Chem.*, **1994**, *98,* 401-403.

[Pet07]   K. S. Peters, *Chem. Rev.*, **2007**, *107*, 859-873.

[Pom95]   S. Pommeret, T. Gustavsson, R. Naskrecki, G. Baldacchino, J.-C. Mialocq, *J. Mol. Liq.*, **1995**, *64*, 101-112.

[Pri96]   J. Perez-Prieto, M. A. Miranda, E. Font-Sanchis, K. Konya, J. C. Scaiano, *Tetrahedron Lett.*, **1996**, *37*, 4923-4926.

[Pug10]   I. Pugliesi, P. Krok, S. Lochbrunner, A. Błaszczyk, C. von Hänisch, M. Mayor, E. Riedle, *J. Phys. Chem.* **2010**, *114*, 12555-12560.

[Rau82]   H. Rau, E. Lüddecke, *JACS*, **1982**, *104*, 1616-1620.

[Rus10]   M.-M. Russew, S. Hecht, *Adv. Mater.* **2010**, *22*, 3348-3360.

[Sah92]   M. R. V. Sahyun, D. K. Sharma, *Chem. Phys. Lett.* **1992**, *189*, 571-576.

[Sai11a]   C. F. Sailer, R. B. Singh, J. Ammer, E. Riedle, I. Pugliesi, *Chem. Phys. Lett.* **2011**, *512*, 60-65..

[Sai13a]   C. F. Sailer, S. Thallmair, B. P. Fingerhut, C. Nolte, J. Ammer, H. Mayr, I. Pugliesi, R. de Vivie-Riedle, E. Riedle, *Chem.Phys.Chem.* **2013**, *14*, 1423–1437.

[Sai13b]   C. F. Sailer, E. Riedle, *Pure Appl. Chem.* **2013**, *85*, 1487–1498.

[Sai13c]   C. F. Sailer, N. Krebs, B. P. Fingerhut, R. de Vivie-Riedle, E. Riedle, *Wavepacket Splitting in the First 100 fs Determines the Products from the Bond Cleavage of Diphenylmethylchloride*. Proceedings of the XVIIIth International Conference on Ultrafast Phenomena, Lausanne, Switzerland. *EPJ Web of Conferences* **2013**, *41*, 05042

[San 05]   M. M. Berberan-Santos, E. N. Bodunov, B. Valeur, *Chem. Phys.* **2005**, *315*, 171-182.

[Scf90]   F. P. Schäfer, *Dye lasers*, 3rd enlarged and rev. ed., Springer, Berlin, Heidelberg, **1990.**

[Sch08]   H. F. Schaller, H. Mayr, *Angew. Chem. Int. Ed.* **2008**, *47*, 3958-3961.

[Schr09]   W. J. Schreier, J. Kubon, N. Regner, K. Haiser, T. E. Schrader, W. Zinth et al.

JACS, **2009**, *131*, 5038-5039.

[Sha88]   M. Shapiro, *Ultrashort laser pulses*, Springer, Berlin, **1988**.

[Sha97]   M. Shapiro, P. Brumer, *J. Chem. Soc. Faraday Trans.*, **1997**, *93*, 1263-1277.

[Sie09]   R. Siewertsen, H. Neumann, B. Buchheim-Stehn, R. Herges, C. Näther, F. Renth et al. *JACS*, **2009**, *131*, 15594-15595.

[Sin02]   T. Singer, *Synthese und Reaktivität von 1,3-Diarylallylkationen*, diploma thesis, Ludwig-Maximilians-Universität München, **2002**.

[Sta09]   A. D. Stahl, M. Di Donato, I. van Stokkum, R. Van Groedelle, M. L. Groot, *Biophys. J.*, **2009**, *97*, 3215-3223.

[Stc12]   P. Stacko, P. Sebej, A. T. Veetil, P. Klan, *Org. Lett.*, **2012**, *14*, 4918-4921.

[Sto04]   I. van Stokkum, D. S. Larssen R. van Groedelle, M. L. Groot, *Biochim et Biophys. Acta*, **2004**, *1657*, 82-104.

[Szo07]   S. Szobota, P. Gorositza, F. Del Bene, C. Wyart, D. I. Fortin, K. D. Kolstad et al. *Neuron*, **2007**, *54*, 535-545.

[Szo10]   S. Szobota, E. Y. Isacoff, *Annu. Rev.Biophys.*, **2010**, *39*, 329-348.

[Tho91]   N. C Thomas*, J. Chem. Ed.*, **1991**, *68*, 631-634.

[Tro11]   K. Troshin, C. Schindele, H. Mayr, *J. Org. Chem.*, **2011**, *76*, 9301-9408.

[Tro13a]   K. Troshin, H. Mayr, *J. Org. Chem.* **2013**, *78*, 2649-2660.

[Tro13b]   K. Troshin, H. Mayr, *J. Am. Chem. Soc.* **2013**, *135*, 252-265.

[Ujj98]   L. Ujj, S. Devanathan, T. E. Meyer, M. A. Cusanovich, G. Tollin, G. H. Atkinson, *Biophys. J.*, **1998**, *75*, 406-412.

[Wac96]   J. Wachtweitl, T. Nägele, B. Puell, W. Zinth, M. Krüger, S. Rudolph-Böhner et al. *J. Photochem. Photobiol A*, **1996**, *105*, 283-288.

[Wac11]   J. Wachtveitl, A. Zumbusch, *Chem. Bio. Chem.*, **2011**, *12*, 1169-1170.

[Wei08]   A. Weigel, A. L. Dobryakov, M. Veiga, J. L. P. Lustres, *J. Phys. Chem.*, **2008**, *112*, 12054-12065.

[Wen10]   M. Wenninger, *Spektroskopische Charakterisierung der ultraschnellen Reaktionsmechanismen flavinbasierter Photochemie*, diploma thesis, Ludwig-Maximilians-Universität München, **2010**.

[Wil70]   G. Williams, D. C. Watts, *Trans. Farad. Soc.*, **1970**, *66*, 80-85.

[Yel09]   C. S. Yelleswarapu, Y. Chu, B. R. Kimball, D. V. G. L. N. Rao, *Opt. Commun.* **2009**, *282*, 2259-2262.

[Zar98]   R. N. Zare, *Science*, **1998**, *279*, 1875-1879.

[Zew80]   A. H. Zewail, *Physics today*, **1980**, *33*, 1-8.

[Zew00]   A. H. Zewail, *J. Phys. Chem. A*, **2000**, *104*, 5660-5694.

[Zin11]   W. Zinth, A. Laubereau, W. Kaiser, *Eur. Phys. J. H*., **2011,** *36*, 153-181.

Appendix A: photos of the home-built transient absorption spectrometer

Figure A1: Regenerative Ti:Sa amplifier system (CPA 2001; Clark MXR) (top), tunable Nd:YAG laser system (NT242; EKSPLA) (bottom).
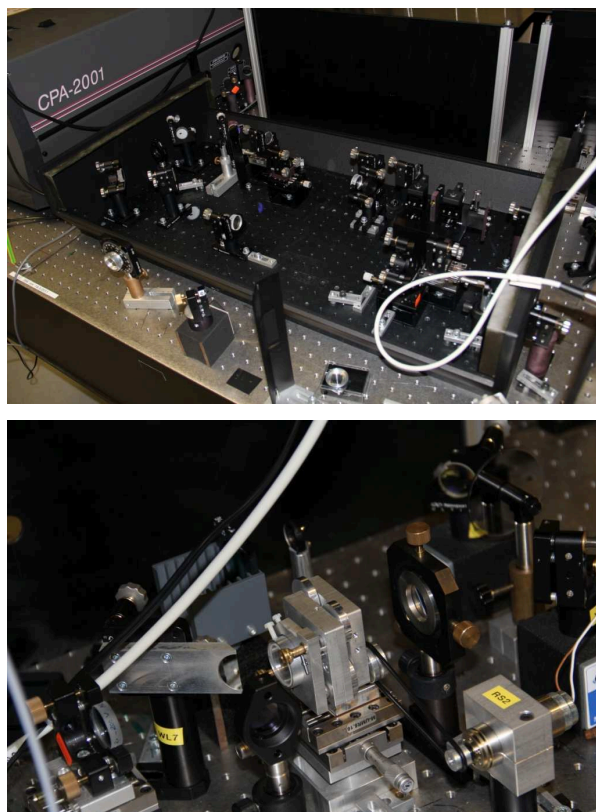
Figure A2: The two-stage NOPA (top), CaF2 white light stage (bottom).
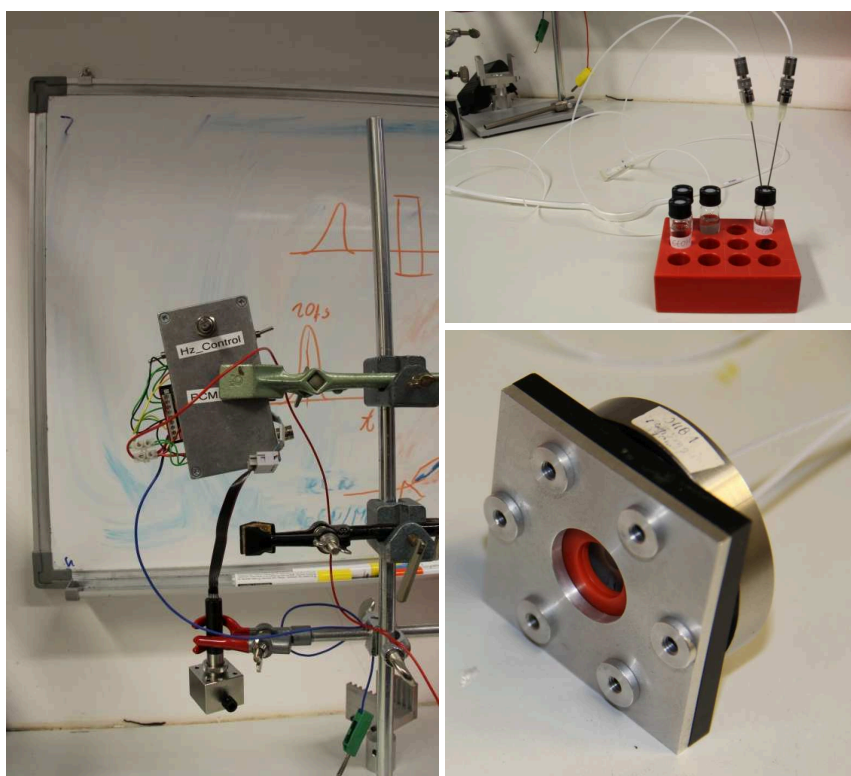
Figure A3: The micro annular gear pump mzr-2921-M2 controller (left), the sample flask with needles equipped with the standard catheter connectors (right top), the flow cell with 200-µm windows and 110-µm spacer.
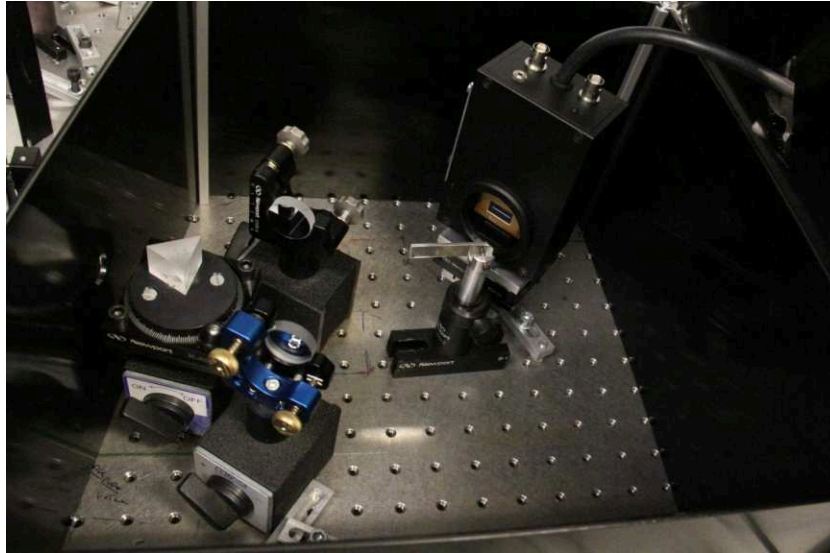
Figure A4: The prism-based polychromator coupled to a CCD-based detector (Entwick-lungsbüro Stresing).

Appendix B: spectral data for some laser dyes

In this appendix the spectral data for some laser dyes is presented. Every picture has the following structure: the selected transient absorption spectra in the top and the stationary absorption spectra (taken from [Bra00]) under the transient spectra (measured by Peter Lang). Vertical lines are plotted for a better overlap of the wavelength scales.
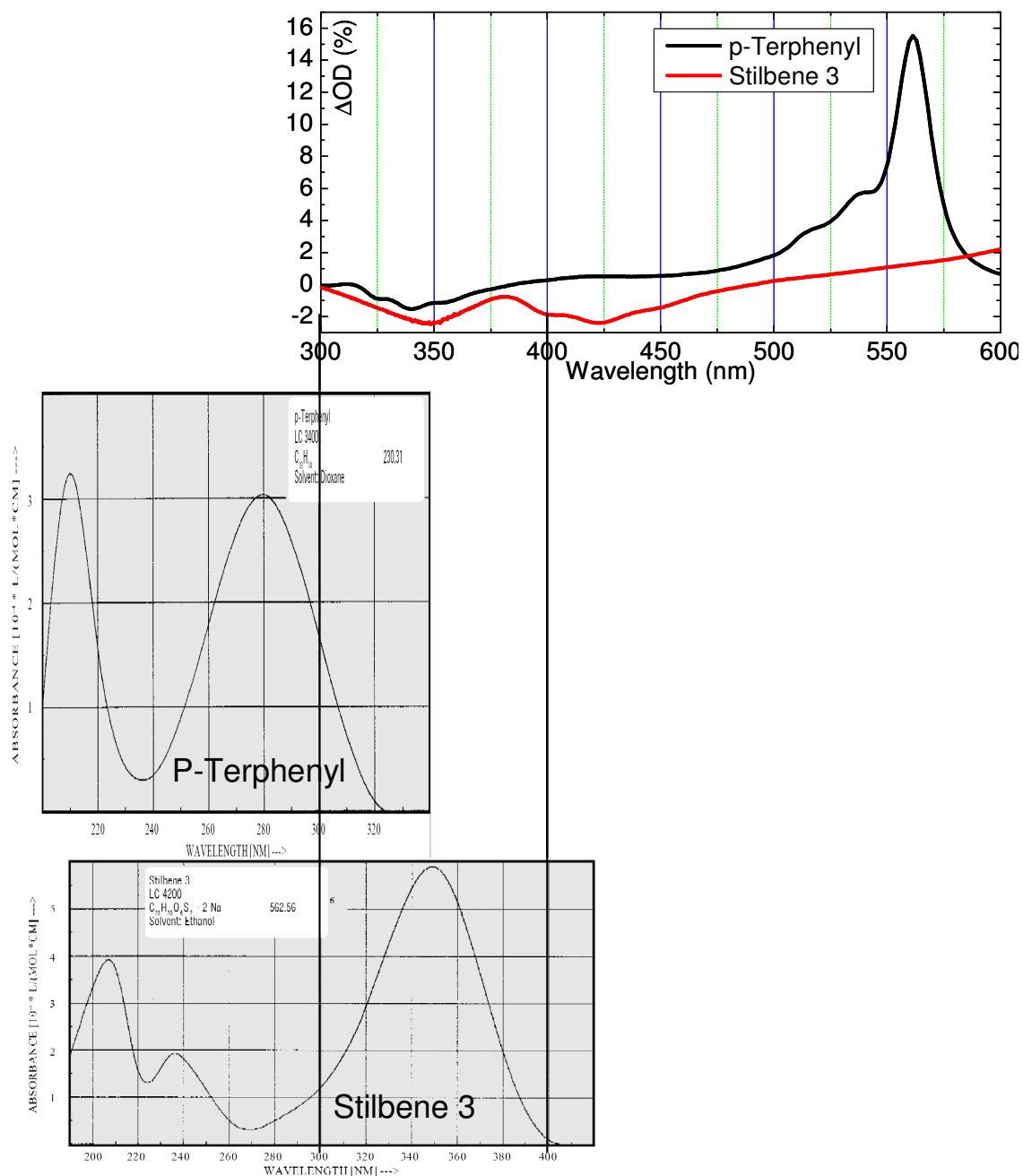
Figure B1: Transient absorption spectra from the experiment (top) and stationary absorption spectra (bottom) of p-terphenyl and stilbene 3 laser dyes.
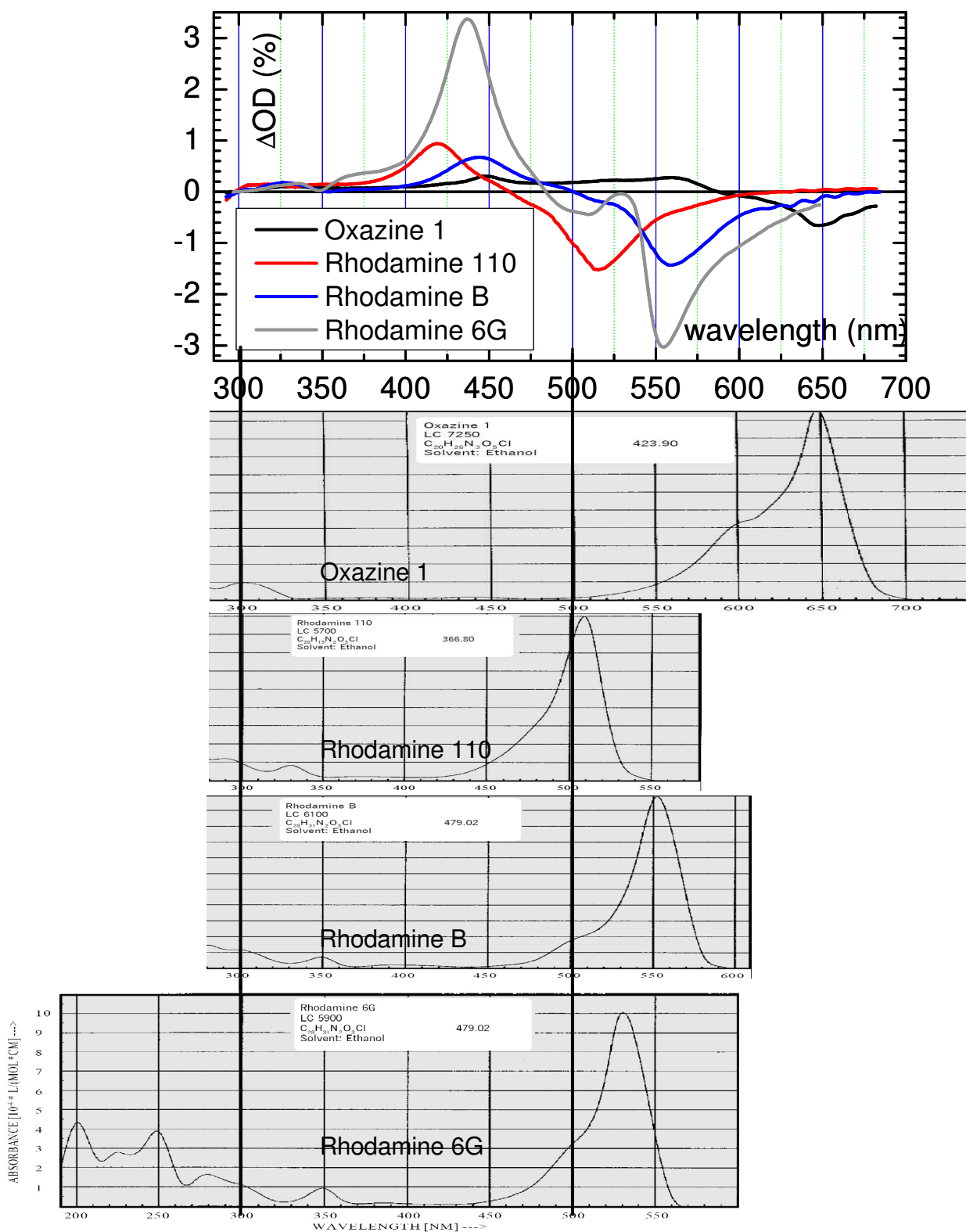
Figure B2: Transient absorption spectra from the experiment (top) and stationary absorption spectra (bottom) of oxazine 1 and some rhodamine laser dyes.
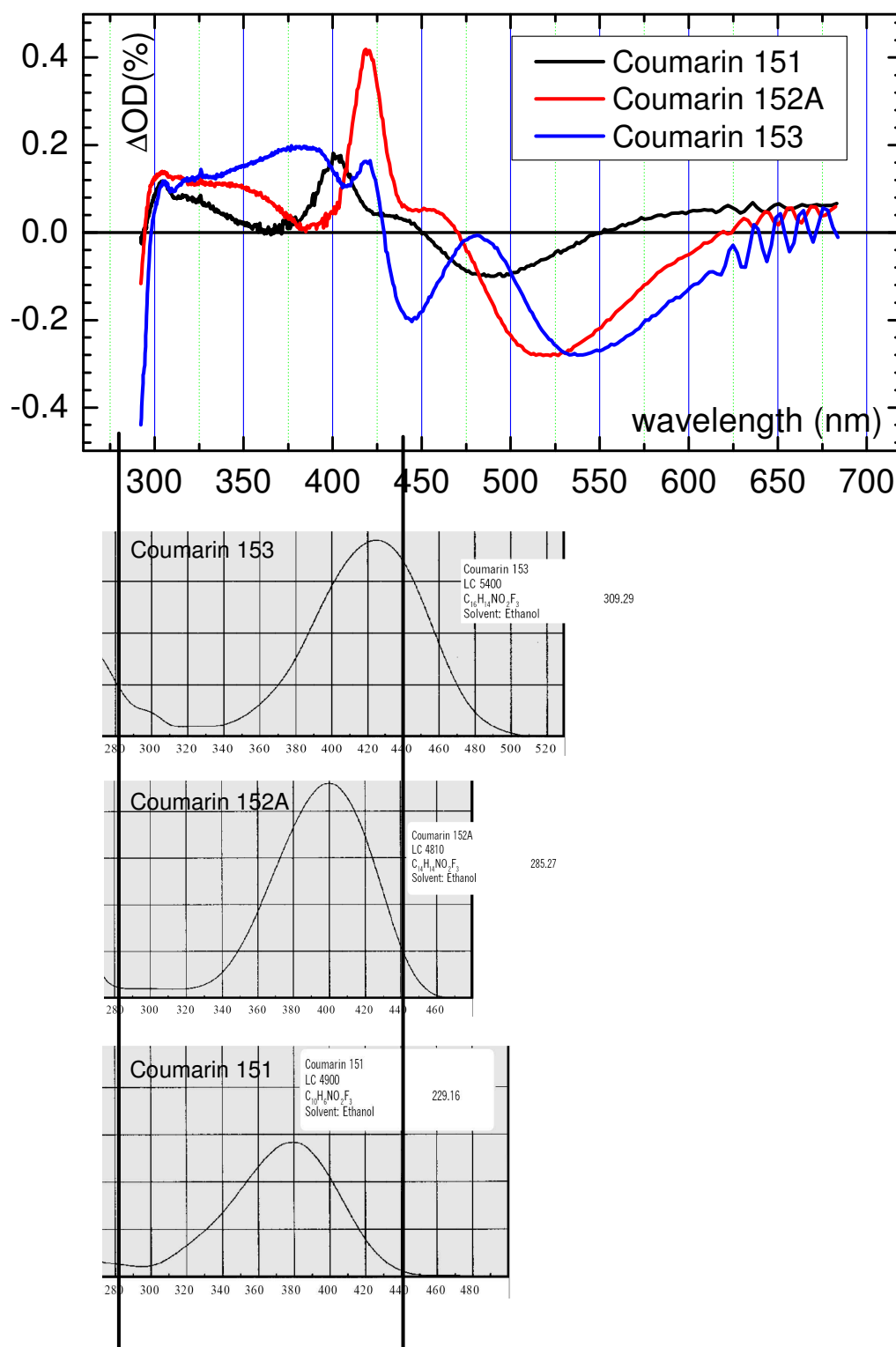
Figure B3: Transient absorption spectra from the experiment (top) and stationary absorption spectra (bottom) of some coumarin laser dyes.
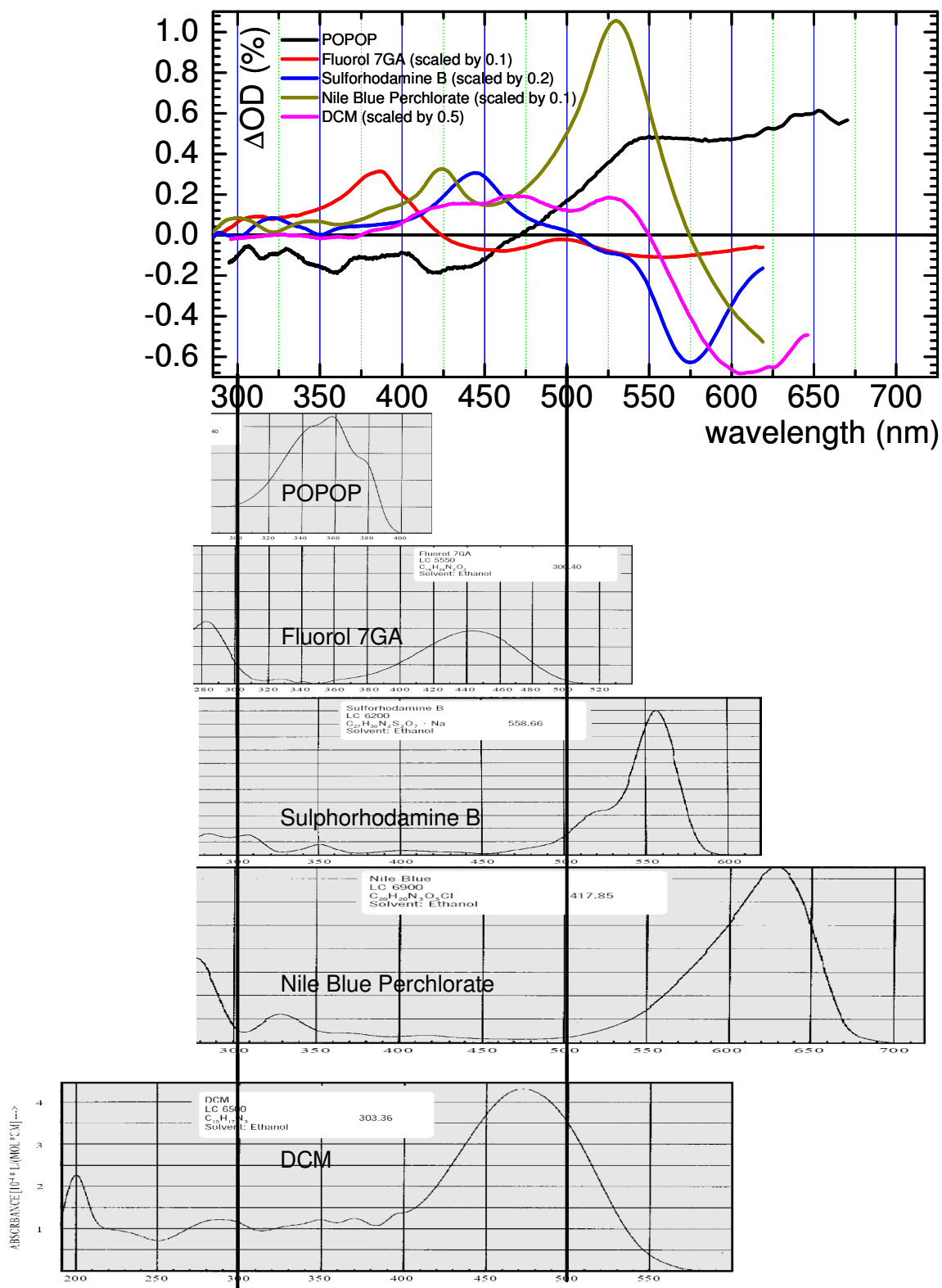
Figure B4: Transient absorption spectra from the experiment (top) and stationary absorption spectra (bottom) of POPOP, fluorol 7GA, sulforhodamine B, Nile Blue Perchlorate and DCM laser dyes.

Appendix C: stationary and transient absorption investigation of the parasitic photooligomerization process

If we look at the stationary absorption spectrum of 1(HH)-Cl, a small spectral feature in the form of a relatively long (50 nm) structureless band centered at 325 nm can be noticed.

Later it was noticed that the solution of 1(HH)-Cl in acetonitrile or dichloromethane changes its color from transparent to light yellow (Fig. C1) with the simultaneous increase of the extinction in 325-nm band after the irradiation of the sample during the measurement.
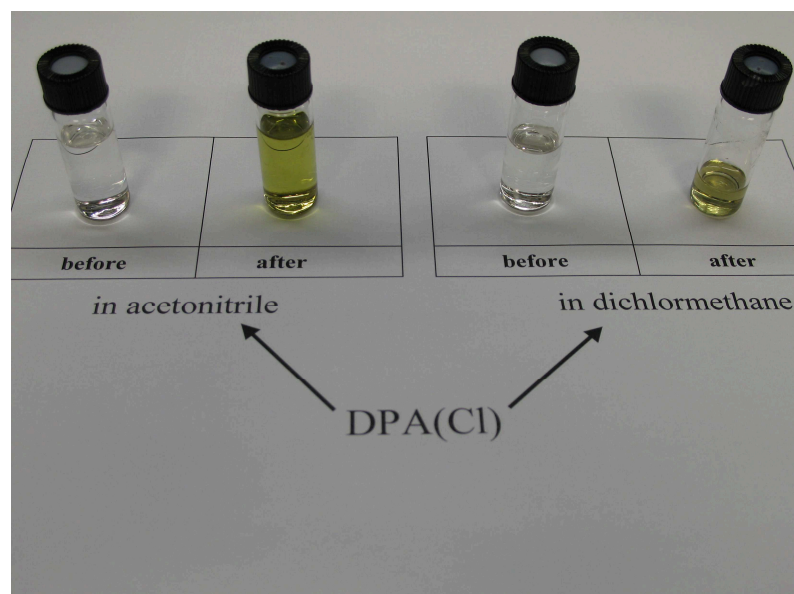
Figure C1: The color change of the 1(HH)-Cl solution observed after the irradiation at 261 nm during the TA experiment.

In order to analyze the nature of the band, the following experiment was conducted: the solution of 1(HH)-Cl in acetonitrile was irradiated during 10 hours in the 120-µm flow cell used for the TA experiments. The irradiation wavelength was 325 nm (the centre of the unknown band) and the energy was 400 nJ. After this time the sample was analyzed with stationary absorption and NMR-spectroscopy which yielded the following results:

- The absorption of the 1(HH)-Cl band decreases with the simultaneous increase of the 325-nm band (Figure C2).
- The completely new band centered at 360 nm, arises (Figure C2).

- The NMR-analysis yielded the spectra almost identical to the NMR-spectra of polystyrene (Figure C3).

Thus, the following conclusion was drawn: the 325-nm band originates from the absorption of the dimer molecule (formed from allyl radicals obtained due the photoinduced bond cleavage). The band centered at 360 nm originates from the oligomer absorption (formed from the dimer precursors during the irradiation with the UV radiation).
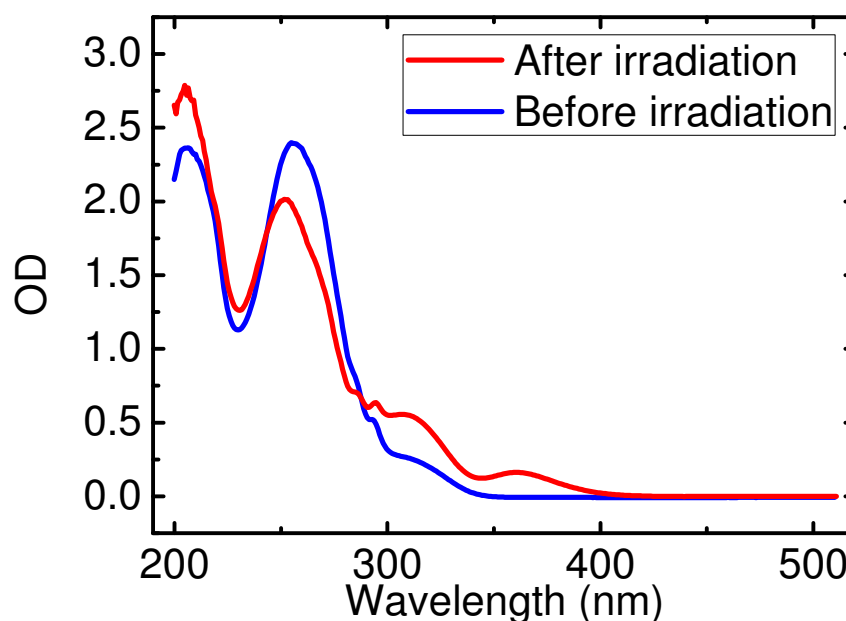
Figure C2: The stationary absorption spectra of 1(HH)-Cl before and after 10-hour irradiation with UV laser beam (325 nm, 400 nJ).

In order to test if the 325-nm band really originates from the dimer, the TA measurement (excitation wavelength: 325 nm) was conducted. The resulting spectra (see Figure C4) did not demonstrate similarity to the spectra of 1(HH)-Cl excited at the middle of its absorption band (see Fig. D1). In contradiction to 1(HH)-Cl transient spectra, only one quite broad band centered at 363 nm was present. This band can be identified as the ESA band of the 1(HH)-Cl dimer. The single-channel fit yields the following results: the major part of the dimer signal decays with the 3 ps time, and the rest exists for much longer time. These long-lived dimer species signals can overlap with the radical signal (at 361 nm), creating the second decay time of 98 μs, observed in the nanosecond TA experiment of 1(HH)-Cl in acetonitrile.

Therefore, the competing parasitic reaction channel was discovered. Since the TA signals of

the oligomer products overlap with the signal of the radical, it can make the interpretation of the radical signal more complicated.

Figure C3: The NMR-spectra of the irradiated 1(HH)-Cl in acetonitrile (left) and of the iso-tactic polystyrene in tetrachloroethylene (right, adapted from F. A. Bovey, F. P. Hood III, E. W. Anderson, L. C. Snyder, *J. Chem. Phys.* **1965**, *42*, 3900-3910).
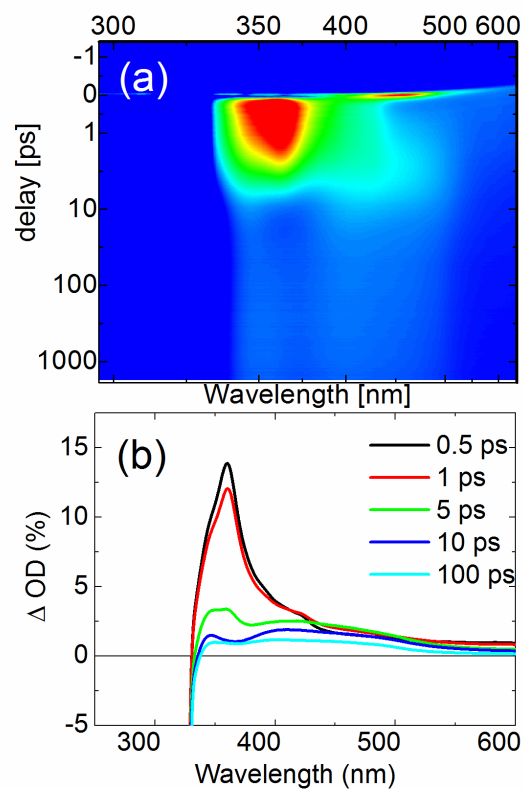
Figure C4: False color representation of the transient data and transient spectra of the transient data (a) and selected transients (b) of the oligomer band of 1(HH)-Cl in CH$_3$CN, fs-ps experiment (325 nm excitation).

Appendix D: Transient absorption spectra for all investigated diphenylallyl and diarylallyl systems

As the excitation energies between the femtosecond and nanosecond UV/Vis experiments are different and the false color representations of the transient data have been chosen to clearly visualize spectral features, the false color scales are not comparable to each other.
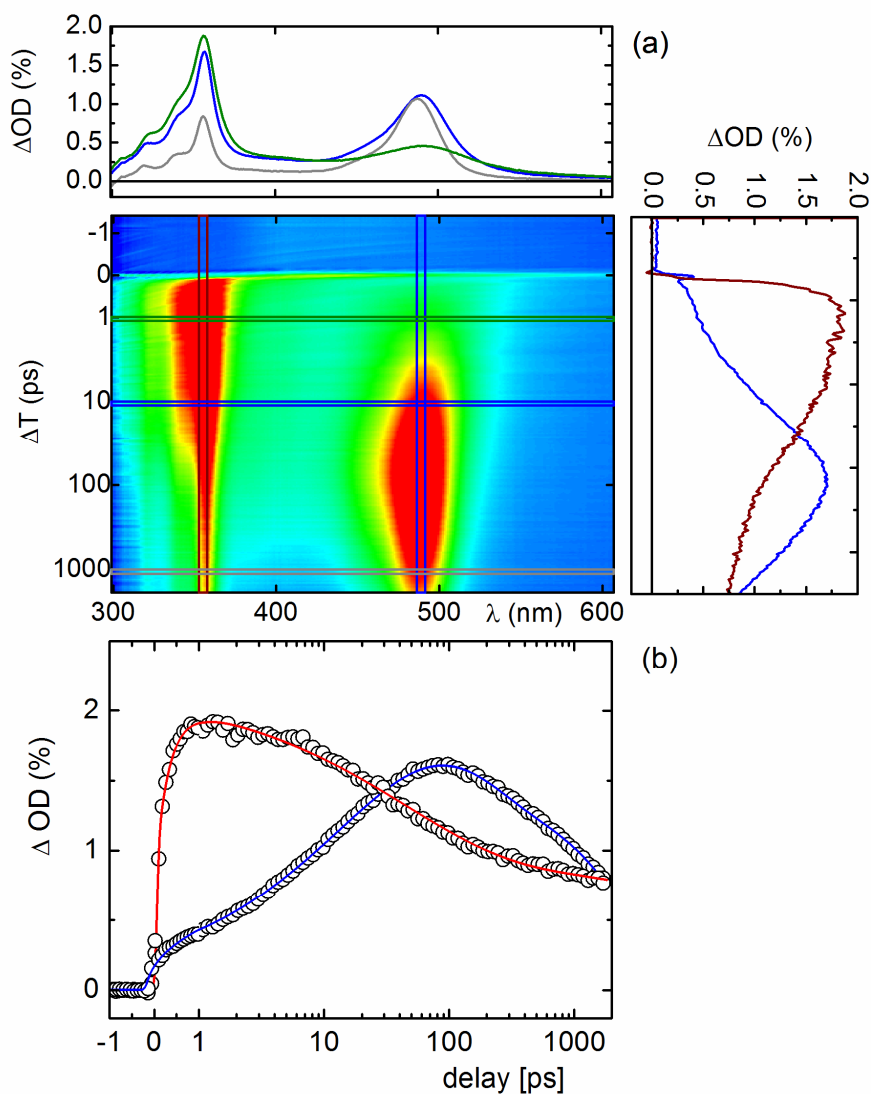
Figure D1: Transient spectra, false color representation of the transient data (a) and time traces (b) of radical (red) and cation (blue) of 1(HH)-Cl in CH_3CN, fs-ps experiment (261 nm excitation).
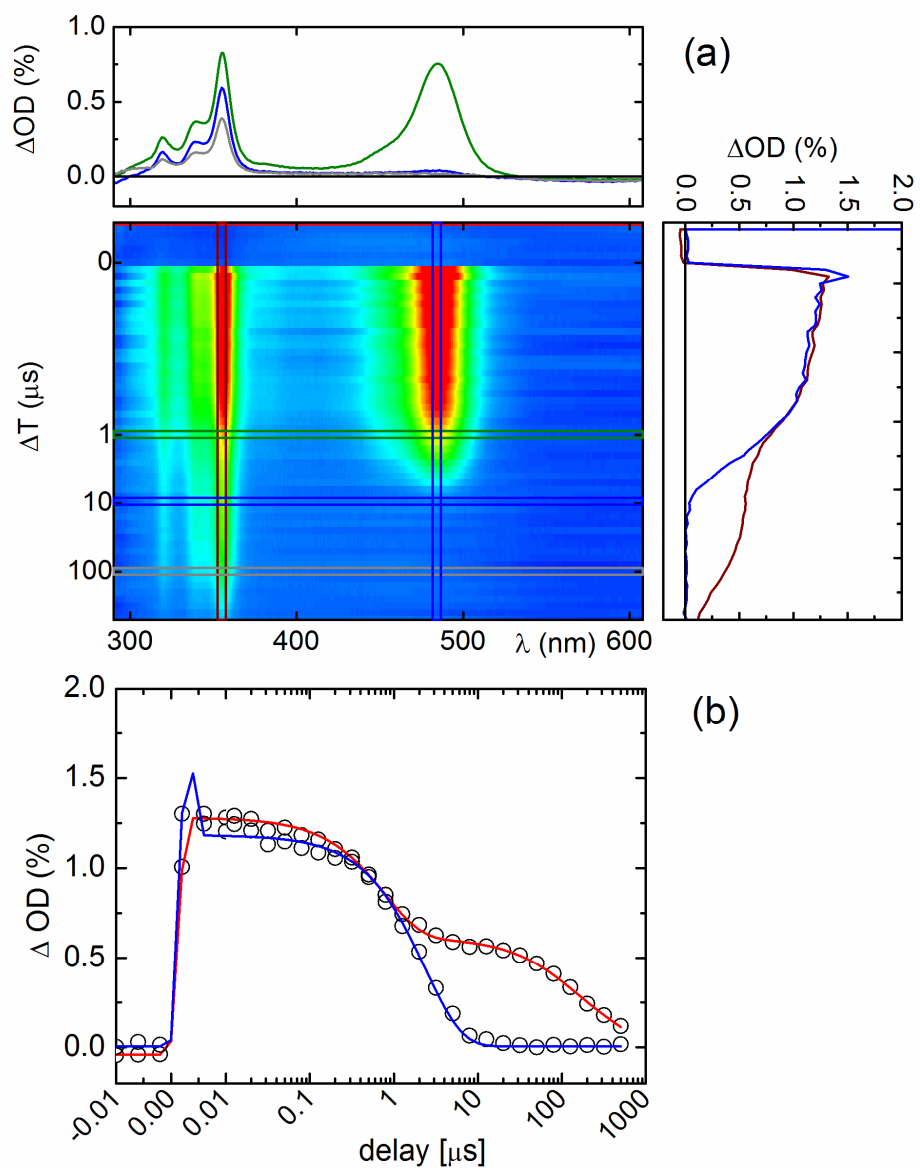
Figure D2: Transient spectra, false color representation of the transient data (a) and time traces (b) of radical (red) and cation (blue) of 1(HH)-Cl in CH_3CN, ns-μs experiment (261 nm excitation).
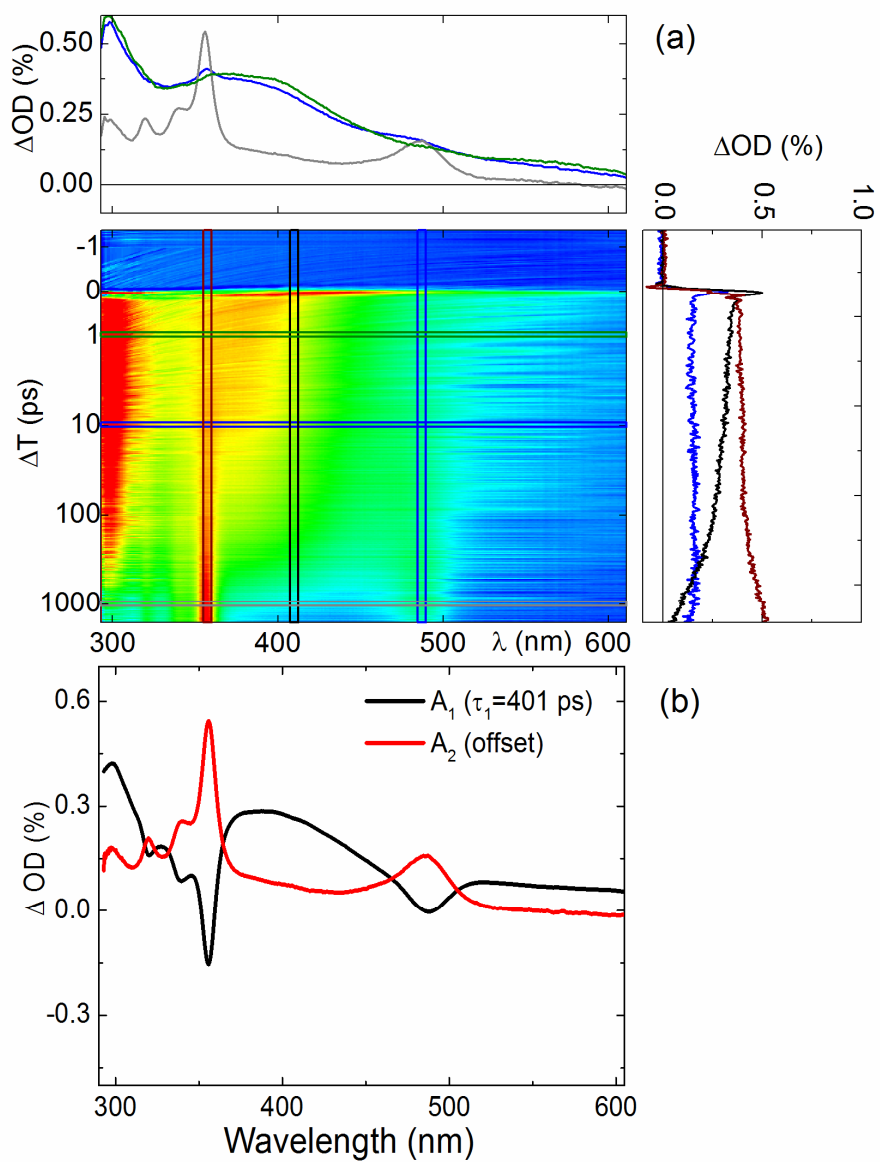
Figure D3: Transient spectra, false color representation of the transient data (a) and global fit (b) of radical and cation bands of 1(HH)-OAc in CH_3CN, fs-ps experiment (261 nm excitation).
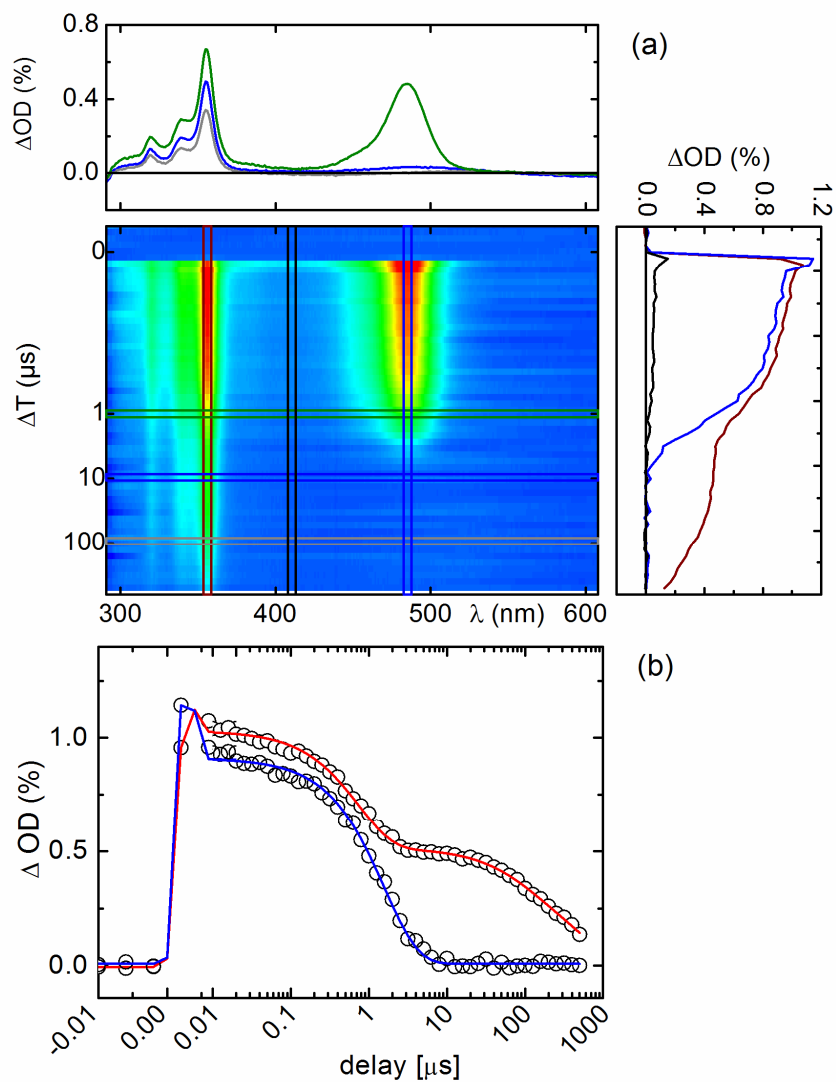
Figure D4: Transient spectra, false color representation of the transient data (a) and time traces (b) of radical (red) and cation (blue) of 1(HH)-OAc in CH$_3$CN, ns-μs experiment (261 nm excitation).
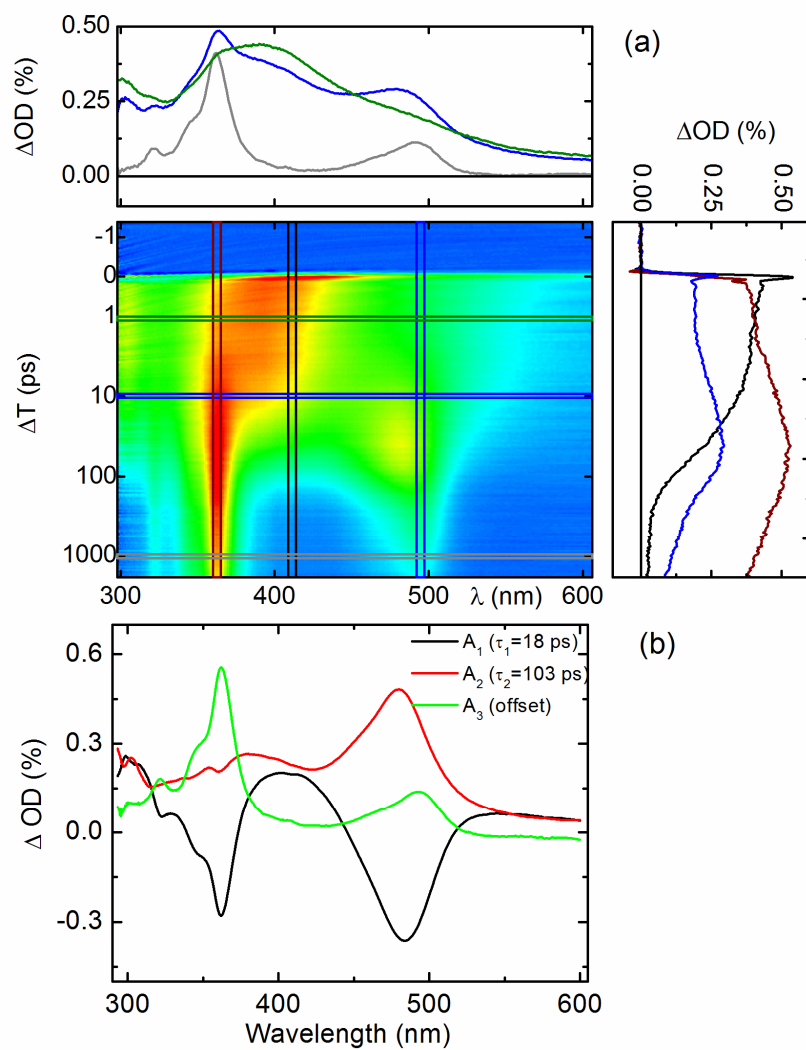
Figure D5: Transient spectra, false color representation of the transient data (a) and global fit (b) of radical and cation bands of 1(MeFF)-OAc in CH$_3$CN, fs-ps experiment (261 nm excitation).
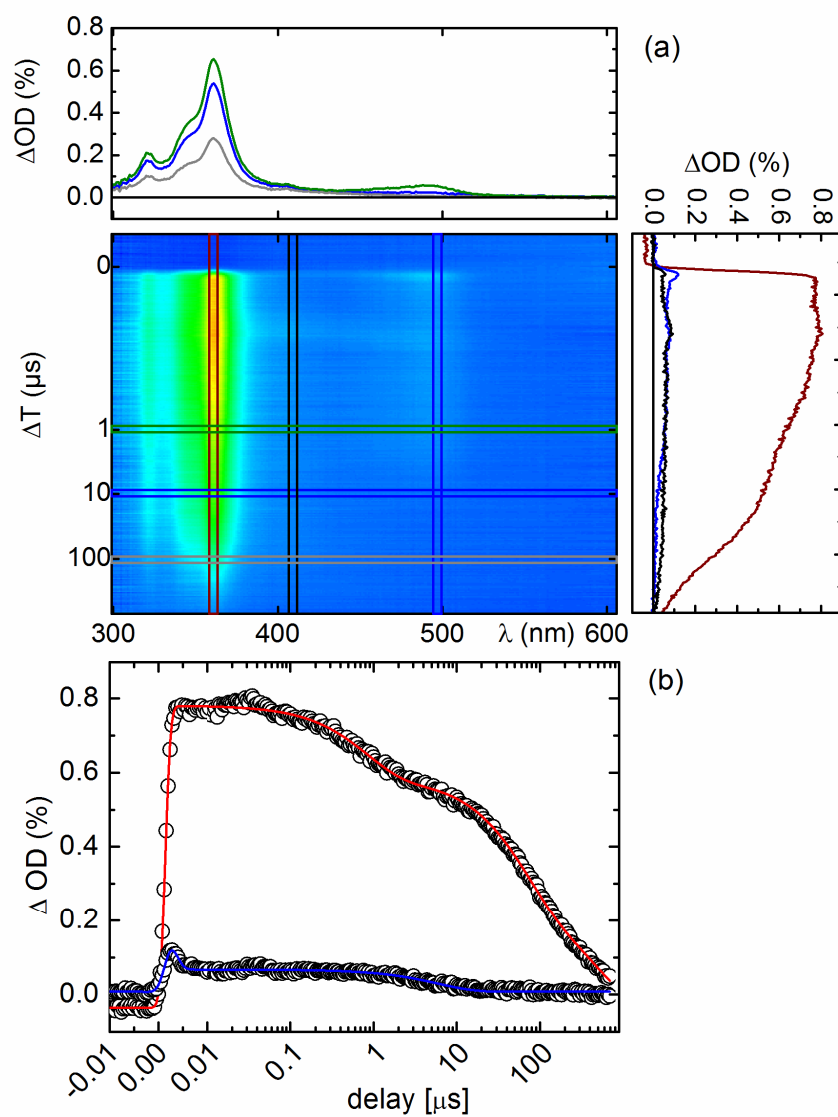
Figure D6: Transient spectra, false color representation of the transient data (a) and time traces (b) of radical (red) and cation (blue) of 1(MeFF)-OAc in CH$_3$CN, ns-μs experiment (261 nm excitation).
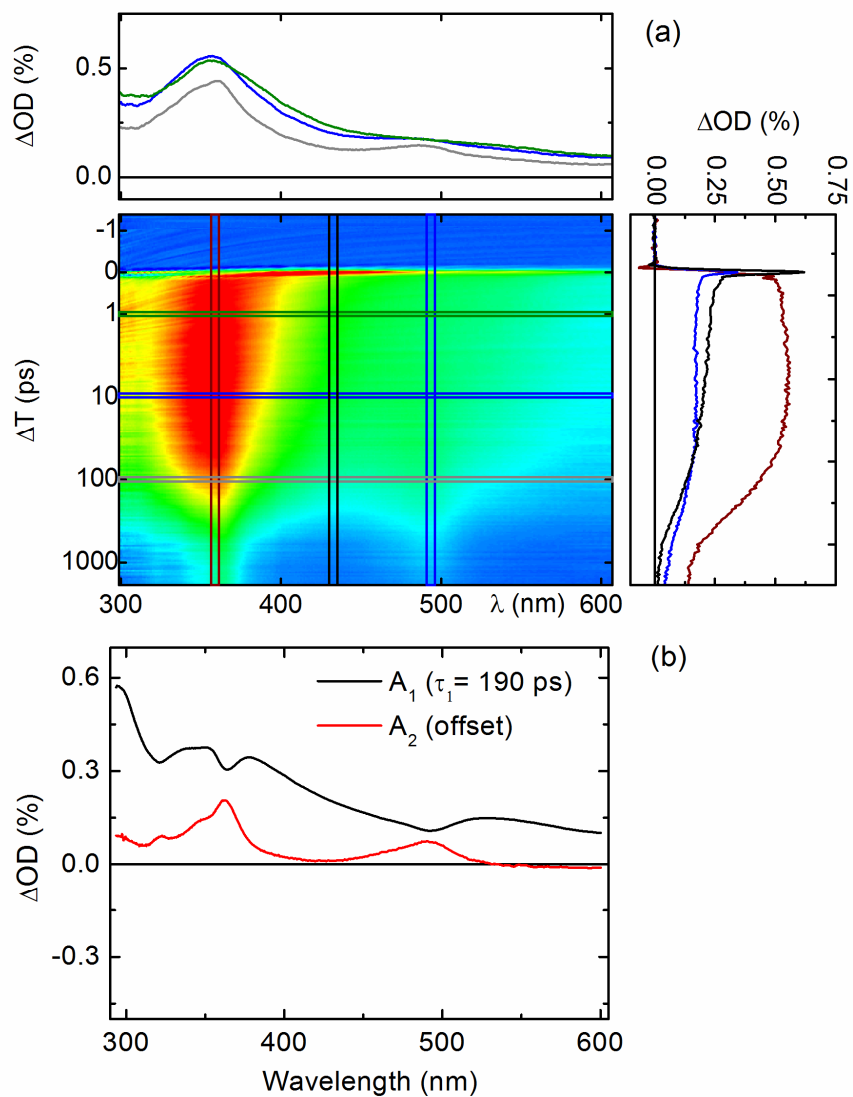
Figure D7: Transient spectra, false color representation of the transient data (a) and global fit (b) of radical and cation bands of 1(FFMe)-OAc in CH_3CN, fs-ps experiment (261 nm excitation).
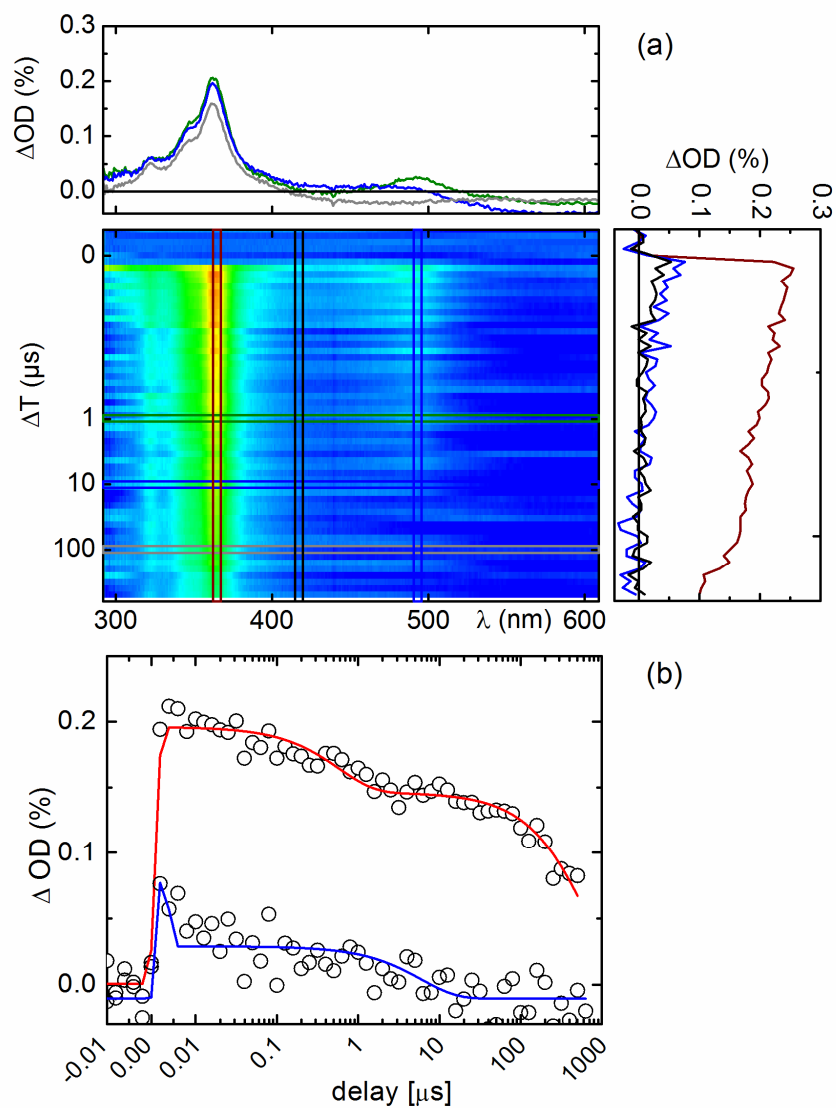
Figure D8: Transient spectra, false color representation of the transient data and time traces (b) of radical (red) and cation (blue) of 1(FFMe)-OAc in CH_3CN, ns-μs experiment (261 nm excitation).
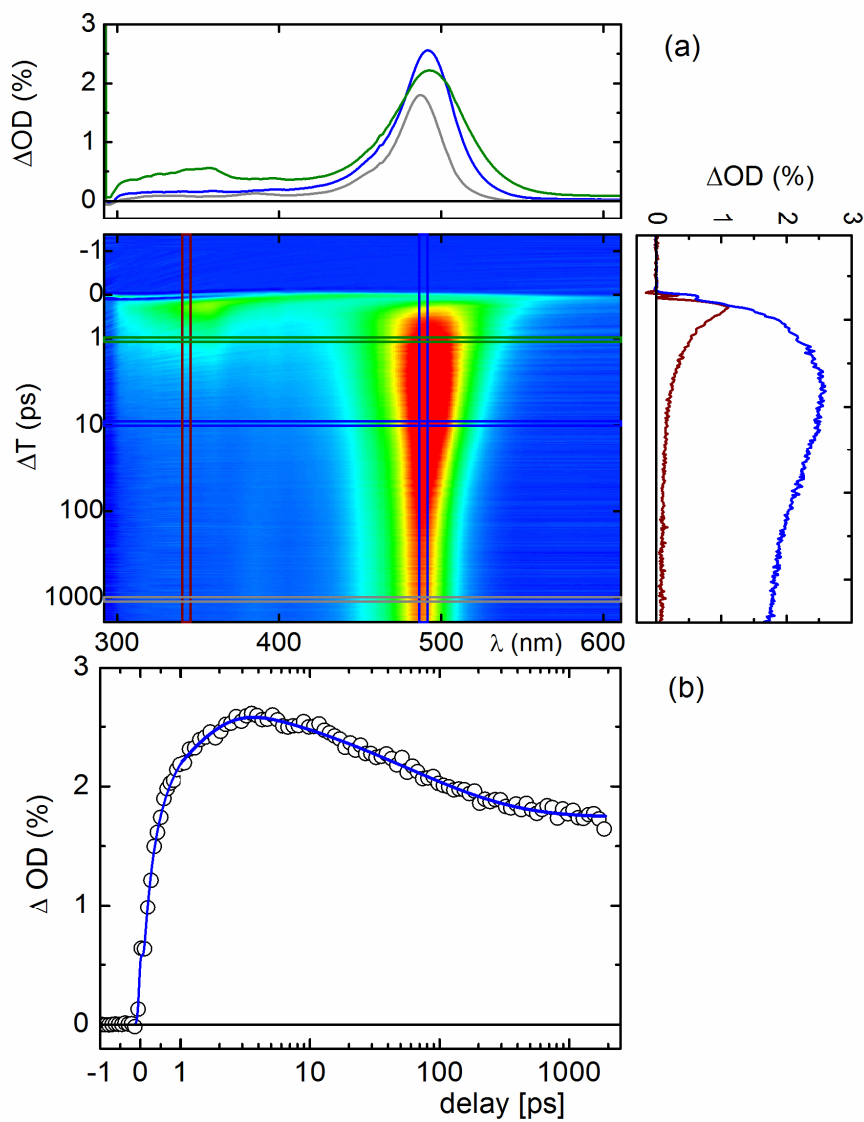
Figure D9: Transient spectra, false color representation of the transient data (a) and time trace (b) of cation band of 1(HH)-PPh$_3$BF$_4$ in CH$_3$CN, fs-ps experiment (270 nm excitation).
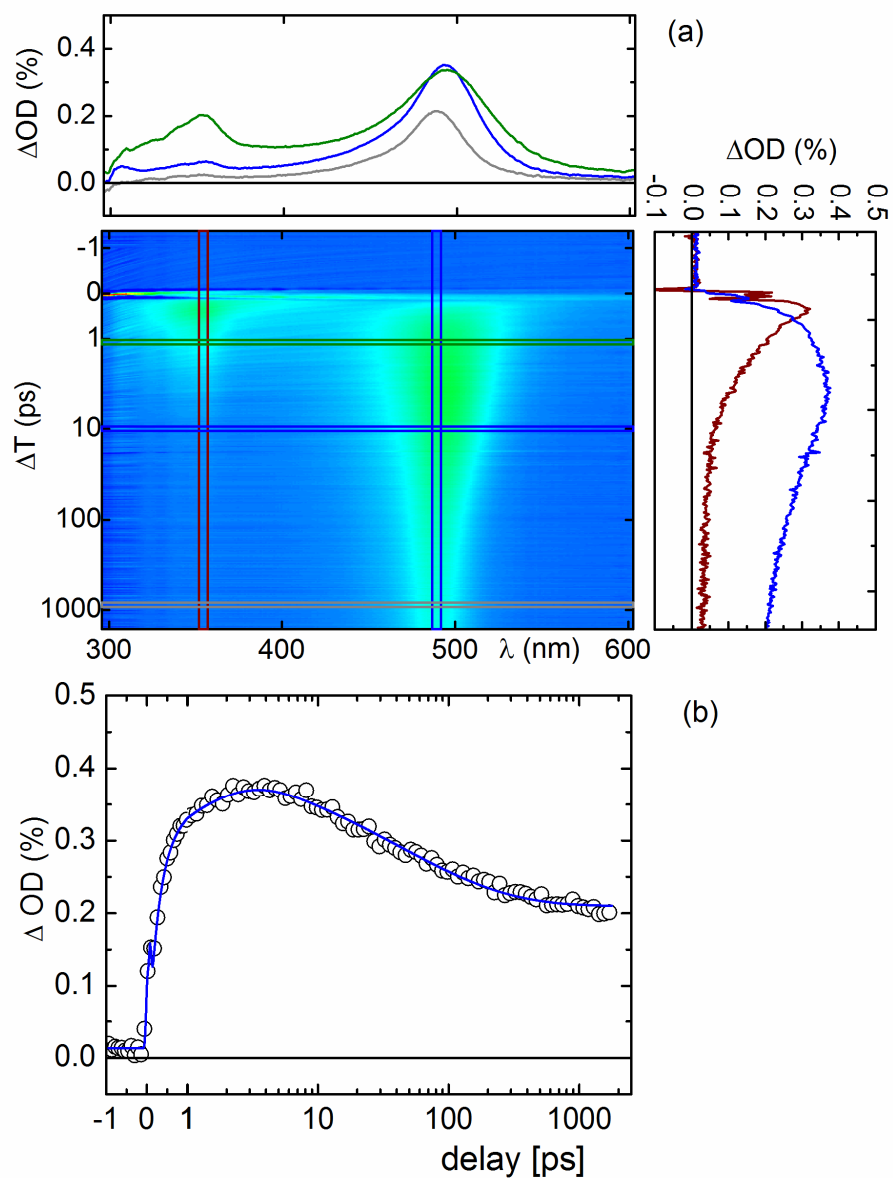
Figure D10: Transient spectra, false color representation of the transient data (a) and time trace (b) of cation band of 1(FF)-PPh$_3$BF$_4$ in CH$_3$CN, fs-ps experiment (270 nm excitation).
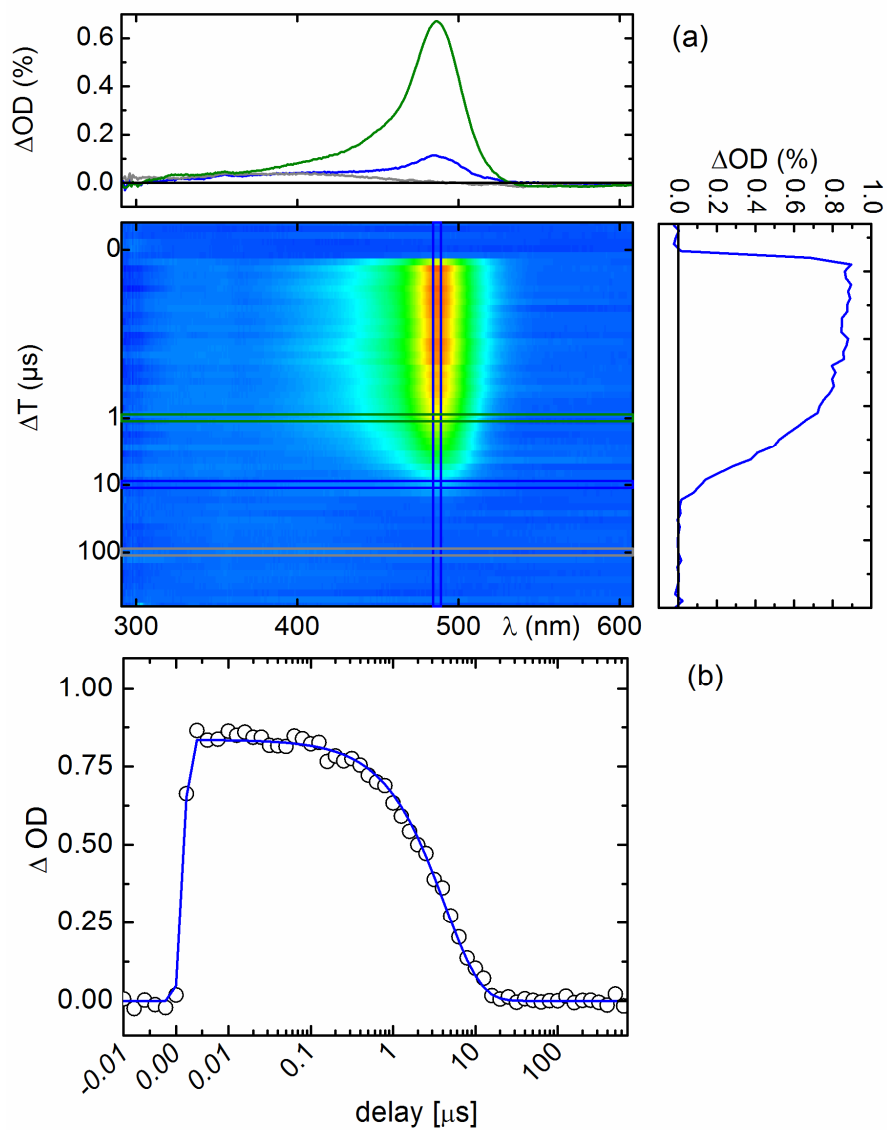
Figure D11: Transient spectra, false color representation of the transient data (a) and time trace of cation band (b) of 1(FF)-PPh$_3$BF$_4$ in CH$_3$CN, ns-µs experiment (270 nm excitation).
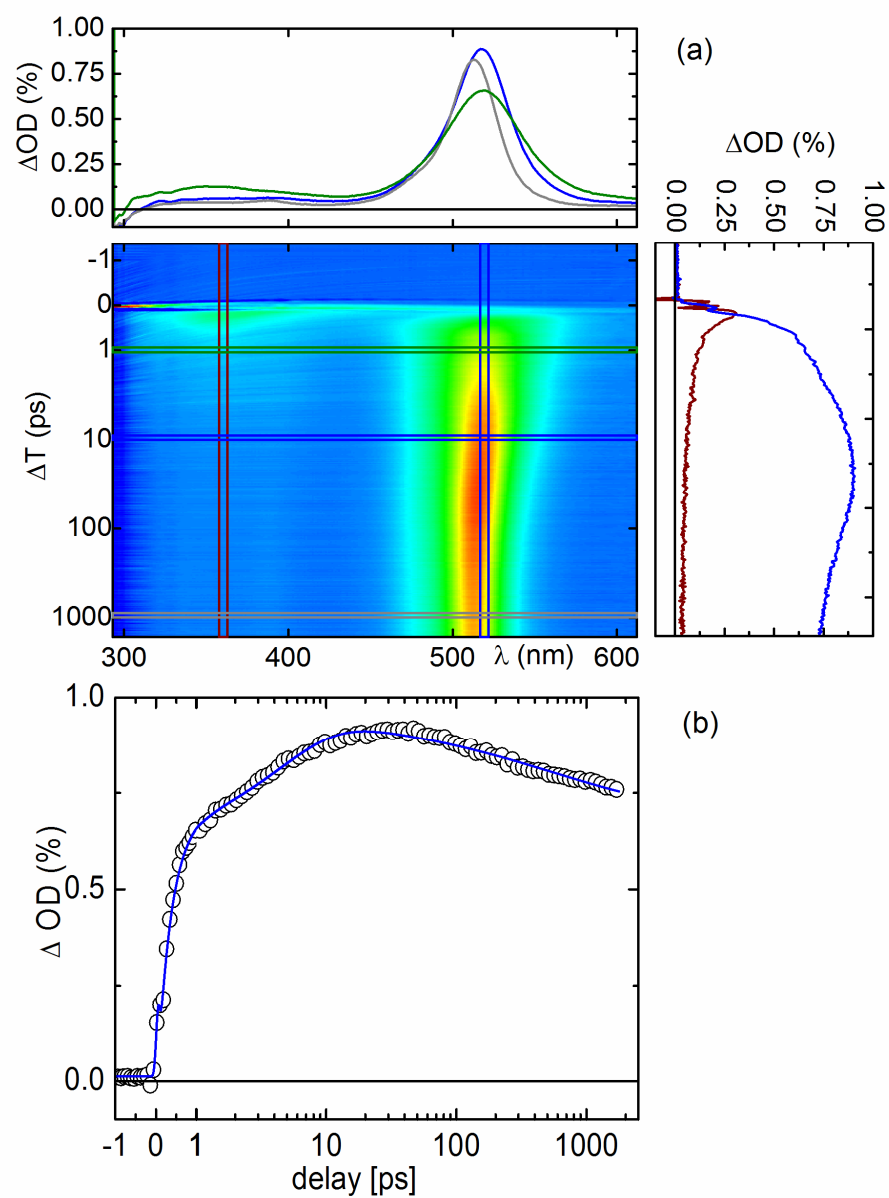
Figure D12: Transient spectra, false color representation of the transient data (a) and time trace (b) of cation band of 1(MeMe)-PPh$_3$BF$_4$ in CH$_3$CN, fs-ps experiment (270 nm excitation).
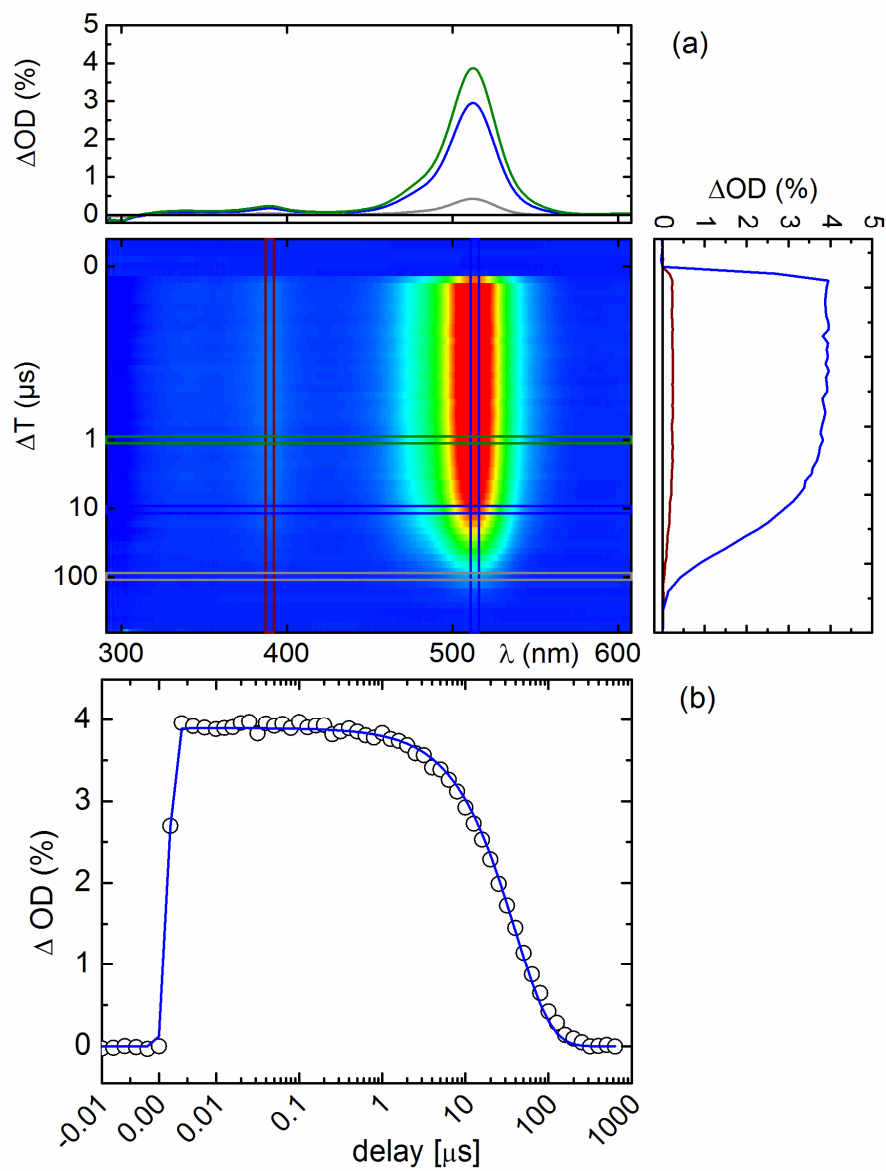
Figure D13: Transient spectra, false color representation of the transient data (a) and time trace of cation band (b) of 1(MeMe)-PPh$_3$BF$_4$ in CH$_3$CN, ns-μs experiment (270 nm excitation).
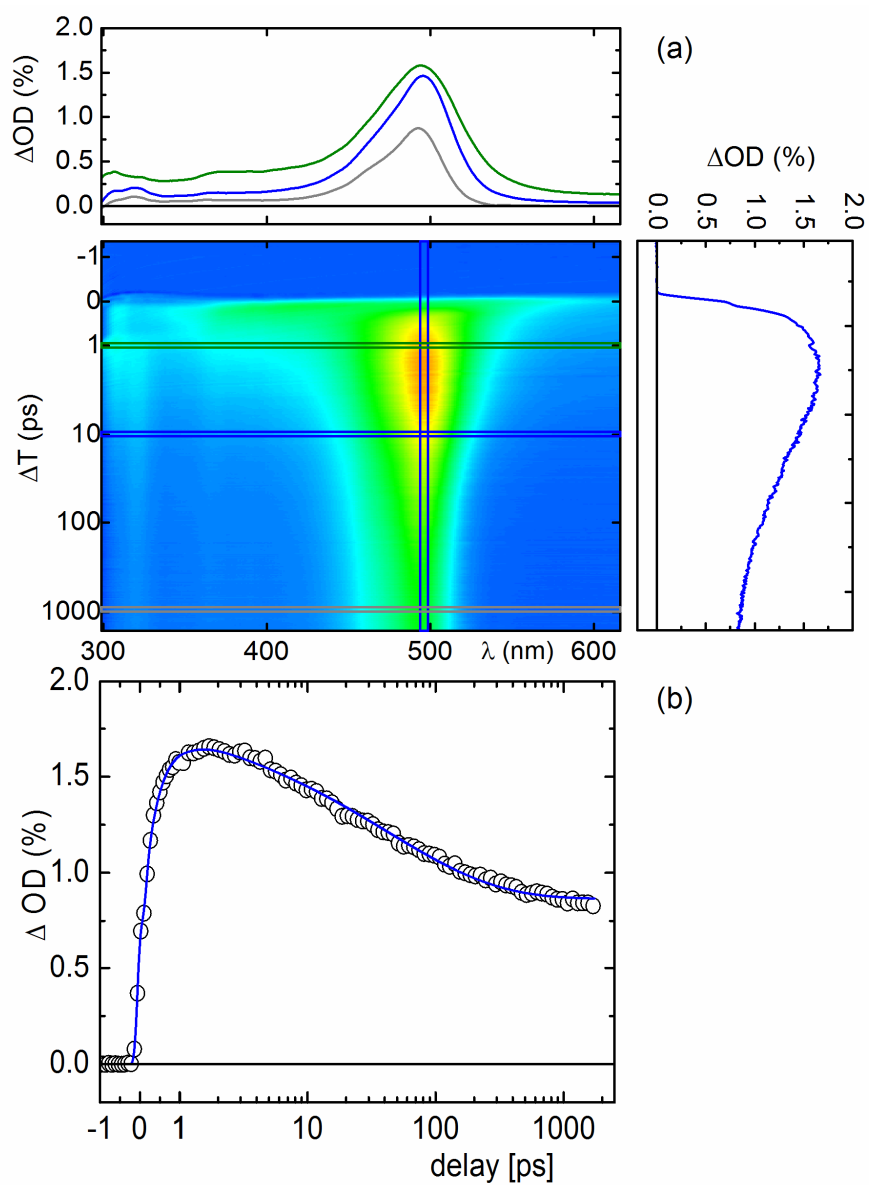
Figure D14: Transient spectra, false color representation of the transient data (a) and time trace (b) of cation band of 1(MeFF)-PPh$_2$MeBF$_4$ in CH$_3$CN, fs-ps experiment (270 nm excitation).
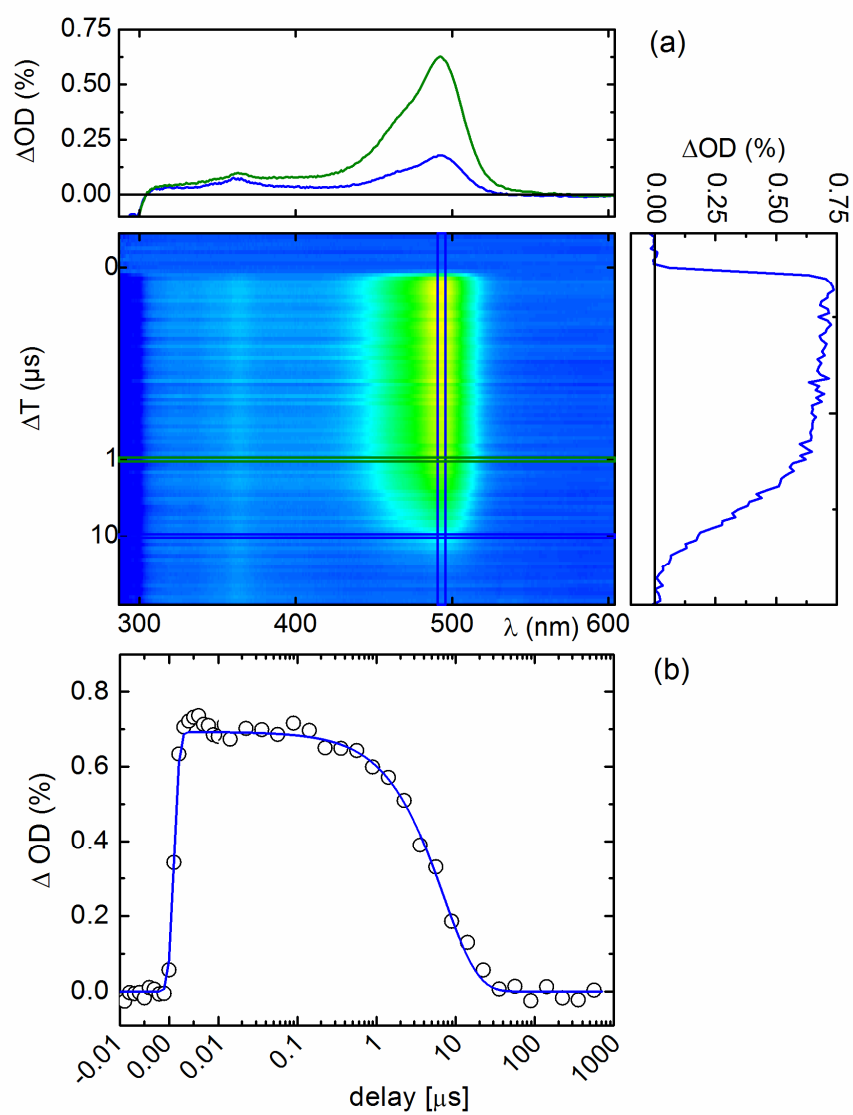
Figure D15: Transient spectra, false color representation of the transient data (a) and time trace of cation band (b) of 1(MeFF)-PPh$_2$MeBF$_4$ in CH$_3$CN, ns-µs experiment (270 nm excitation).
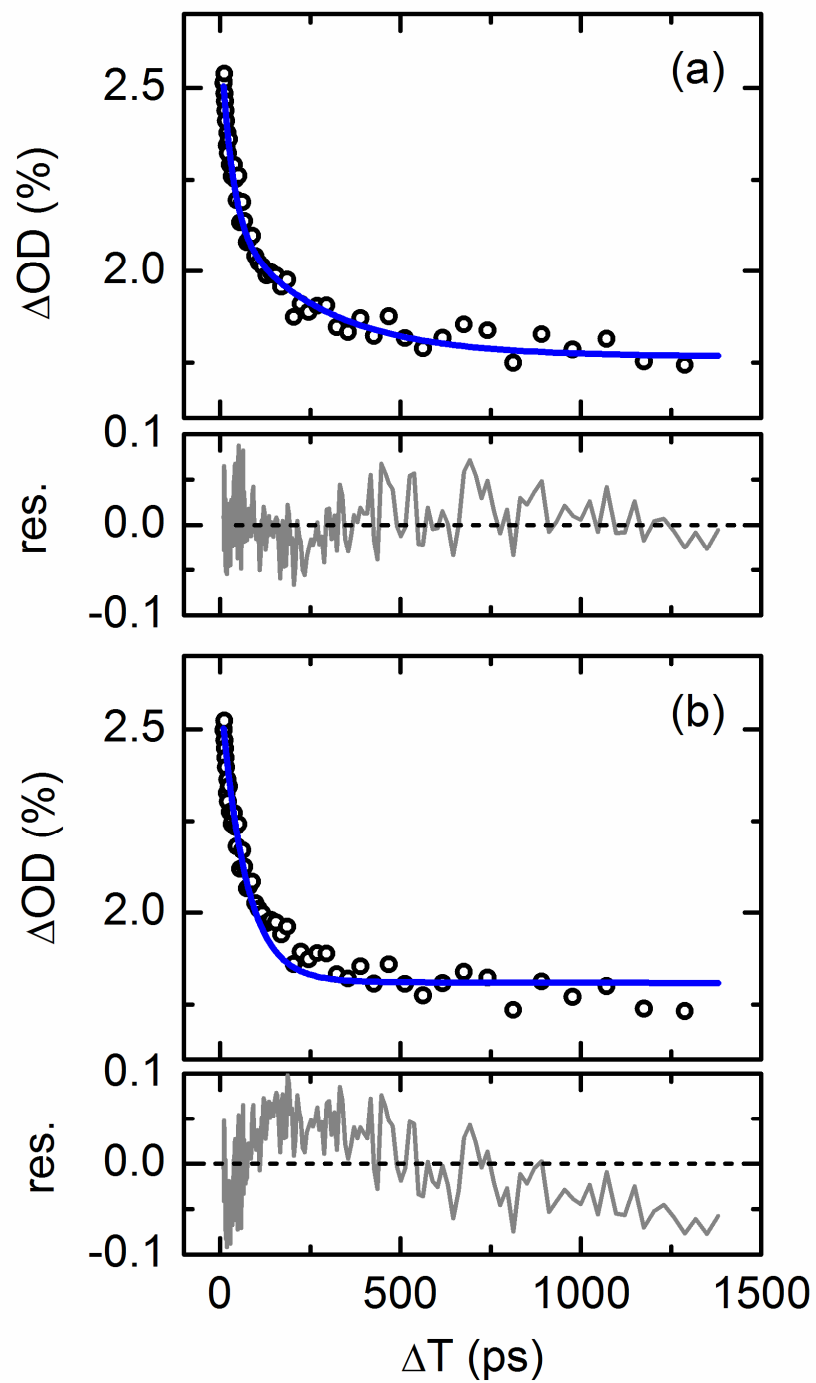
Figure D16: Comparison of the fits (blue lines) and residua (grey lines) obtained from a stretched exponential (a) and a monoexponential function (b) for the geminate recombination of the cation band of 1(HH)-PPh$_3$BF$_4$ in CH$_3$CN, fs-ps experiment (270 nm excitation).
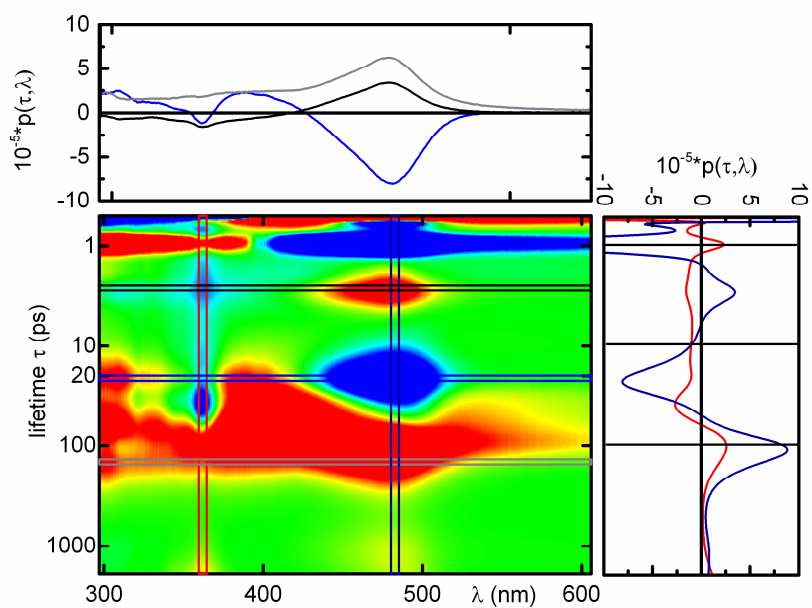
Figure D17: Results of the Maximal Entropy analysis for 1(MeFF)-OAc in CH$_3$CN, fs-ps experiment (261 nm excitation).

Appendix E: article preprint

Direct Observation of Memory Effects in SN1 Reactions by Femto- to Microsecond Spectroscopy of Allylium Ion Pairs

Michael Mikhailov, Konstantin Troshin, Herbert Mayr, Eberhard Riedle, Igor Pugliesi

In preparation

Direct Observation of Memory Effects in S_N1 Reactions by Femto- to Microsecond Spectroscopy of Allylium Ion Pairs

Michael Mikhailov,[1] Konstantin Troshin,[2] Herbert Mayr [2], Eberhard Riedle [1*], Igor Pugliesi[1]

[1] *Lehrstuhl für BioMolekulare Optik, Ludwig-Maximilians-Universität München, Oettingenstrasse 67, 80538 München, Germany*

[2] *Department Chemie, Ludwig-Maximilians-Universität München, Butenandstrasse 5-13, 81377 München, Germany*

*Authors to whom correspondence should be addressed.

Eberhard Riedle:

Tel: +49 (0)89 2180 9210

Fax: +49 (0)89 2180 9202

E-mail address: Eberhard.Riedle@physik.uni-muenchen.de

Abstract

In comparison to the benzhydryl systems, in diarylallyl systems unsymmetric substitution should have an effect on the photoinduced dynamics, as the excitation is localized on the styrene moiety. Herein we present a novel investigation of the photoinduced dynamics of 1,3-diarylallyl systems ranging from femtoseconds to microseconds and comprising chemical variations of the leaving group as well as the substitution in the aromatic rings. We start our investigation with the 1,3-Diphenylallyl chloride to create a direct comparison to the previously published benzhydryl chloride. The spectroscopic analysis is then extended to unsymmetrically substituted diarylallyl carboxylates and diarylallyl phosphonium salts.

For the 1,3-diphenylallyl chloride the photoinduced mechanism is similar to that of the related benzhydryl chloride, albeit all steps are slower but have comparable quantum yields. For the 1,3-diarylallyl acetates radicals and cations appear to be generated exclusively with the photoinduced bond cleavage. An in depth analysis of the dynamics suggests that the process of direct radical and cation generation occur on a slower or similar time scale to the electron transfer. This masks the observation of the electron transfer channel in the transient measurements. Asymmetric substitution leads to substantial differences in the dissociation dynamics and yields of cation and radical as the excitation is localized on the styrene moiety. For the diarylallyl phosphonium salts we observe exclusive cation generation. The geminate recombination follows a stretched exponential dynamics. This is the first spectroscopic confirmation of a fast suprafacial migration of the leaving group from one terminal allyl carbon to another resulting in a distribution of the distances between these carbons and the leaving group. This observation is in line with the finding that suprafacial migration of the leaving group occurs much faster than the ion pair diffusional separation and recombination during solvolysis of 1,3-diarylallyl carboxylates [Tro13b].

Keywords: diarylallyl, carbocations, electron transfer, ion pairs, reaction mechanism, time-resolved spectroscopy

1. Introduction

Solvolyses of allyl derivatives played an important role in the development of the electronic theory of organic chemistry, particularly for the understanding of S_N1 reactions. Apart from kinetic arguments, the stereochemical course was a crucial criterion in Ingold's differentiation of S_N2 and S_N1 mechanisms. While S_N2 reactions led to inversion of configuration of chiral carbon centers, S_N1 reactions were associated with racemization due to the achiral nature of the sp^2-hybridized carbenium intermediates. However, memory effects were observed when the subsequent reaction of the carbenium ion with the nucleophile was faster than the diffusional separation of the carbocation from the leaving group, i. e., when the second step of the S_N1 cascade did not proceed through free ions but through ion pairs.

Since in many S_N1 reactions the first step, i. e., the heterolytic cleavage of the C-X bond is reversible, racemization of chiral substrates by common ion return was often found to be faster than formation of the solvolysis products, and the comparison of the rates of racemization and product formation became an important tool for the investigation of the initially formed ion pairs.

Due to their unique structure, allyl derivatives adopted a key role in these investigations, because isomerization of the substrates cannot only occur through migration of the leaving group X^- to the other face of the allyl cation (see pathway a in Chart 1) but also through migration to the other allylic terminus (see pathways b and c in Chart 1).
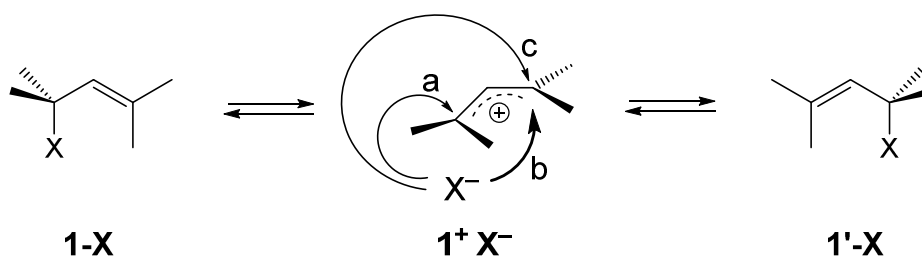
Chart 1:   Isomerization pathways in allyl derivatives

Goering et al. [Goe54 - Goe78] differentiated these processes in cyclic allyl derivatives by comparing the rates of racemization (≙ mode b) and cis-trans isomerization (≙ modes a and c) of the cyclohexenyl derivative **2** in Chart 2.
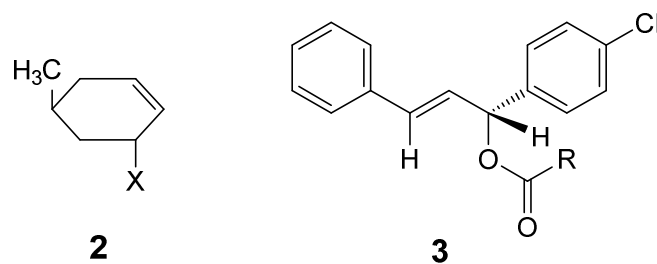
2   **3**
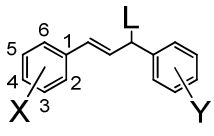
Chart 2:   Cyclohexenyl derivative and allylic ester

Troshin et al. [Tro11] [Tro12] [Tro13b] managed to follow the time-dependent concentrations of all four isomeric esters of **3** in Chart 2 (two regioisomeric pairs of enantiomers) formed by common-ion return of the intermediate ion pairs as well as the concentrations of all four isomeric alcohols (two regioisomeric pairs of enantiomers) formed by trapping of the intermediate allyl cations with water and thus obtained relative rates of the internal reorganization of the initially formed ion pairs as well as the rates of their dissociation into free ions.

We now report on the direct observation of photolytically generated 1,3-diarylallyl cations on the fs to μs time scale, which allows us to provide unprecedented information about absolute rates of movements within ion pairs. We start the investigation by comparing the femtosecond and nanosecond dynamics of 1,3-diphenylallyl chloride with the chemically related system benzhydryl chloride discussed in references [Sai13a] and [Sai13b]. We then move on to study the influence of asymmetric substitution in diarylallyl acetates. Finally we focus on the ion pair dynamics, which is best investigated with diarylallyl phosphonium salts.

2. Experimental Section

Table 1: 1,3-Diarylallyl compounds investigated in this work together with empirical electrophilicity parameters E of the corresponding cations and the absorption maxima of the corresponding diarylallyl radicals and diarylallyl cations in CH_3CN.

X	Y	L^a	Abbreviation	E^b	$1(XY)^{\bullet}$	$1(XY)^+$
					λ_{max} / nm	
H	H	Cl	1(HH)-Cl	2.70	356	490
H	H	OAc	1(HH)-OAc	2.70	355	487
4-Me	3,5-F_2	OAc	1(MeFF)-OAc	---	360	490
3,5-F_2	4-Me	OAc	1(FFMe)-OAc	---	360	490
H	H	PPh_3BF_4	1(HH)-PPh_3BF_4	2.70	c	488
4-Me	4-Me	PPh_3BF_4	1(MeMe)-PPh_3BF_4	1.23	c	518
3-F	3-F	PPh_3BF_4	1(FF)-PPh_3BF_4	4.15	c	495
4-Me	3,5-F_2	$PPh_2Me\ BF_4$	1(MeFF)-PPh_2MeBF_4	---	c	494

[a] Leaving group of the 1,3-diarylallyl compound; Cl and OAc can leave as radicals or anions, PPh_3 and PPh_2Me only as neutral molecules

[b] Electrophilicity parameter of the corresponding 1,3-diarylallyl cations from reference [Tro11]

[c] No radicals detected

2.1 Materials

Structural formulae and abbreviations for the full names of the compounds investigated in this work are shown in Table 1. The compounds 1(HH)-Cl and 1(HH)-OAc were prepared as described in references [Hay89] and [Sch08]. The synthesis of the phosphonium salts was carried out according to the procedures of reference [Tro11]. The unsymmetrically substituted 1,3-diarylallyl acetate 1(MeFF)-OAc was prepared according to the procedure described

in reference [Sch08] from MemFF(OH) (1.000 g, 3.842 mmol), acetyl chloride (550 μL, 605 mg, 7.70 mmol), DMAP (100 mg, 0.818 mmol) and triethylamine (1.3 mL, 0.95 g, 9.4 mmol) with a yield of 0.558 g (1.85 mmol, 48%). The unsymmetrically substituted 1,3-diarylallyl acetate 1(FFMe)-OAc was prepared according to the procedure described in reference [Sch08] from mFFMe(OH) (0.906 g, 3.48 mmol), acetyl chloride (500 μL, 550 mg, 7.00 mmol), DMAP (100 mg, 0.818 mmol) and triethylamine (1.2 mL, 0.87 g, 8.6 mmol) with a yield of 0.450 g (1.49 mmol, 43%). The solvents used for the spectroscopic investigation were of the highest spectroscopic grade available. The absorption strength of the allyl systems is significantly higher than the one of the related benzhydryl systems, facilitating the optical excitation. The detailed absorption spectra are shown for reference in the SI.

2.2 Femtosecond UV/Vis Transient Absorption Measurements

To monitor the ultrafast photoinduced kinetics of the 1,3-diarylallyl systems we used a femtosecond broadband pump-probe setup that has been described in detail elsewhere [Meg09], [Rie13]. Solutions of the compounds in Table 1 (OD ≈ 0.1–0.3, ca. 2×10^{-4} to 1×10^{-3} M) were pumped through a flow cell of 110 μm path length and irradiated with 35-fs pulses (λ_{exc} = 261 nm for diphenylallyl chloride and the 1,3-diarylallyl acetates or 270 nm for the 1,3-diarylallyl phosphonium salts, 70 nJ/pulse) from the frequency-doubled output of a noncollinear optical parametric amplifier (NOPA). The pulses were focused down to a FWHM diameter of about 80 μm inside the sample. A CaF_2 white light continuum spanning from 290 to 720 nm and polarized at the magic angle was used as probe light. The time-dependent transient spectra were recorded with temporal resolutions of 100 fs, which is well below all observed rates. The absorbances were converted to quantum yields using the absorption coefficients of the 1,3-diarylallyl cations [Tro11] and the accurately determined excitation probability [Meg09] as described extensively in references [Sai13a] and [Amm12]. For the 1,3-diarylallyl radicals we took the extinction coefficients of the cations, as in the related benzhydryl system the coefficients between cation and radical are very similar.

2.3 Nanosecond UV/Vis Transient Absorption Measurements

To monitor the photoinduced kinetics of the 1,3-diarylallyl systems on the nanosecond time-scale we used the nanosecond setup described in reference [Sai13b]. A pulsed nanosecond laser system (NT242, Ekspla) with 1 kHz repetition rate and integrated OPO for spectral tunability was used to excite the sample. The nanosecond laser is externally triggered and electronically synchronized with the Ti:sapphire amplifier system, running at 1 kHz repetition rate as well. Solutions of the compounds in Table 1 (OD ≈ 0.5–0.7, ca. 3×10^{-5} to 1.5×10^{-4} M) were pumped through a flow cell of 1 mm and irradiated with pulses centered

at $\lambda_{exc} = 261$ nm or 270 nm and 100 nJ/pulse. The pulses were focused down to a diameter of about 100 µm inside the sample. For spectrally resolved probing the CaF_2 supercontinuum described in the previous section was employed.

3. Photoinduced Dynamics of 1,3-Diphenylallyl Chloride and its photoproducts in comparison to Benzhydryl Chloride

Figure 1b shows the evolution of the transient absorption spectrum after UV-irradiation of 1,3-Diphenylallyl chloride 1(HH)-Cl in acetonitrile (CH_3CN): The probe wavelength is plotted on the horizontal axis and the pump-probe delay on the vertical axis. Blue color indicates low absorbance and red color high absorbance. The delay on the vertical axis is shown in a linear scale for the first ps and in a logarithmic scale afterwards.
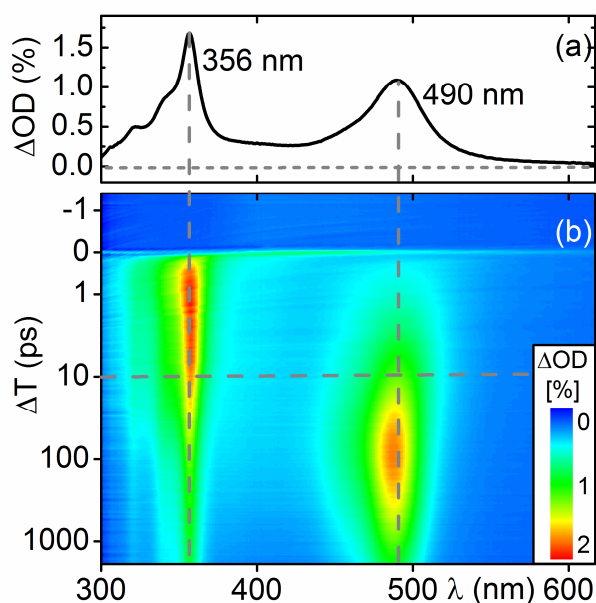
Figure 1:   (a) Transient spectrum at a pump-probe delay of 10 ps and (b) false color representation of the transient data on the femto- to picosecond timescale of 1(HH)-Cl in CH_3CN after 261 nm UV excitation.

UV irradiation at 261 nm generates two bands at 356 nm and 490 nm (see Figure 1a for the spectrum observed after10 ps). The spectral signature at 490 nm coincides with the product bands observed in nanosecond laser flash photolysis experiments on allyl phosphonium ions and chemically generated cations from 1,3-diarylallyl trimethylsilyl ethers [Tro11]. We therefore assign the band at 490 nm to the 1,3-diphenylallyl cation. The band at 356 nm belongs to the 1,3-diphenylallyl radical in analogy to the observations made on the related benzhydryl chloride [Sai13, Bar90] and 1,3-   dichloro-1,3-diphenylpropane   systems

[Mir01]. As depicted in Figure 2b the radical band reaches its maximum shortly before 1 ps and subsequently decays within a few 100 ps to about half of its initial intensity. In contrast, the cation band reaches its maximum within 100 ps and subsequently decays within a few hundred picoseconds. To monitor the reaction of the radicals and cations, transient measurements on the nano- and microsecond timescale were performed (see Figure 3). A higher excitation energy than in the fs recording was used to ensure sufficient signal. The data show that after the dynamics on the picosecond timescale the cation signal persists for up to a few microseconds signaling a corresponding life time of the cation and the radical signal persists even up to several hundred microseconds.
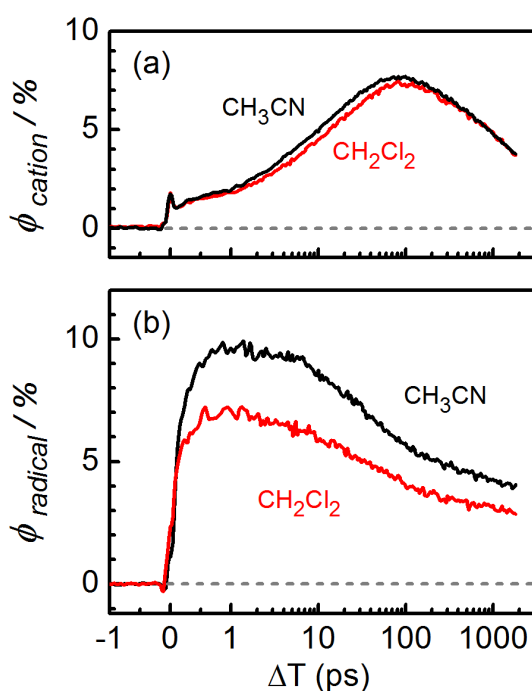
Figure 2: Temporal evolution of (a) the cation quantum yield and (b) the radical quantum yield of 1(HH)-Cl in CH_3CN and CH_2Cl_2.

The temporal evolution of the signal attributed to the cation and radical population in CH_3CN along the vertical lines in Figure 1b is shown in Figure 2 (black lines). The product dynamics is quantified by exponential fits on the band maxima of cation and radical. The results are listed in Table 2. The radical shows a fast initial rise of 300 fs. No fast femtosecond rise is observed for the cation band. Analysis of the time traces off-resonance to the radical and cation bands show that the instantaneous signal present in the radical and cation band is due to excited state absorption of the precursor. Similarly to the benzhydryl system described in [Sai13a], the subsequent picosecond decay of the radical and the rise of the cation

can only be satisfactorily fitted with a stretched-exponential function $A(t) = A_{SE} \exp\left(-\left(t/\tau_{SE}\right)^{\beta_{SE}}\right)$ with $\beta_{SE} = 0.5$. For the decay of the radical and the rise of the cation we obtain an identical time constant of $\tau_{SE} = 18$ ps. At later times the cation absorption shows a substantial decay before it reaches a constant level after 3 ns. This decay has also to be fitted with a stretched exponential function with a time constant of $\tau_{SE} = 324$ ps. The need to use a stretched exponential for the ion pair decay will be explained and rationalized in Section 5.
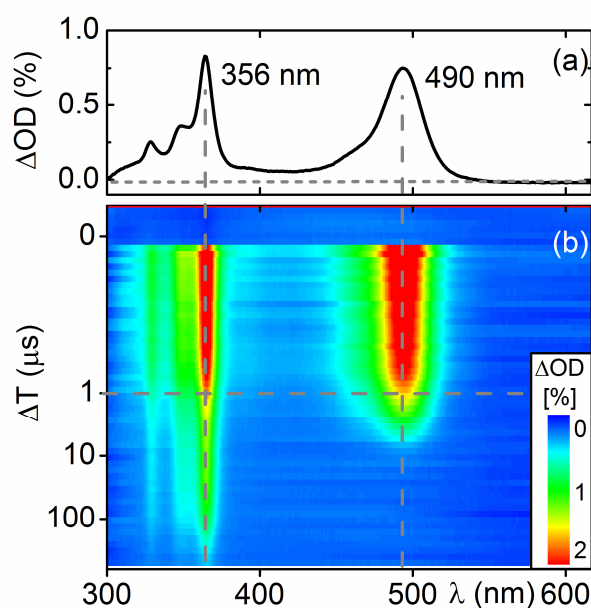
Figure 3: (a) Transient spectrum at a pump-probe delay of 1 µs and (b) false color representation of the transient data on the nano- to microsecond timescale of 1(HH)-Cl in CH_3CN after 261 nm UV excitation. A higher excitation energy compared to Figure 1 was used.

Scheme 1: Reaction mechanism (not to scale) generalized to all investigated compounds for the processes investigated with the femtosecond UV/Vis transient absorption. DAA= 1,3-diarylallyl; L = Leaving group.
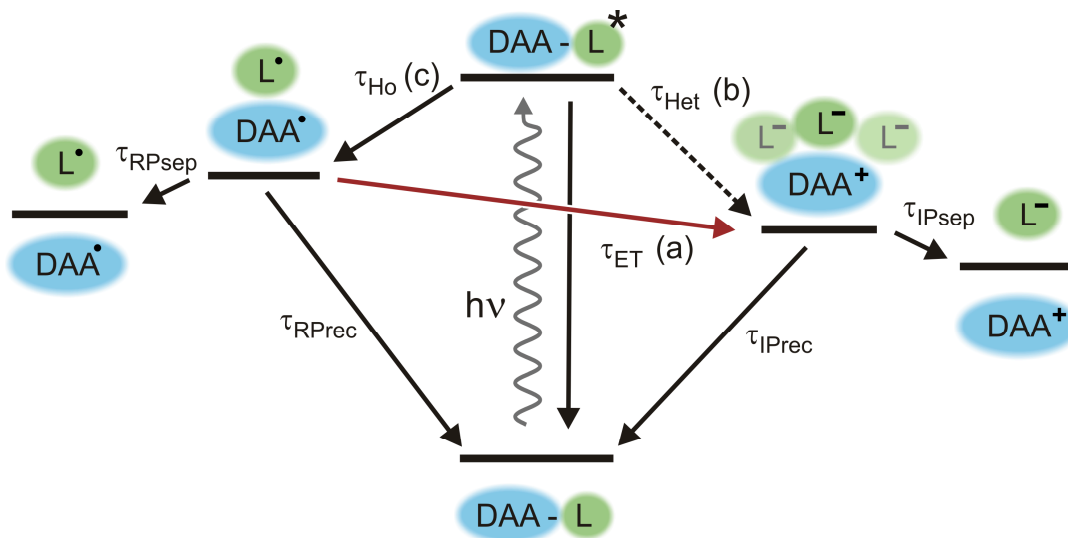
(a) The electron transfer channel is only detectable for 1,3-diarylallyl compounds with the leaving group L = Cl

(b) The heterolysis channel exists only for 1,3-diarylallyl compounds with the leaving group L = OAc and PPh$_3$

(c) The homolysis channel exists only for 1,3-diarylallyl compounds with the leaving group L = Cl and OAc

Based on the experimental data and fits presented so far, we develop a kinetic reaction scheme for the population dynamics of the photoproducts which is shown in Scheme 1. We assign the τ_{Ho} = 300 fs time constant to the photoinduced homolytic C–Cl bond cleavage and subsequent solvent and geometric relaxation of the 1,3-diphenylallyl radical. Details of this complex evolution of the earliest signals have been discussed for the related benzhydryl system [Fin12]. The quantum yield for the initially photogenerated radicals is 10%, which is about four times lower than for benzhydryl chloride. We attribute this difference to a larger potential energy barrier the wavepacket has to cross in order to reach the conical intersection leading to the radical pair.

The stretched exponential time constant τ_{SE} = 18 ps is associated with a dramatic rise of the cation signal and a substantial decrease of the radical signal. This coordinated rise and fall indicates that the cations are formed from the radicals via an electron transfer from the 1,3-diphenylallyl radical to the chlorine radical in close vicinity. Ab initio calculations at the M062X/6-311+G(d) level of theory on the radical and cation optimized in the solvent model IEFPCM yield an exergonic change in Gibbs free reaction energy for the electron transfer of

ΔG_{ET} = -1.74 eV [Gau09]. This clearly indicates that electron transfer is energetically allowed. As has been extensively shown by Sailer et al. [Sai13a], the fact that the electron transfer has to be fitted with a non-exponential function indicates that the observed ensemble kinetics is actually a superposition of dynamics in sub-ensembles. These sub-ensembles are represented by a distribution of fragment distances created by the homolytic bond cleavage leading to a time-dependent electron transfer rate, which is seen in the experiment as stretched exponential decay. The mean electron transfer time is given by twice τ_{SE} [San05], i.e. $<\tau_{ET}>$ = $2\tau_{SE}$ = 36 ps. The ensemble dynamics is reflected in the temporal shift of the band position. The peak position of the cation band undergoes a blue shift from 491 to 487 nm with a time of 30 ps comparable to the electron transfer process associated with the ps rise of the cation and the ps fall of the radical. The cation absorption in ion pairs with short interionic distance is red-shifted compared to that of cation in ion pairs of larger interionic distances or free cations The shift thus occurs as the electron transfer generates ion pairs with increasing interionic distances [Sai13a].

The electron transfer is the main process depleting the radical population by nearly 50%. The remaining radical pairs can avoid electron transfer or recombination and separate by diffusion to free radicals. More than half of the formed cation population decays via geminate recombination. Unlike benzhydryl chloride, here this process can only be modelled properly with a stretched exponential time constant of τ_{SE} = 324 ps. The remaining part lives for up to a microsecond. There is a competition between geminate recombination of the ion pair and diffusional separation of the ions: After the photoinduced C–Cl bond cleavage, the ion pairs generated by electron transfer can either separate to give rise to long-lived free ions or recombine to 1(HH)-Cl. The geminate recombination can only occur as long as the fragments are in close vicinity and is terminated by diffusional separation. The observed mean cation decay time of a $<\tau_{Rec+Diff}>$ = 648 ps therefore is determined jointly by the geminate recombination and the cation separation. Characteristic times for the individual processes can be extracted from the data and turn out to be a $<\tau_{IPrec}>$ = 1.0 ns for the recombination and a $<\tau_{IPsep}>$ = 1.8 ns for the separation.

There is a chemically interesting difference that can be is observed in the solvent dependent behavior between the 1,3-diphenylallyl and benzhydryl systems. While in the case of benzhydryl chloride only in highly polar solvents such as CH_3CN a significant fraction of the ion pairs separates diffusionally to free ions, for 1,3-diphenylallyl chloride we observe long-lived free radicals and cations for less polar solvents such as dichloromethane (CH_2Cl_2) (see Figure 2, red lines). As the positive charge is distributed over the allyl moiety, the lower

permittivity of CH_2Cl_2 affords a shielding of the Coulomb attraction that is large enough for the generation of free ions.

Scheme 2: Reaction mechanism (not to scale) generalized to all investigated compounds for the processes investigated with the nanosecond UV/Vis transient absorption. DAA= 1,3-diarylallyl; L = Leaving group.
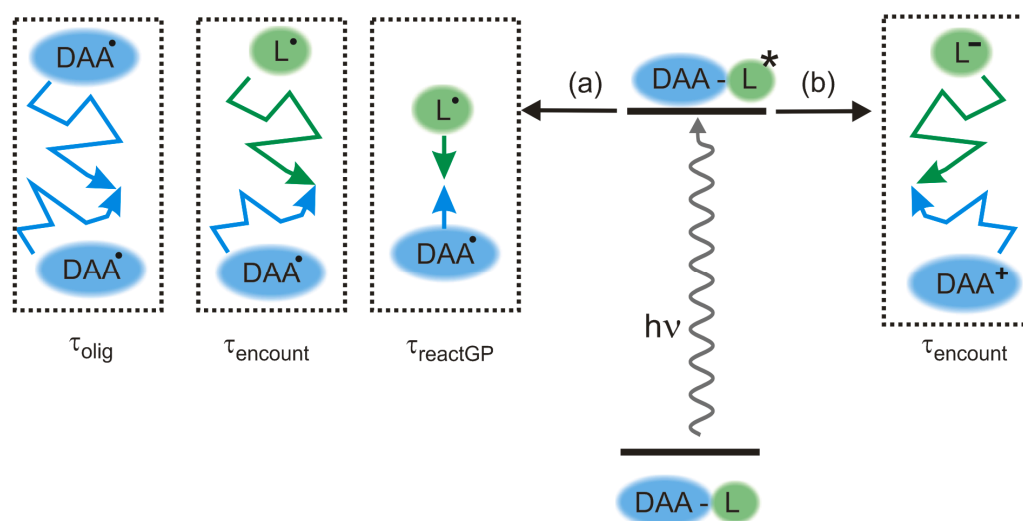
(a) Femto and picosecond processes leading to free radicals depicted in Scheme 1

(b) Femto and picosecond processes leading to free ions depicted in Scheme 1

The photoinduced evolution of the transient absorption spectrum of 1(HH)-Cl in CH_3CN on the nano- to microsecond timescale is shown in Figure 3b. Both the 1,3-diphenylallyl radical and cation are present at the same spectral position as in the femto- to nanosecond measurement (Figure 1b). Time traces of the radical and cation band are shown in Figure S8 and the fit results are listed in Table 3. The processes associated with these time constants are shown in Scheme 2. The cation signal decays within the first two microseconds and the radical signal within several hundred microseconds. No residual signal is found throughout the spectrum at the end of the measurement. Compared to the radical and cation originating from benzhydryl chloride, the 1,3-diphenylallyl radical and cation live nearly an order of magnitude longer. This is related to the delocalization of the radical / charge character over the allyl subunit which reduces their reactivity [Tro11]. The absorption signal evolution of the cation decays monoexponentially with a time constant of a $\tau_{encount}$ = 2.4 µs. This is well in line with the first order decay rates found by Troshin et al. [Tro11]. We assign this process to dif-

- 12 -

fusion controlled re-encounter of the free 1,3-diphenylallyl cation and chloride anion along with reactions with the solvent and nucleophilic impurities (e,g,, water) present in it.

The absorption signal evolution of the radical has a more complex temporal behavior that has to be fitted with the sum of three exponential functions. About 50% of the radical population decays with a time constant of $\tau_{\text{react GP}} = 0.8\,\mu s$. A further 23% decay with a longer time constant of $\tau_{\text{olig}} = 98\,\mu s$ while the remaining 27% are very long lived with a time constant of $\tau_{\text{encount}} = 585\,\mu s$. This behavior is significantly different compared to the radicals originating from benzhydryl chloride, which decay with only two time constants [Sai13b]. The $\tau_{\text{react GP}} = 0.8\,\mu s$ time constant is most likely due to radicals that are still geminate pairs that have not separated far enough or statistically re-encounter. In order to shed light on the process behind the two longer time constants illumination experiments on 1,3-diphenylallyl chloride in CH_3CN have been performed and the photoproducts analyzed with standard chemical methods. The details are described in the Supporting Information, Section 2. In short, we find that light exposure induces oligomerization of the diphenylallyl unit yielding a product whose NMR spectrum is comparable to polystyrene. Based on these results we believe that the process behind the time constant of $\tau_{\text{olig}} = 98\,\mu s$ is oligomerization while the time constant of $\tau_{\text{encount}} = 585\,\mu s$ is due to radicals that have distributed equally in solution and slowly find a reaction partner by diffusion.

4. Influence of asymmetric substitution on the photoinduced dynamics of 1,3-diphenylallyl acetate

Figure 4b shows the evolution of the transient absorption spectrum of 1(HH)-OAc in CH_3CN. After UV excitation at 261 nm, we observe the appearance of an instantaneous long-lived broad and featureless absorption band ranging from the visible into the UV range, which decays within 500 ps. The similarity of this spectral feature to the broad and long-lived excited state absorption (ESA) of styrene and diphenylpropene (Figure S10) allows to assign this spectral feature to the absorption of the optically excited 1(HH)-OAc precursor. At pump-probe delays larger than 500 ps two product bands around 355 nm and 487 nm appear, which can be ascribed to the 1,3-diphenylallyl radical and cation by the same line of argumentation as in the case of the 1,3-diphenylallyl chloride.

As the transient spectrum is rather congested, we quantify the photoinduced dynamics with a global fit procedure [Fit06] based on a rate model. The results are listed in Table 2 and the processes associated with these time constants are illustrated in Scheme 1. The decay associated difference spectra (DADS), the wavelength dependent pre-exponential factors, can be found in Figure S9. The best fit is ob-   tained with an exponential time constant of

$\tau_{Ho/Het}$ = 401 ps and an offset. The DADS associated with the $\tau_{Ho/Het}$ = 401 ps time constant describes the decay of the broad featureless ESA of the excited precursor and the simultaneous rise of the radical and cation band which live for several microseconds as shown by the transient measurements on the nano- microsecond timescale in Figure S11. The characteristic concerted fall of the radical band and rise of cation band due to electron transfer cannot be observed. This is also the case in the temporal evolution of the unsymmetrically substituted 1(MeFF)-OAc shown in Figure 5, where the cation band is substantially more intense compared to that of 1(HH)-OAc. One can clearly see that the radical (red line) and cation traces (blue line) rise with comparable time scales. The ESA seems to decay on a similar time scale (black line).
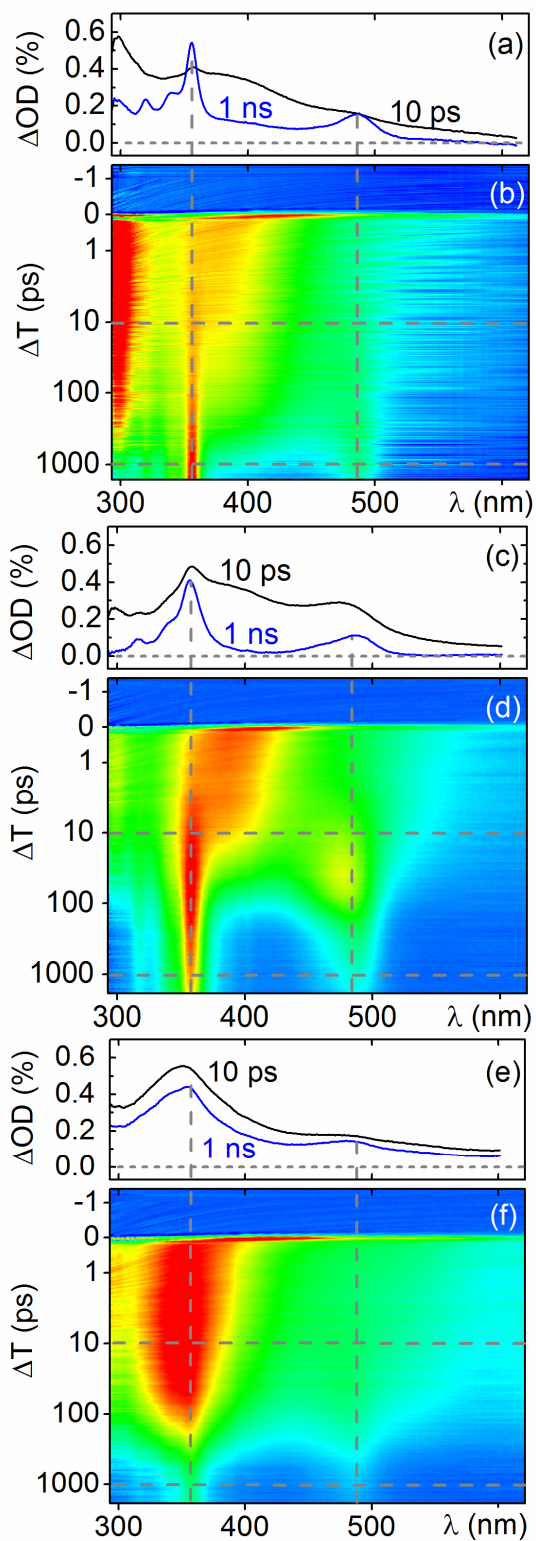
Figure 4: Transient spectrum at pump-probe delays of 10 ps and 1 ns (a) of 1(HH)-OAc, (c) 1(MeFF)-OAc and (e) 1(FFMe)-OAc in CH$_3$CN after 261 nm UV excitation. (b), (d) and (f) are false color representations of the transient data of 1(HH)-OAc, 1(MeFF)-OAc and 1(FFMe)-OAc.

Direct heterolysis has already been observed in benzhydryl chloride [Sai13a] albeit it does not represent the major channel for cation generation. Just as the lone pairs on the chlorine leaving group in benzhydryl chloride it is conceivable that the lone pairs of the acetate open up both the homolytic and heterolytic channels [Sai13c]. The observation that radical and cation appear to be generated in comparable amounts suggests that the conical intersections for radical and ion pair formation are closer to each other on the potential energy surface than in the case of benzhydryl chloride [Fin12, Sai13c]. A detailed theoretical analysis of influence of the position of the conical intersections on the relative reaction yields is subject to a forthcoming publication.

The calculated change in Gibbs free reaction energy for the electron transfer of the radical pair to the cation pair of 1(HH)-OAc is exergonic (ΔG_{ET} = -1.10 eV) indicating that electron transfer should still occur. The ΔG_{ET} value suggests a mean electron transfer rate comparable to 1(HH)-Cl, where the ΔG_{ET} =-1.74 eV, in the region of 30 ps. In the case of 1(HH)-OAc, where the rise of the radical and cation band occurs with 401 ps, the electron transfer being much faster would not be detectable. However, for 1(MeFF)-OAc, where the radical and cation rise is completed well within 100 ps, the effects of electron transfer should become observable in the temporal evolution. As the timescales for heterolysis and the electron transfer are very similar, we carried out a Maximum Entropy analysis [Kut13]. This method is a model free analysis yielding a direct visual evaluation of the distribution of lifetimes present in the experimental data and thus allows to see if there are small differences between the rise of the radical and the cation signal, that cannot be modeled any longer with a global fit procedure. We would expect that if electron transfer is present, the radical signal would have a slightly faster rise compared to the cation signal. As can be seen from the results of the analysis (see Figure S24), this is indeed the case. The resulting matrix of the lifetime distribution $p(\tau, \lambda)$ is visualized as a false colour plot, where the blue regions represent lifetimes contributing to signal rises, while red regions represent lifetimes contributing to signal falls. After 1 ps we observe an extended lifetime distribution from 5 ps to 30 ps for the rise of the radical, while for the rise of the cation we observe a more localized lifetime distribution around 20 ps. The fall around 5 ps at the spectral position of the cation can be assigned to the decay of ESA of the excited state precursor. Based on these results we suggest that after excitation and radical generation, there is an equilibration of the system in both the hemolytic and heterolytic channels and the process of direct generation of cations via heterolysis and indirect generation via electron transfer in the radical pairs become equally probable.

An even more interesting result is obtained when comparing the evolution of the transient

absorption spectrum of the two unsymmetrically substituted diarylallyl acetates 1(MeFF)-OAc and 1(FFMe)-OAc in Figure 4d and 4f. Unlike in the case of the related benzhydryl systems, exchanging the substituents between the styrene and toluene moiety has a dramatic effect on both the dissociation dynamics and the yield of cation and radical. With the toluene moiety we define the phenyl ring directly attached to the sp^3 carbon, while the styrene moiety is the stryryl group attached to the sp^3 carbon. In the case of 1(MeFF)-OAc the global fit yields a time constant of $\tau_{Ho/Het} = 18$ ps for the generation of cation and radical, while for 1(FFMe)-OAc the same process occurs with $\tau_{Ho/Het} = 190$ ps. Furthermore, the yield is 5 times higher for 1(MeFF)-OAc than for 1(FFMe)-OAc. To understand this behavior we analyse the stationary absorption spectra of the 1,3-diarylallyl systems.
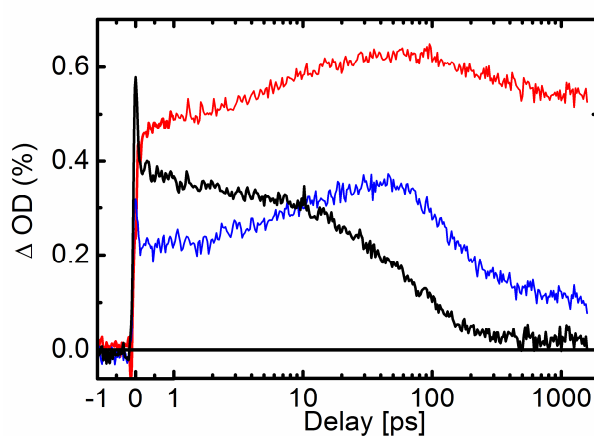
Figure 5:   Temporal evolution of the absorption changes of the cation band (blue line), the radical band (red line) and the precursor ESA band (black line) of 1(MeFF)-OAc in CH_3CN after 261 nm UV excitation.
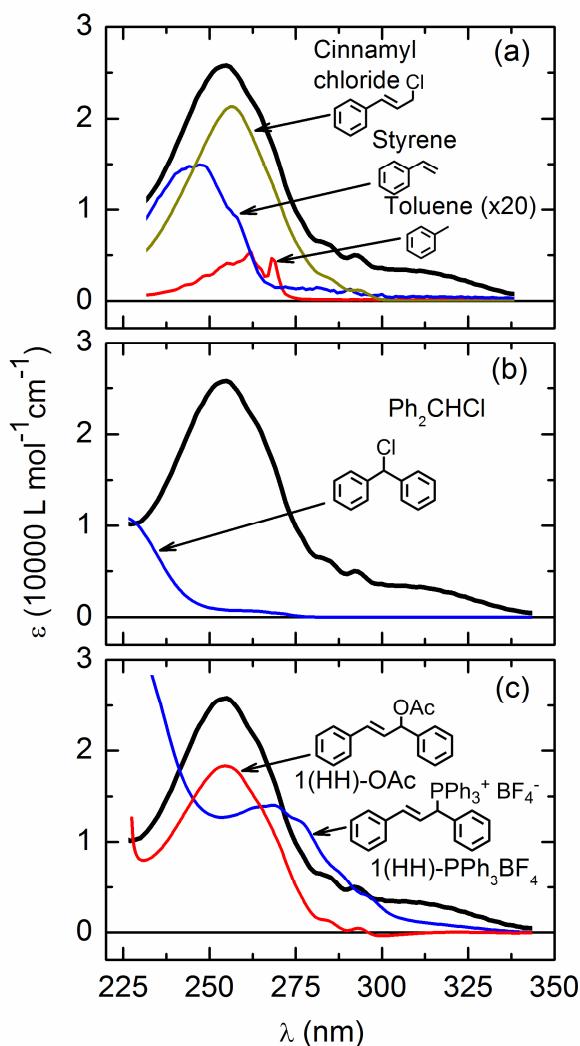
Figure 6: Comparison of the stationary absorption spectrum of 1(HH)-Cl (black line) in CH$_3$CN with the stationary absorption spectra of (a) toluene (red line), styrene (blue line) and cinnamyl chloride (dark yellow line) (b) benzhydryl chloride Ph$_2$CHCl (blue line) and (c) 1(HH)-OAc (red line), and 1(HH)-PPh$_3$BF$_4$ (blue line).

In contrast to benzhydryl chloride, 1,3-diphenylallyl chloride has an absorption maximum at 255 nm with a 33 times larger extinction coefficient of 25.800 L*mol^{-1}*cm^{-1} (see Figure 6b). A comparison of this absorption spectrum with the absorption spectra of the two aromatic moieties comprising 1,3-diphenylallyl chloride, styrene and toluene, indicates that the strong absorption band at 255 nm is due to the styrene moiety (see Figure 6a), which has the maximum extinction coefficient of 15000 L*mol^{-1}*cm^{-1} at 248 nm. This is much larger than for toluene (260 L*mol^{-1}*cm^{-1} at 262 nm) but still approximately half the absorption strength of 1(HH)-Cl and blue-shifted. If the chloromethyl group is added to styrene to form cinnamyl chloride, an absorption spectrum with an extinction coefficient and band spectral

position is obtained that compares very well with that of 1(HH)-Cl. This clearly shows, that the styrene moiety plays the role of the chromophore during the optical excitation of 1(HH)-Cl. As exchanging the chlorine leaving group with an acetate leaving group has no major effect on the position of the band maximum of the 1,3-diarylallyl system (see Figure 6c), we conclude that also for 1(HH)-OAc the styrene moiety plays the role of the chromophore.

In contrast to the benzhydryl system [Fin08], here the excitation is localized on the styrene moiety. Thus only substituents on the styrene moiety can affect the dissociation dynamics and yield of cations and radicals. The sp^3 hybridized carbon centre on which the leaving group is attached prevents any communication between the p-system of the styrene moiety and the toluene moiety. Substituents on the toluene moiety therefore cannot influence the photoinduced dissociation dynamics.

The fit results from the femtosecond transient measurements show that electron donating substituents on the styrene side lead to faster dissociation dynamics and increase the yield of cation and radical compared to electron withdrawing substituents. From ab initio studies on the benzhydryl system we know that heterolysis and homolysis occur at conical intersections between the excited state precursor and the ground state product potential energy surface [Fin08, Fin12, Sai13c]. Recent theoretical investigations show that the position and topology of conical intersections are strongly affected by substituent effects [Nen12]. There is however no general recipe that allows to determine in which direction the electron donating / withdrawing character of the substituent shifts the dissociation dynamics and product yield. This requires the knowledge of the orbitals involved in the conical intersections as well as the topology of the nearby energy landscape. Such an extended theoretical investigation is beyond the scope of this work, but we envision that unsymmetrically substituted 1,3-diarylallyl systems are very good model systems for the theoretical investigation of the effects of substitution on conical intersections.

On the nano- microsecond time scale the asymmetric substitution has no effects on the dynamics of the cations and radicals (see Figures S12 and S14). For both 1,3-diarylallyl acetates we obtain comparable time constants (see Table 3). The cation decays with a time constant of $\tau_{encount} = 6\,\mu s$. The radical traces can be modelled with a triple exponential decay of $\tau_{react\,GP} = 0.8\,\mu s$, $\tau_{olig} = 63\,\mu s$ and $\tau_{encount} = 501\,\mu s$. We assign these time constants just as in the case of 1,3-diphenylallyl chloride to recombination of 1,3-diphenylallyl radical and acetate radical in close proximity, the oligomerization of 1,3-diphenylallyl radicals and the diffusive encounter of 1,3-diphenylallyl and acetate radicals. These processes are shown in Scheme 2.

After photoinduced bond cleavage the diarylallyl cation and radical undergo ultrafast planarization, just like the benzhydryl system [Fin12]. Due to this planarization, the radicals and cations originating from the unsymmetrically substituted 1(MeFF)-OAc and 1(FFMe)-OAc become chemically indistinguishable and thus give rise to the same recombination dynamics.

5. Non-exponential ion pair dynamics in 1,3-diarylallyl phosphonium salts

In order to investigate the dynamics of photogenerated ion pairs, we used 1,3-diarylallyl phosphonium salts as model substances. The photolysis of 1,3-diarylallyl phosphonium salts only generates cations [Tro11] and no radicals. Thus there are no competing channels that can interfere with the ion pair dynamics.
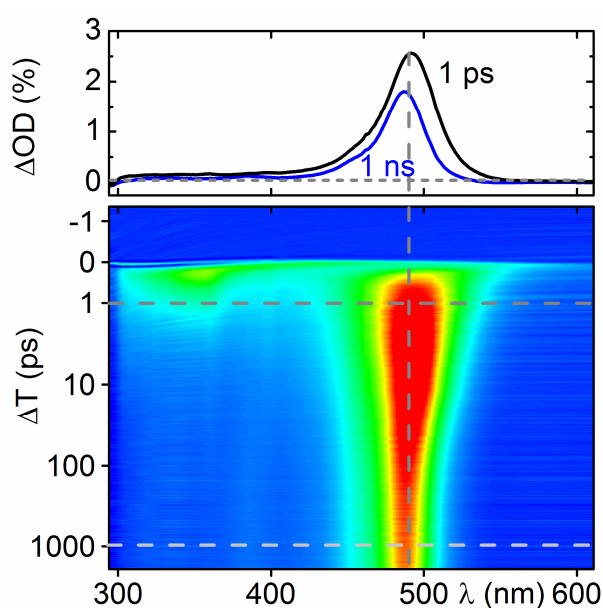
Figure 7:   (a) Transient spectrum at a pump-probe delay of 1 ps and 1 ns and (b) false color representation of the transient data of 1(HH)-PPh$_3$BF$_4$ in CH$_3$CN after 270 nm UV excitation.

Figure 7b shows the evolution of the transient absorption spectrum of 1(HH)-PPh$_3$BF$_4$ in CH$_3$CN. UV excitation at 270 nm generates two types of bands: (i) a broad absorption band below 400 nm, which decays within the first picoseconds, which is assigned to the excited state absorption of the phosphonium salt precursor; (ii) a long-lived product band around 488 nm, which is due to the 1,3-diarylallyl cation [Tro11].
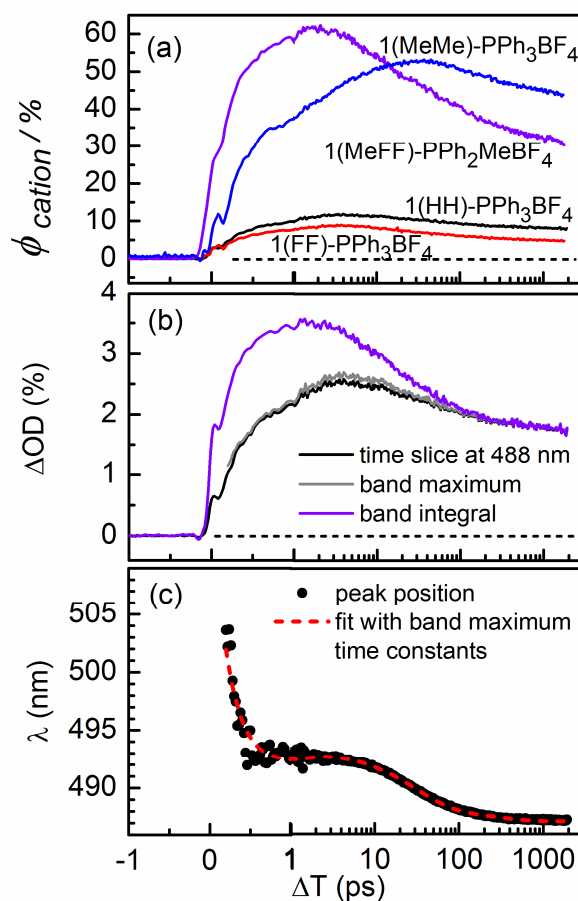
Figure 8: (a) Temporal evolution of the cation quantum yield originating from the precursors with the phosphonium leaving group in CH_3CN, (b) the comparison of time slice, band maximum and band integral of the cation band at 488 nm and (c) measured (dots) and fitted (red dashed line) temporal evolution of the cation peak position after photolysis of 1(HH)-PPh$_3$BF$_4$.

The temporal evolution of the signal attributed to the cation in CH_3CN along the vertical line at 488 nm in Figure 7b is shown in Figure 8a and b (black line). The dynamics are quantified by an exponential fit, the results of which are listed in Table 2. The processes associated with these time constants are illustrated in Scheme 1. The major part of the cation band is formed with an initial fast rise of $\tau_{Het} = 200$ fs. This time is much faster than that for the benzhydryl phosphonium salts of 10 ps reported in references [Sai11, Amm12]. We assign the $\tau_{Het} = 200$ fs time constant to the photoinduced C–P bond cleavage and subsequent solvent rearrangement and geometric planarization of the cation. A further rise of $\tau_{cool} = 0.9$ ps brings the cation band to its maximum. We attribute this time constant to vibrational cooling as in the fit of the band integral over the cation band this time constant disappears entirely (see black and violet lines in Figure 8b). A subsequent picosecond decay due to diffusion terminated geminate recombination decreases the cation population by about 30% before a

population is reached, that is stable on the microsecond time scale. The picosecond decay can only be satisfactorily fitted with a stretched exponential function just as in the case of 1(HH)-Cl and 1(MeFF)-OAc. A comparative monoexponential fit for this decay is shown in Figure S23 (Supporting Information). In order to confine the number of free fit parameters β_{SE} was set to 0.5, as the dynamics of all the phosphonium salts reported below can be well fitted with $\beta_{SE} = 0.5$. For the decay of the cation we obtain a $\tau_{SE} = 55$ ps. In order to exclude that the need for a stretched exponential function is due to a spectral shift of the cation band, we evaluated the spectral position of the cation band maximum and compared the temporal evolution of the band maximum with the time slice at 488 nm. We used the same procedure outlined in detail in reference [Sai13a].

The spectral shift of the band maximum is shown in Figure 8c. We observe a large blue shift of 10 nm within the first 200 fs time constant accompanied by a small red shift of 2 nm within the first picoseconds before the final blue shift of 5 nm on the time range of 100 ps. The time scale of this last blue shift coincides with the picosecond decay of the diffusion terminated geminate recombination. It is due to the slightly different cation spectrum of close and well separated ion-leaving-group-pairs [Sai13b, Sch87]. However the spectral band shift is not large enough to alter the temporal evolution of the 488 nm time slice in such a way that a stretched exponential function would be needed. This becomes clear by the nearly perfect match between the time slice at 488 nm (black line in Figure 8b) and the temporal evolution of the band maximum (grey line in Figure 8b). We therefore have to conclude that the stretched exponential behavior of the geminate recombination is due to a characteristic of the process itself, rather than a spectral artifact.

The fact that the geminate recombination has to be fitted with a non-exponential function indicates therefore that the observed ensemble kinetics is again a superposition of dynamics in sub-ensembles. In the case of the geminate recombination these sub-ensembles are represented by a distribution of geminate ion-leaving-group-pair distances. As has been shown in reference [Sai13a] the geminate recombination is distance dependent. Geminate pairs at shorter ion-leaving-group distances recombine faster than those at larger ion-leaving-group distances. Therefore a time-dependent rate for geminate recombination is obtained, which is seen in the experiment as stretched exponential decay. The mean recombination time is given by twice τ_{SE} [San05], i.e. $<\tau_{rec+diff}> = 2\tau_{rec+diff} = 110$ ps. As the geminate recombination is terminated by diffusional separation, the observed mean recombination time of $<\tau_{rec+diff}> = 110$ ps is a sum of geminate recombination and ion pair separation. The characteristic times for the individual are $<\tau_{IPrec}> = 325$ ps for the recombination and

$<\tau_{IPsep}> = 166$ ps for the separation.

The process that generates the distribution of interionic distances is not due to the photoinduced bond cleavage as in the case of the benzhydryl system, but rather due to the suprafacial migration of the phosphonium leaving group along the allylic chain. This motion has already been observed by Goering and coworkers [Goe54 - Goe78] in cyclic allyl cations. Troshin et al. [Tro13b] could show that in the case of the geminate pair formed between the 1-(4-chlorophenyl)-3-phenylallyl cation and the paranitrobenzoate anion, suprafacial migration leads to partial stereoselectivity in the geminate recombination. From their data they extracted the rate of the suprafacial migration to be $(10$ ps$)^{-1}$. The *E* parameter of 2.67 for the 1-(4-chlorophenyl)-3-phenylallyl cation is almost identical to that of the 1,3-diphenylallyl cation. Therefore the rate of suprafacial migration cannot be substantially different in the geminate pair between the 1,3-diarylallyl cation and the triphenylphosphonium. The suprafacial migration is about 30 times faster than the rate of geminate recombination of $<\tau_{IPrec}> = 325$ ps. This motion is therefore fast enough for the geminate pairs to form a significant distribution of interionic distances before geminate recombination occurs.

The attachment of substituents on the phenyl rings does not have any substantial effects on the photoinduced bond cleavage and subsequent solvent rearrangement and geometric planarization of the cation (300 – 500 fs). This is also the case for the low picosecond cooling. However we observe significant differences in the rate for geminate recombination. While for 1(MeMe)-PPh$_3$BF$_4$ it occurs with much slower rate ($<\tau_{IPrec}> = 6.7$ ns) than in the case of the unsubstituted 1,3-diphenylallyl cation, a significant speed up is observed in the case of 1(FF)-PPh$_3$BF$_4$ ($<\tau_{IPrec}> = 182$ ps). This difference is directly related to the increase of the cation electrophilicity (larger *E* parameter), which is modulated by the substitution in the aromatic rings. Electron withdrawing groups result in a more reactive allyl cation (higher *E*), while electron donating substituents decrease the *E* parameter and reactivity with the nucleophilic leaving group. For the unsymmetrically substituted 1,3-diarylallyl phosphonium salt 1(MeFF)-PPh$_2$MeBF$_4$ we observe a rate for geminate recombination of $<\tau_{IPrec}> = 177$ ps that is very similar to that of 1(FF)-PPh$_3$BF$_4$. We conclude that the influence of the two fluorine substituents on the one phenyl ring outweighs the electron donating effects of the methyl group on the other phenyl ring.

6. Conclusions

We have shown that the 1,3-diarylallyl systems offer a wealth of interesting properties par-

tially different from those of the related benzhydryl systems extensively studied before. In the case of allyl halides the time resolved experiments show that the picosecond dynamics is somewhat slower than in the related benzhydryl halides. The photoinduced reaction mechanism and the yields of cations and radicals are however well comparable with the benzhydryl halides.

As the excitation is localized on the styrene moiety, the asymmetric substitution in the 1,3-diarylallyl acetates has a dramatic effect on the picosecond dissociation dynamics and the yield of the cation. Electron withdrawing substituents on the styrene side lead to slower dissociation dynamics and decrease the yield of the cation compared to electron donating substituents. The asymmetric substitution has no influence on the diffusion controlled re-encounter of the free 1,3-diarylallyl cation and acetate anion due to the planarization of the cation after the heterolysis.

The 1,3-diarylallyl phosphonium salts allowed for a detailed investigation of the dynamics of the geminate ion pairs as the photoinduced bond cleavage exclusively generates carbocations. The partial stereoselectivity of internal ion return in the solvolysis of optically active allyl compounds observed by Goering et al. [Goe78] and Troshin et al. [Tro13b] could only be explained by a suprafacial migration of the leaving group that is substantially faster than the migration of the leaving group to the other face of the cation leading to the racemization of the substrate and the ion pair recombination. The suprafacial motion was estimated to be as fast as 10 ps. In our time resolved experiments we observed a stretched exponential dynamics of the geminate recombination. As this recombination depending on the substitution occurs on a time scale of a few hundred picoseconds, the stretched exponential dynamics is direct spectroscopic evidence of the suprafacial migration of the photoleaving group along the allylic chain generating a distribution of interionic distances on the low picosecond timescale.

Supporting Information

Additional stationary spectra and transient spectra, details of the illumination study on 1(HH)-Cl and comparison between single and stretched exponential fits.

Acknowledgements

Table 2: List of all time constants obtained from femtosecond UV/Vis transient absorption measurements for the 1,3-diarylallyl compounds in CH_3CN investigated in this work listed with decreasing electrophilicity parameter E and decreasing nucleophilicity parameter N of the leaving group. E n.d. = Electrophilicity parameter has not been determined. L = Leaving group.

		Cl^- (N = 17.20)		OAc^- (N = 16.90)		PPh_3 (N = 14.33)	
		$1(XY)^\bullet$	$1(XY)^+$	$1(XY)^\bullet$	$1(XY)^+$	$1(XY)^\bullet$	$1(XY)^+$
FF(L) E = 4.15	$\tau_{Ho/Het}$ (ps)					---	0.5
	τ_{cool} (ps)					---	1.7
	$\tau_{Rec+Diff}$ (ps)					---	82 [d]
HH(L) E = 2.70	$\tau_{Ho/Het}$ (ps)	0.3	---	401	401	---	0.2
	τ_{ET} (ps)	36 [a]	36 [a]	---	---	---	---
	τ_{cool} (ps)	---	---	---	---	---	0.9
	$\tau_{Rec+Diff}$ (ps)	---	648 [b]	---	---	---	110 [e]
MeMe(L) E = 1.23	$\tau_{Ho/Het}$ (ps)					---	0.3
	τ_{cool} (ps)					---	4.6
	$\tau_{Rec+Diff}$ (ps)					---	1094 [f]
MemFF(L) E n.d.	$\tau_{Ho/Het}$ (ps)			18	18	---	0.4
	τ_{cool} (ps)			---	---	---	2.0
	$\tau_{Rec+Diff}$ (ps)			---	206 [c]	---	84 [g]
mFFMe(L) E n.d.	$\tau_{Ho/Het}$ (ps)			190	190		
	τ_{cool} (ps)			---	---		
	$\tau_{Rec+Diff}$ (ps)			---	---		

[a] mean electron transfer time $<\tau_{ET}>$ obtained from the stretched exponential

[b] mean recombination time $<\tau_{Rec+Diff}>$ composed of $<\tau_{IPrec}>$ = 1.0 ns and $<\tau_{IPsep}>$ = 1.8 ns

[c] mean recombination time $<\tau_{Rec+Diff}>$ obtained from stretched exponential

[d] $<\tau_{Rec+Diff}>$ composed of $<\tau_{IPrec}>$ = 182 ps and $<\tau_{IPsep}>$ = 149 ps

[e] $<\tau_{Rec+Diff}>$ composed of $<\tau_{IPrec}>$ = 325 ps and $<\tau_{IPsep}>$ = 166 ps

[f] $<\tau_{Rec+Diff}>$ composed of $<\tau_{IPrec}>$ = 6.7 ns and $<\tau_{IPsep}>$ = 1.3 ns

[g] $<\tau_{Rec+Diff}>$ composed of $<\tau_{IPrec}>$ = 177 ps and $<\tau_{IPsep}>$ = 160 ps

Table 3: List of all time constants in CH_3CN obtained from nanosecond UV/Vis transient absorption measurements for the 1,3-diarylallyl compounds investigated in this work listed with decreasing electrophilicity parameter E and decreasing nucleophilicity parameter N of the leaving group. E n.d. = Electrophilicity parameter has not been determined. L = Leaving group.

		Cl⁻ ($N = 17.20$)		OAc⁻ ($N = 16.90$)		PPh₃ ($N = 14.33$)	
		$1(XY)^{\bullet}$	$1(XY)^{+}$	$1(XY)^{\bullet}$	$1(XY)^{+}$	$1(XY)^{\bullet}$	$1(XY)^{+}$
FF(L) $E = 4.15$	$\tau_{\text{react GP}}$ (µs)					---	---
	τ_{olig} (µs)					---	---
	τ_{encount} (µs)					---	4.3
HH(L) $E = 2.70$	$\tau_{\text{react GP}}$ (µs)	0.8	---	0.7	---		
	τ_{olig} (µs)	98	---	88	---		
	τ_{encount} (µs)	585	2.4	577	1.6		
MeMe(L) $E = 1.23$	$\tau_{\text{react GP}}$ (µs)					---	---
	τ_{olig} (µs)					---	---
	τ_{encount} (µs)					---	39
MemFF(L) E n.d.	$\tau_{\text{react GP}}$ (µs)			0.8	---	---	---
	τ_{olig} (µs)			63	---	---	---
	τ_{encount} (µs)			501	6.0	---	7.0
mFFMe(L) E n.d.	$\tau_{\text{react GP}}$ (µs)			0.8	---		
	τ_{olig} (µs)			63	---		
	τ_{encount} (µs)			501	6.0		

References

Papers Troshin

[Tro13a]   Troshin, K.; Mayr, H. Electrofugalities of 1,3-Diarylallyl Cations. *J. Org. Chem.* **2013**, *78*, 2649-2660.

[Tro13b]   Troshin, K.; Mayr, H. Ion Pair Dynamics: Solvolyses of Chiral 1,3-Diarylallyl Carboxylates as a Case Study. *J. Am. Chem. Soc.* **2013**, *135*, 252-265.

[Tro12]   Troshin, K.; Mayer, P.; Mayr, H. How does Palladium Coordination Affect the Electrophilicities of Allyl Cations? Development of a Robust Kinetic Method for Following Reactions of [(η3-Diarylallyl)Pd(Ph3P)2]+ with Nucleophiles. *Organometallics* **2012**, *31*, 2416-2424.

[Tro11]   Troshin, K.; Schindele, C.; Mayr, H. Electrophilicities of Symmetrically Substituted 1,3-Diarylallyl Cations. *J. Org. Chem.* **2011**, *76*, 9391-9408.

Synthesis

[Hay89]   Hayashi, T.; Yamamoto, A.; Yoshihiko, I.; Nishioka, E.; Miura, H.; Yanagi, K. Asymmetric Synthesis Catalyzed by Chiral Ferrocenylphosphine-Transition-Metal Complexes. 8. Palladium-Catalyzed Asymmetric Allylic Amination. *J. Am. Chem. Soc.* **1989**, *111*, 6301 – 6311.

[Sch08]   Schaller, H. F.; Mayr, H. "Carbocation Watching" in Solvolysis Reactions. *Angew. Chem.* **2008**, *120*, 4022-4025; *Angew. Chem. Int. Ed.* **2008**, *47*, 3958-3961.

Our papers

[Amm12]   Ammer, J.; Sailer C. F.; Riedle, E.; Mayr H. Photolytic Generation of Benzhydryl Cations and Radicals from Quaternary Phosphonium Salts: How Highly Reactive Carbocations Survive Their First Nanoseconds. *J. Am. Chem. Soc* **2012**, *134*, 11481-11494.

[Fin08]   Fingerhut, B. P.; Geppert, D.; de Vivie-Riedle, R. Ultrafast dissociation pathways of diphenylmethyl chloride to generate reactive carbo cations. *Chem. Phys.* **2008**, *343*, 329-339.

[Fin12]   Fingerhut, B. P.; Sailer, C. F.; Ammer, J.; Riedle, E.; de Vivie-Riedle, R. Buildup and Decay of the Optical Absorption in the Ultrafast Photo-Generation and Reaction of Benzhydryl Cations in Solution. *J. Phys. Chem. A* **2012**, *116*, 11064-11074.

[Sai11]   Sailer, C. F.; Singh R. B.; Ammer, J.; Riedle, E.; Pugliesi, I. Encapsulation of diphenylmethyl phosphonium salts in reverse micelles: Enhanced bimolecular reaction of the photofragments. *Chem. Phys. Lett.* **2011**, *512*, 60-65.

[Sai13a]   Sailer, C. F.; Thallmair, S.; Fingerhut, B. P.; Nolte, C.; Ammer, J.; Mayr, H.; Pugliesi, I.; de Vivie-Riedle, R.; Riedle, E. A Comprehensive Microscopic Picture of the Benzhydryl Radical and Cation Photogeneration and Interconversion through Electron Transfer. *Chem.Phys.Chem.* **2013**, *14*, 1423–1437.

[Sai13b]   Sailer, C. F.; Riedle, E. Photogeneration and reactions of benzhydryl cations and radicals: A complex sequence of mechanisms from femtoseconds to microseconds *Pure Appl. Chem.* **2013**, *85*, 1487–1498.

[Sai13c]   Sailer, C. F.; Krebs, N.; Fingerhut, B. P.; de Vivie-Riedle, R.; Riedle, E. Wavepacket Splitting in the First 100 fs Determines the Products from the Bond Cleavage of Diphenylmethylchloride. *Proceedings of the XVIIIth International Conference on Ultrafast Phenomena, Lausanne, Switzerland. EPJ Web of Conferences* **2013**, *41*, 05042

Spectrometer

[Meg09]   Megerle, U.; Pugliesi, I.; Schriever C.; Sailer C. F.; Riedle, E. Sub-50 fs broadband absorption spectroscopy with tunable excitation: putting the analysis of ultrafast molecular dynamics on solid ground. *Appl. Phys. B* **2009**, *96*, 215-231.

[Rie13]   Riedle, E.; Bradler, M.; Wenninger, M.; Sailer, C. F.; Pugliesi, I. Electronic transient spectroscopy from the deep UV to the NIR: unambiguous disentanglement of complex processes. *Faraday Discuss.*, **2013**, *163*, 139-158.

Lit on Allyls: Allylic rearrangements and ion pair dynamics

[Mir01]   Miranda, M. A.; Perez-Prieto, J.; Font-Sanchis E.; Scaiano, J. C. One- vs Two-Photon Processes in the Photochemistry of 1,n-Dihaloalkanes. *Acc. Chem. Res.* **2001**, *34*, 717-726.

-[Goe54]   Goering, H. L.; Blanchard, J. P.; Silversmith, E. F. Sterochemistry of Allylic Rearrangements. 11. The Kinetics and Stereochemistry of the Rearrangement of

cis- and trans-5-Methyl-2-cyclohexenyl Acid Phthalate. *J. Am. Chem. Soc.* **1954**, *76*, 5409–5418.

[Goe55] (a) Goering, H. L.; Silversmith, E. F. Stereochemistry of Allylic Rearrangements. 111. The Solvolysis of cis- and trans-5-Methyl-2-cyclohexenyl Acid Phthalate in Aqueous Acetone. *J. Am. Chem. Soc*. **1955**, *77*, 1129–1133.

(b) Goering, H. L.; Silversmith, E. F. Stereochemistry of Allylic Rearrangements. VII. The Acid-catalyzed Hydrolysis of cis and trans-5-Methyl-2-cyclohexenyl p-Nitrobenzoate in Aqueous Acetone. *J. Am. Chem. Soc.* **1955**, *77*, 6249–6253.

(c) Goering, H. L.; Nevitt, T. D.; Silversmith, E. F. Stereochemistry of Allylic Rearrangements. VI. The Ethanolysis and Acetolysis of cis- and trans-5-Methyl-2-cyclohexenyl Chloride. *J. Am. Chem. Soc.* **1955**, *77*, 5026–5032.

[Goe60] Goering, H. L.; Takahashi Doi, J. Stereochemistry of Allylic Rearrangements. XI. The Isomeric Rearrangement of trans-5-Methyl-2-cyclohexenyl p-Nitrobenzoate-carbony1-O18 in Aqueous Acetone *J. Am. Chem. Soc.* **1960**, *82*, 5850–5854.

[Goe62] Goering, H. L.; Josephson, R. R. Stereochemistry of Allylic Rearrangements. XII. Oxygen Exchange Associated with the Acid-catalyzed Rearrangement of cis- and trans-5-Methyl-2-cyclohexen. *J. Am. Chem. Soc.* **1962**, *84*, 2779–2785.

[Goe71] Goering, H. L.; Koermer, G. S.; Linsay, E. C. Stereochemistry of Allylic Rearrangements. XVI. Stereochemistry of Ion-Pair Return in the trans-α,γ-Methylphenylallyl p-Nitrobenzoate System. *J. Am. Chem. Soc.* **1971**, *93*, 1230–1234

[Goe78] Goering, H. L.; Anderson, R. P. Stereochemistry of Allylic Rearrangements. 16. Ion-Pair Return Associated with Solvolysis of exo- and endo-Bicyclo[3.2.l]oct-3-en-2-yl p-Nitrobenzoate in Aqueous Acetone. *J. Am. Chem. Soc.* **1978**, *100*, 6469-6474

Miscellaneous

[Bar90] Bartl, J.; Steenken S.; Mayr H.; McClelland, R. A. Photo-Heterolysis and -Homolysis of Substituted Diphenylmethyl Halides, Acetates, and Phenyl Ethers in Acetonitrile: Characterization of Diphenylmethyl Cations and Radicals Generated by 248-nm Laser Flash Photolysis. *J. Am. Chem. Soc.* **1990**, *112*, 6918-

6928.

[Nen12]   Nenov, A.; de Vivie-Riedle, R. Conical intersection seams in polyenes derived from their chemical composition. *J. Chem. Phys.* **2012**, *137*, 074101.

[Fit06]   Fita, P.; Luzina, E.; Dziembowska, T.; Radzewicz, Cz.; Grabowska, A. Chemistry, photophysics, and ultrafast kinetics of two structurally related Schiff bases containing the naphthalene or quinoline ring. *J. Chem. Phys.* **2006**, *125*, 184508.

[Gau09]   For all ab initio calculations the Gaussian 09 ab initio suite was employed: Gaussian 09, Revision A.02, M. J. Frisch, G. W. Trucks, H. B. Schlegel, G. E. Scuseria, M. A. Robb, J. R. Cheeseman, G. Scalmani, V. Barone, B. Mennucci, G. A. Petersson, H. Nakatsuji, M. Caricato, X. Li, H. P. Hratchian, A. F. Izmaylov, J. Bloino, G. Zheng, J. L. Sonnenberg, M. Hada, M. Ehara, K. Toyota, R. Fukuda, J. Hasegawa, M. Ishida, T. Nakajima, Y. Honda, O. Kitao, H. Nakai, T. Vreven, J. A. Montgomery, Jr., J. E. Peralta, F. Ogliaro, M. Bearpark, J. J. Heyd, E. Brothers, K. N. Kudin, V. N. Staroverov, R. Kobayashi, J. Normand, K. Raghavachari, A. Rendell, J. C. Burant, S. S. Iyengar, J. Tomasi, M. Cossi, N. Rega, J. M. Millam, M. Klene, J. E. Knox, J. B. Cross, V. Bakken, C. Adamo, J. Jaramillo, R. Gomperts, R. E. Stratmann, O. Yazyev, A. J. Austin, R. Cammi, C. Pomelli, J. W. Ochterski, R. L. Martin, K. Morokuma, V. G. Zakrzewski, G. A. Voth, P. Salvador, J. J. Dannenberg, S. Dapprich, A. D. Daniels, O. Farkas, J. B. Foresman, J. V. Ortiz, J. Cioslowski, and D. J. Fox, Gaussian, Inc., Wallingford CT, 2009.

[San05]   Berberan-Santos, M. N.; Bodunov, E. N.; Valeur, B Mathematical functions for the analysis of luminescence decays with underlying distributions 1. Kohlrausch decay function (stretched exponential). *Chem. Phys.* **2005**, *315*, 171-182.

[Sch87]   Schneider, R.; Mayr, H.; Plesch, P. H. *Ber. Bunsenges. Phys. Chem.* **1987**, *91*, 1369.

[Kut13]   Kutta, R.-J.; Langenbacher, T.; Kensy, U.; Dick, B. *Appl.Phys. B* **2013**, 111, 203.

The fs to µs dynamics of reactive carbocations and carbon radicals photogenerated from diphenylallyl systems

Michael Mikhailov[1], Konstantin Troshin[2], Herbert Mayr[2,*], Eberhard Riedle[1,*], Igor Pugliesi[1]

[1] *Lehrstuhl für BioMolekulare Optik, Ludwig-Maximilians-Universität München, Oettingenstrasse 67, 80538 München, Germany*

[2] *Department Chemie, Ludwig-Maximilians-Universität München, Butenandstrasse 5-13, 81377 München, Germany*

Supporting Information

List of Contents

*Authors to whom correspondence should be addressed.

Eberhard Riedle:

Tel: +49 (0)89 2180 9210

Fax: +49 (0)89 2180 9202

E-mail address: Eberhard.Riedle@physik.uni-muenchen.de

Herbert Mayr:

Tel: +49 (0)89 2180 77719

Fax: +49 (0)89 2180 77717

E-mail address: Herbert.Mayr@cup.uni-muenchen.de

1. Stationary Absorption Spectra of the diphenylallyl acetates and phosphonium salts.
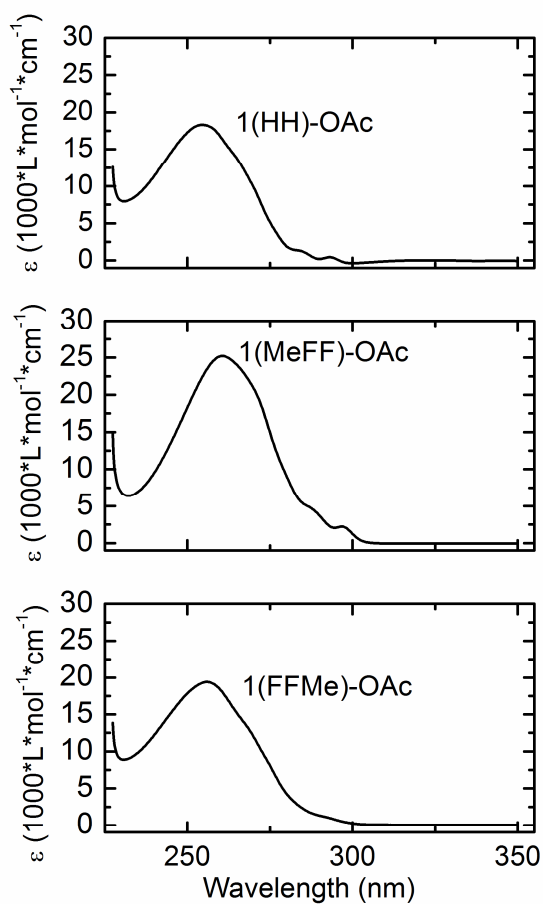
Figure S1: Stationary absorption spectra of all diphenylallyl acetate compounds in CH_3CN investigated in this work.
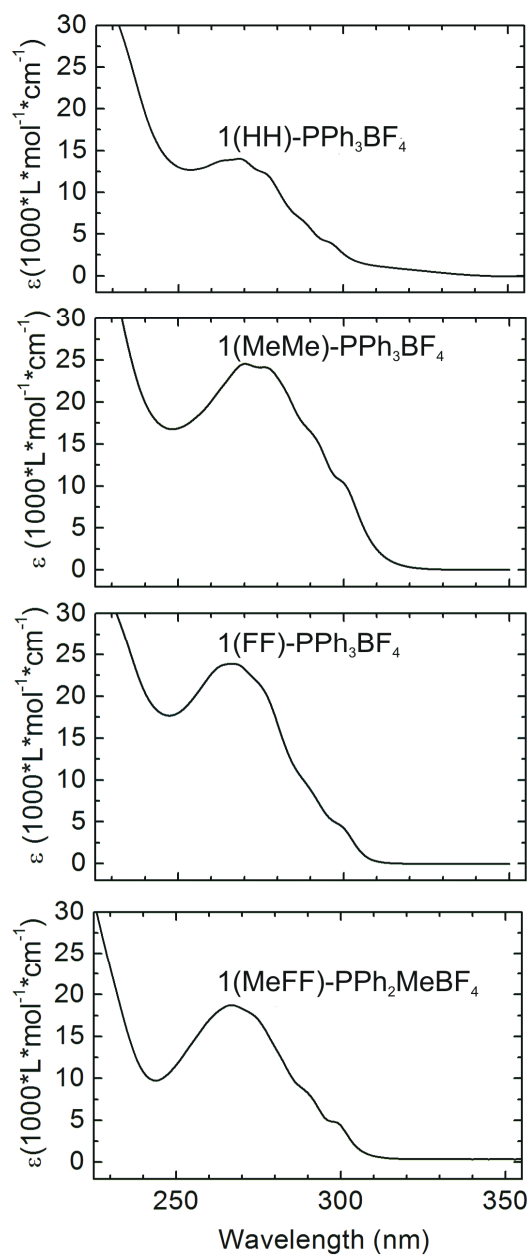
Figure S2: Stationary absorption spectra of all diphenylallyl phosphonium salts in CH_3CN investigated in this work.

2. Stationary and transient absorption investigation of the parasitic photooligomerization process in DPA(Cl) photoinduced bond cleavage

If we look at the stationary absorption spectrum of 1(HH)-Cl, a small spectral feature in the form of a relatively long (50 nm) structureless band centered at 325 nm can be noticed.

Later it was noticed that the solution of 1(HH)-Cl in acetonitrile or dichloromethane changes its color from transparent to light yellow (Fig. S3) with the simultaneous increase of the extinction in 325-nm band after the irradiation of the sample during the measurement.
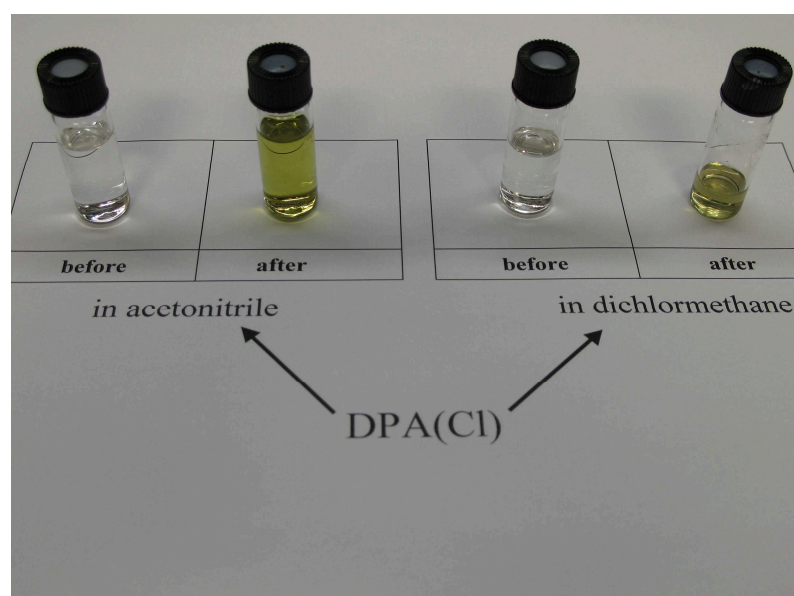
Figure S3: The color change of the 1(HH)-Cl solution observed after the irradiation at 261 nm during the TA experiment.

In order to analyze the nature of the band, the following experiment was conducted: the solution of 1(HH)-Cl in acetonitrile was irradiated during 10 hours in the 120-μm flow cell used for the TA experiments. The irradiation wavelength was 325 nm (the centre of the unknown band) and the energy was 400 nJ. After this time the sample was analyzed with stationary absorption and NMR-spectroscopy which yielded the following results:

- The absorption of the 1(HH)-Cl band decreases with the simultaneous increase of the 325-nm band (Fig. S4).
- The completely new band centered at 360 nm, arises (Fig. S4).

- The NMR-analysis yielded the spectra almost identical to the NMR-spectra of polystyrene (Fig. S5).

Thus, the following conclusion was drawn: the 325-nm band originates from the absorption of the dimer molecule (formed from allyl radicals obtained due the photoinduced bond cleavage). The band centered at 360 nm originates from the oligomer absorption (formed from the dimer precursors during the irradiation with the UV radiation).
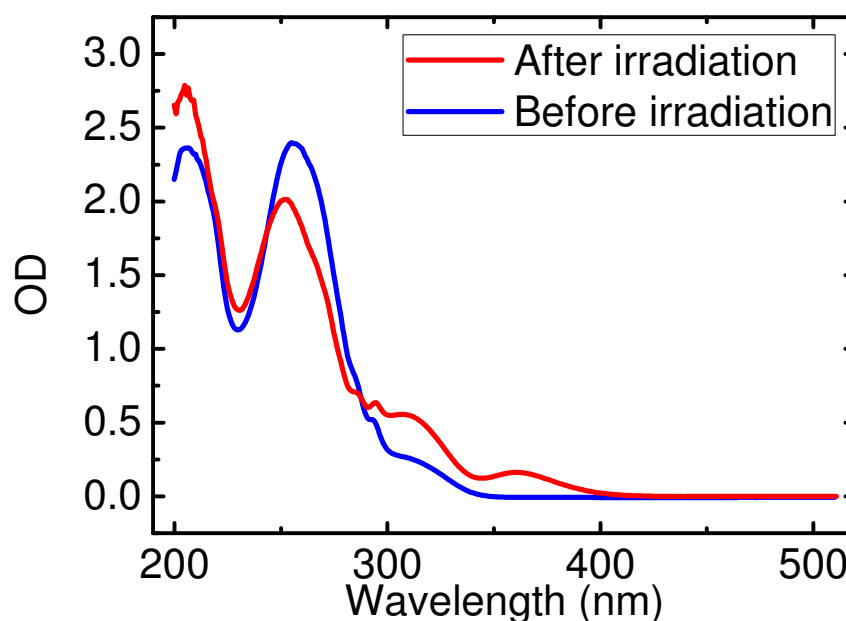
Figure S4: The stationary absorption spectra of 1(HH)-Cl before and after 10-hour irradiation with UV laser beam (325 nm, 400 nJ).

In order to test if the 325-nm band really originates from the dimer, the TA measurement (excitation wavelength: 325 nm) was conducted. The resulting spectra (see Fig. S6) did not demonstrate similarity to the spectra of 1(HH)-Cl excited at the middle of its absorption band (see Fig. S7). In contradiction to 1(HH)-Cl transient spectra, only one quite broad band centered at 363 nm was present. This band can be identified as the ESA band of the 1(HH)-Cl dimer. The single-channel fit yields the following results: the major part of the dimer signal decays with the 3 ps time, and the rest exists for much longer time. These long-lived dimer species signals can overlap with the radical signal (at 361 nm), creating the second decay time of 98 μs, observed in the nanosecond TA experiment of 1(HH)-Cl in acetonitrile.

Therefore, the competing parasitic reaction channel was discovered. Since the TA signals of

the oligomer products overlap with the signal of the radical, it can make the interpretation of the radical signal more complicated.

Figure S5: The NMR-spectra of the irradiated 1(HH)-Cl in acetonitrile (left) and of the isotactic polystyrene in tetrachloroethylene (right, adapted from F. A. Bovey, F. P. Hood III, E. W. Anderson, L. C. Snyder, *J. Chem. Phys.* **1965**, *42*, 3900-3910).
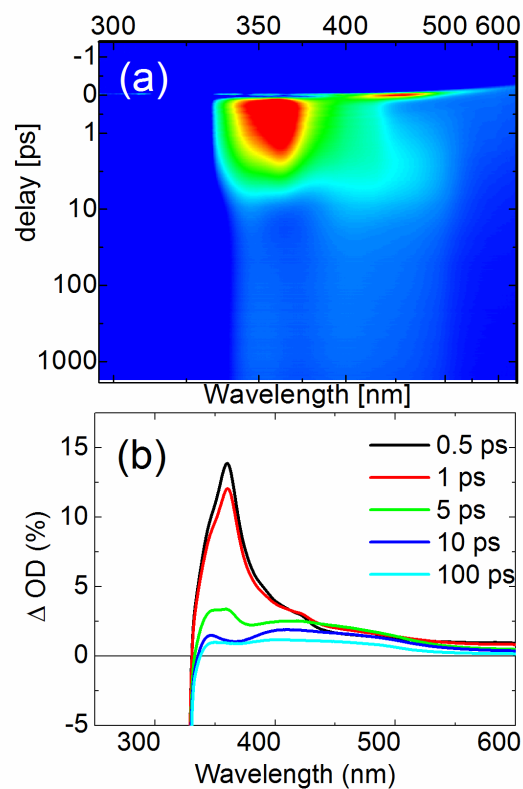
Figure S6: False color representation of the transient data and transient spectra of the transient data (a) and selected transients (b) of the oligomer band of 1(HH)-Cl in CH_3CN, fs-ps experiment (325 nm excitation).

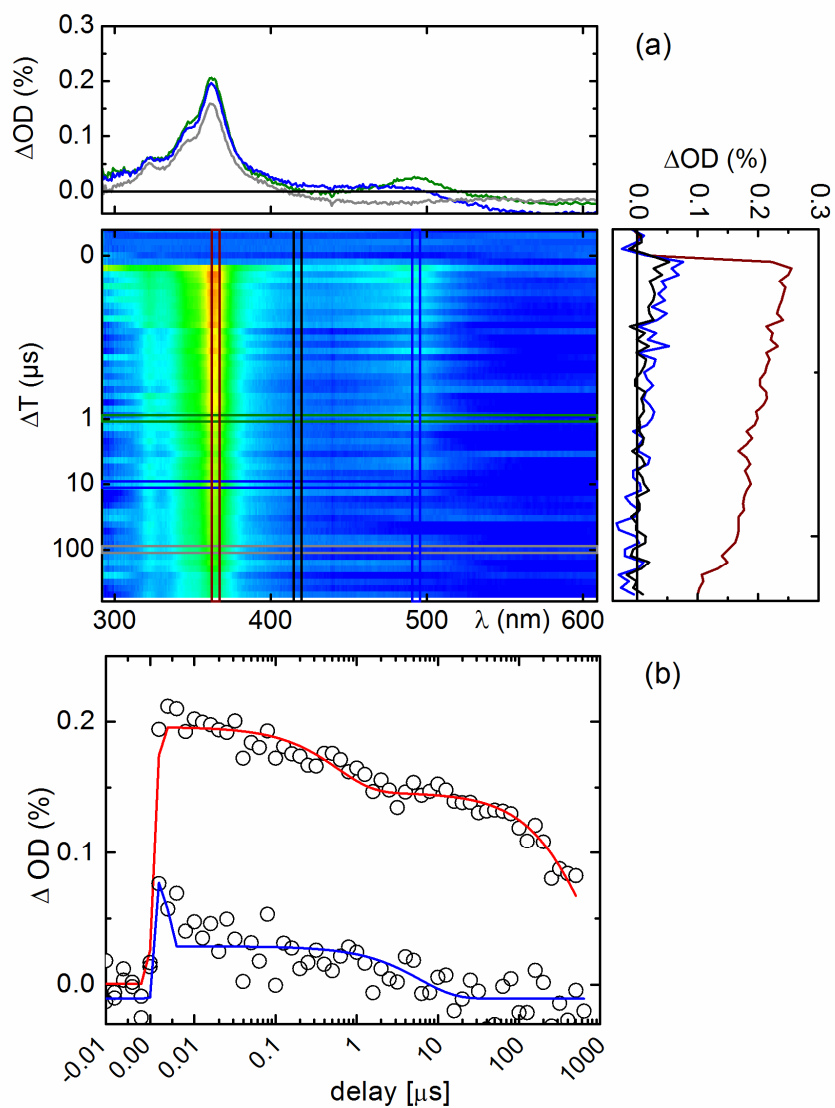# 3. Transient absorption spectra for all investigated diphenylallyl systems
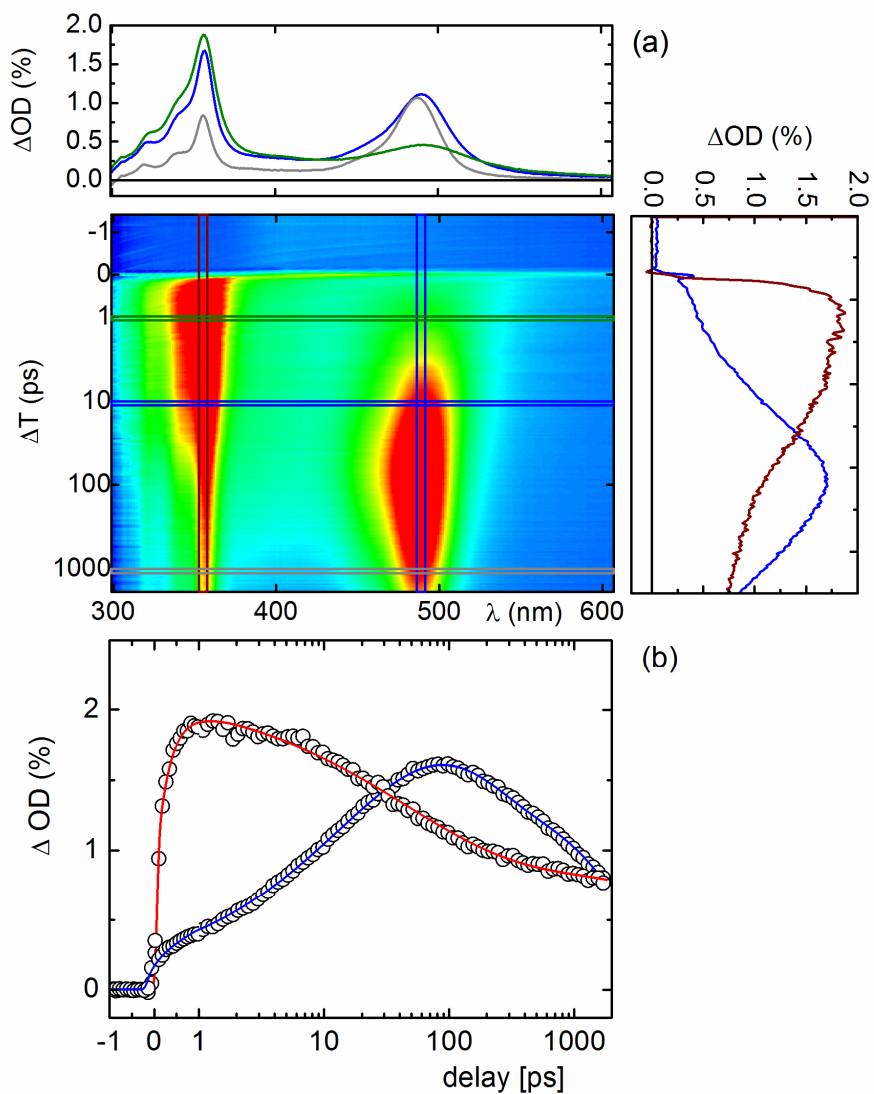
Figure S7: Transient spectra, false color representation of the transient data (a) and time traces (b) of radical (red) and cation (blue) of 1(HH)-Cl in CH_3CN, fs-ps experiment (261 nm excitation).
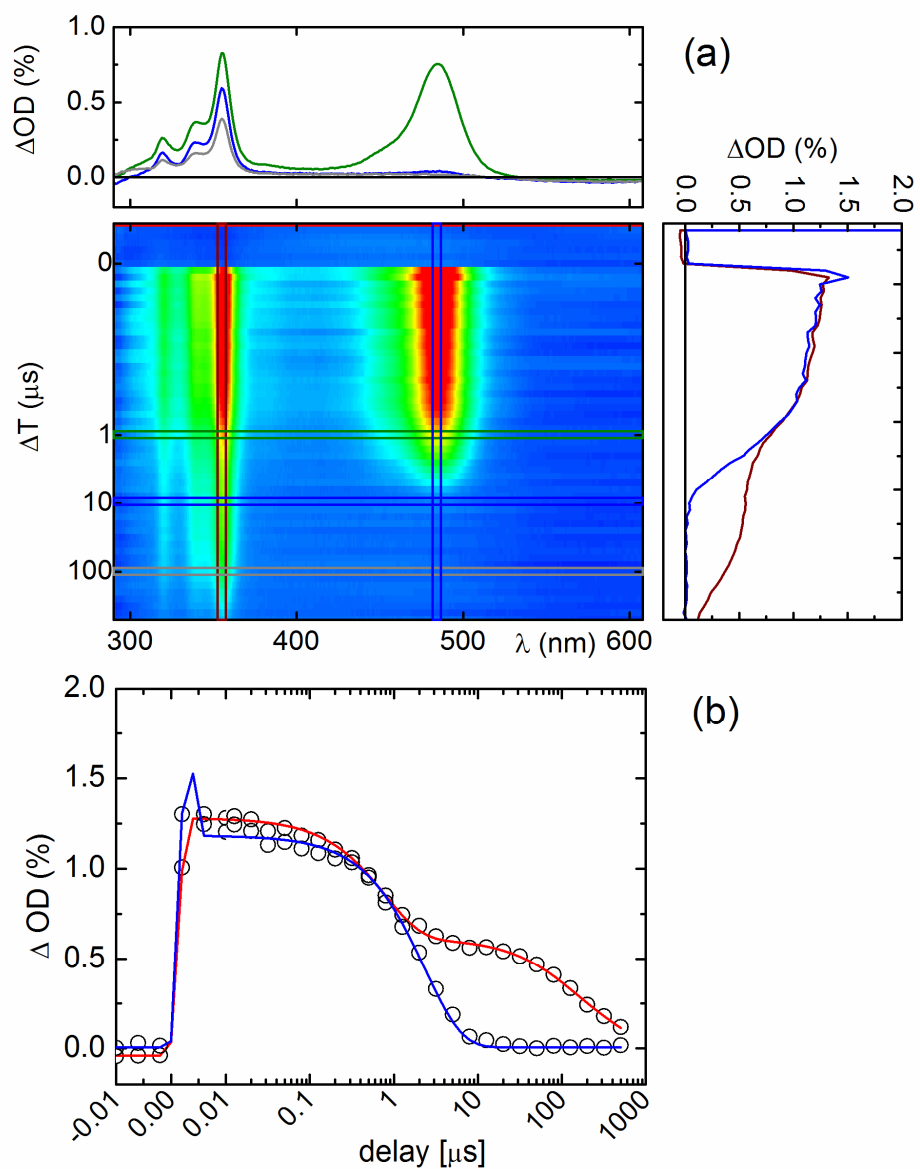
Figure S8: Transient spectra, false color representation of the transient data (a) and time traces (b) of radical (red) and cation (blue) of 1(HH)-Cl in CH_3CN, ns-µs experiment (261 nm excitation).
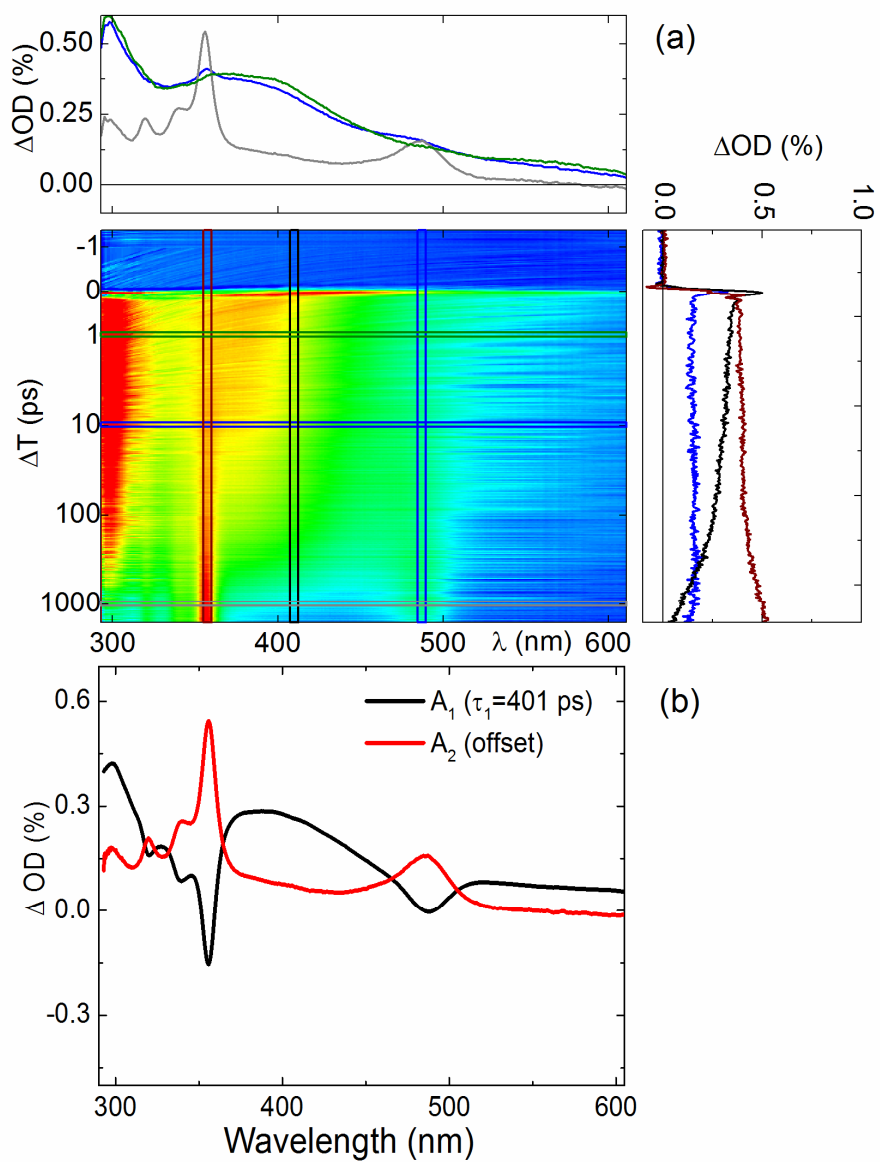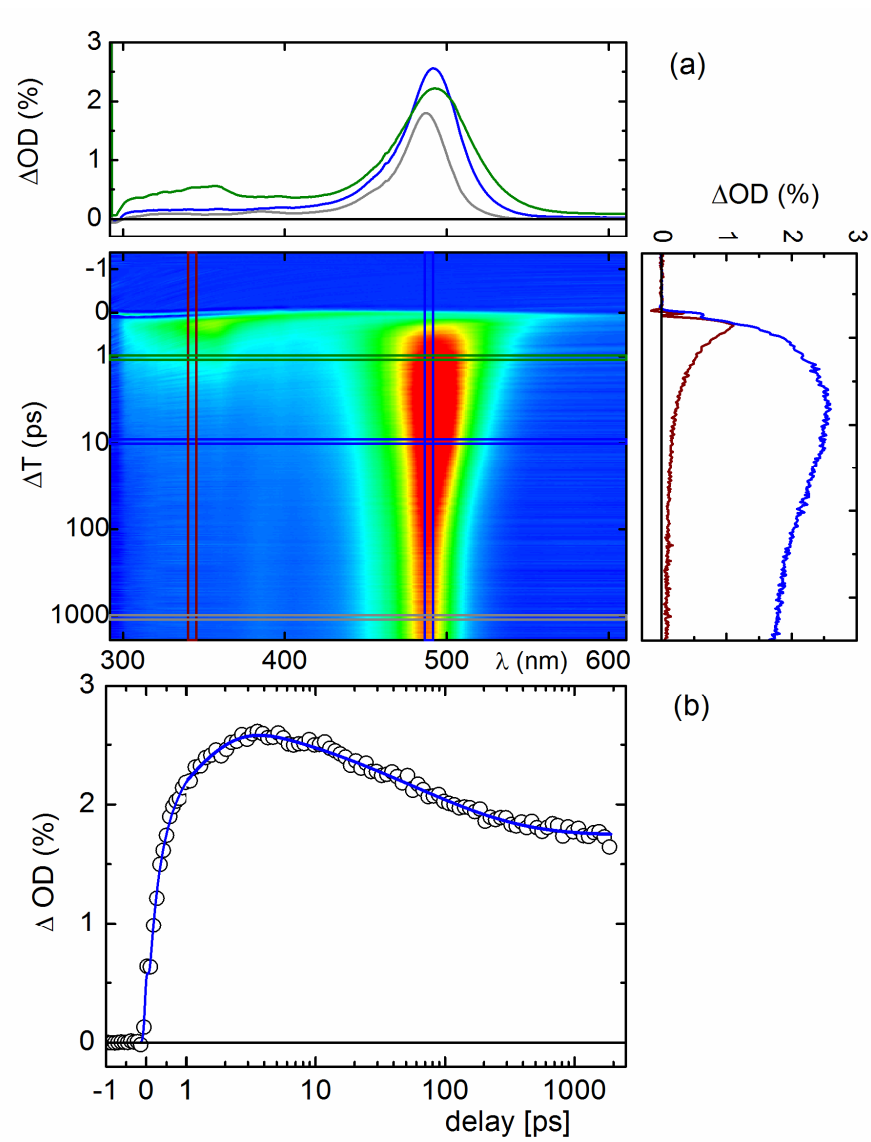
Figure S9: Transient spectra, false color representation of the transient data (a) and global fit (b) of radical and cation bands of 1(HH)-OAc in CH_3CN, fs-ps experiment (261 nm excitation).
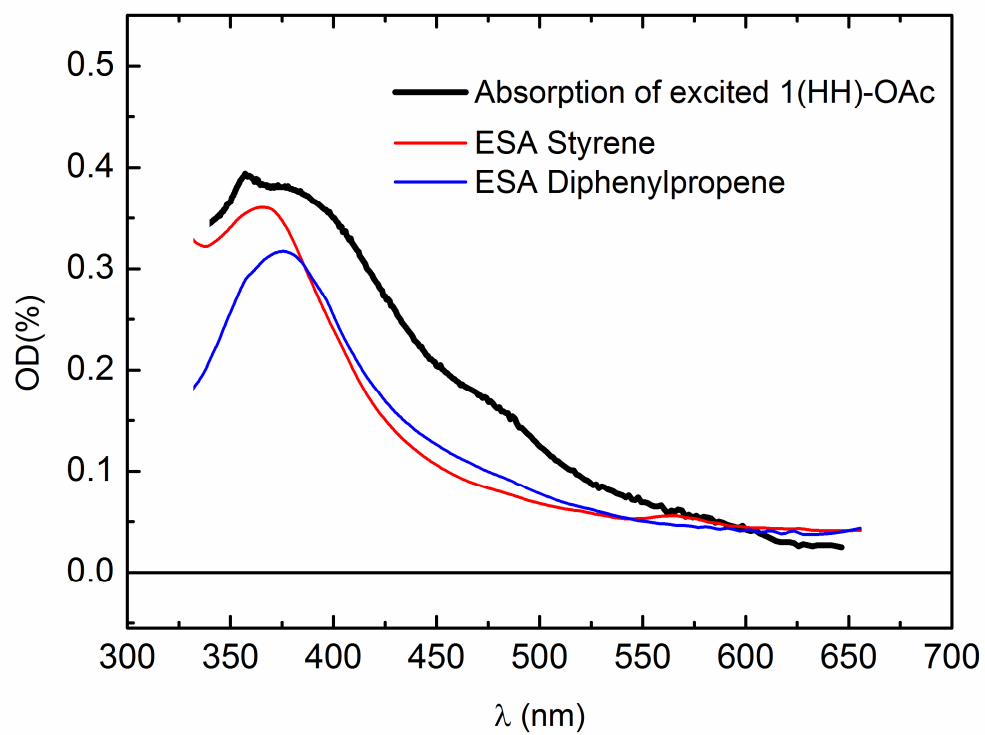
Figure S10: Species-associated spectra of 1(HH)-OAc.
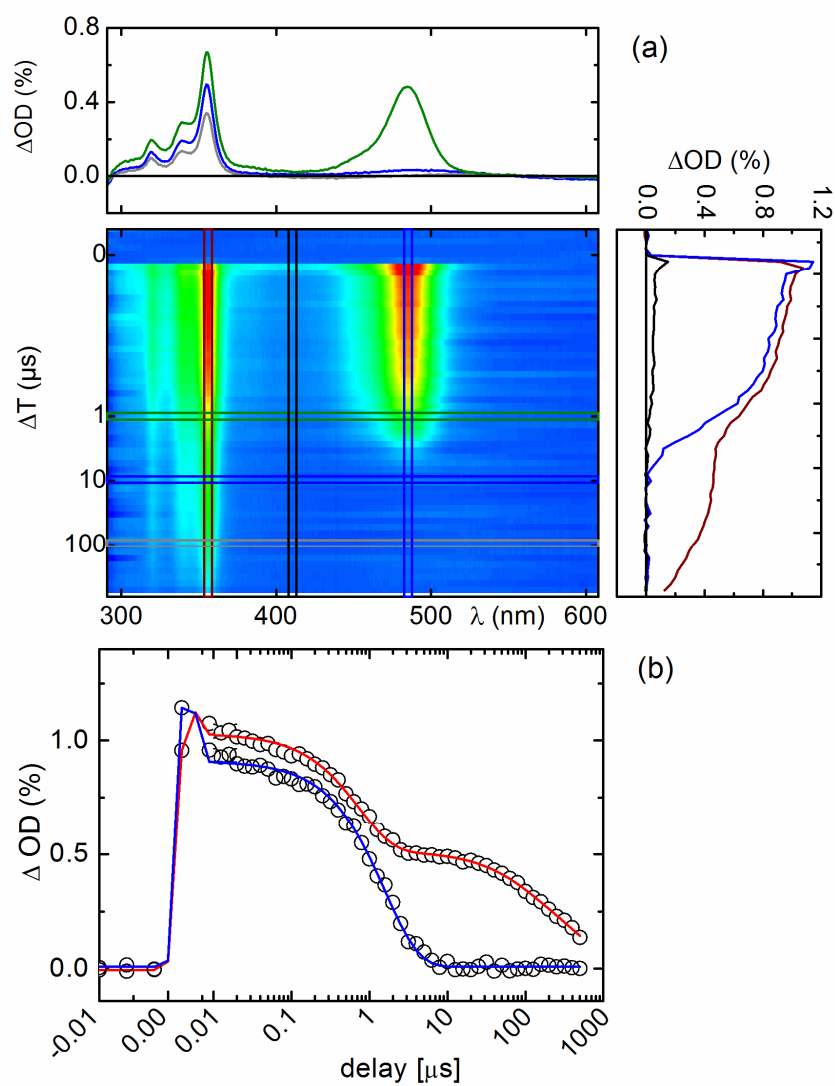
Figure S11: Transient spectra, false color representation of the transient data (a) and time traces (b) of radical (red) and cation (blue) of 1(HH)-OAc in CH_3CN, ns-μs experiment (261 nm excitation).
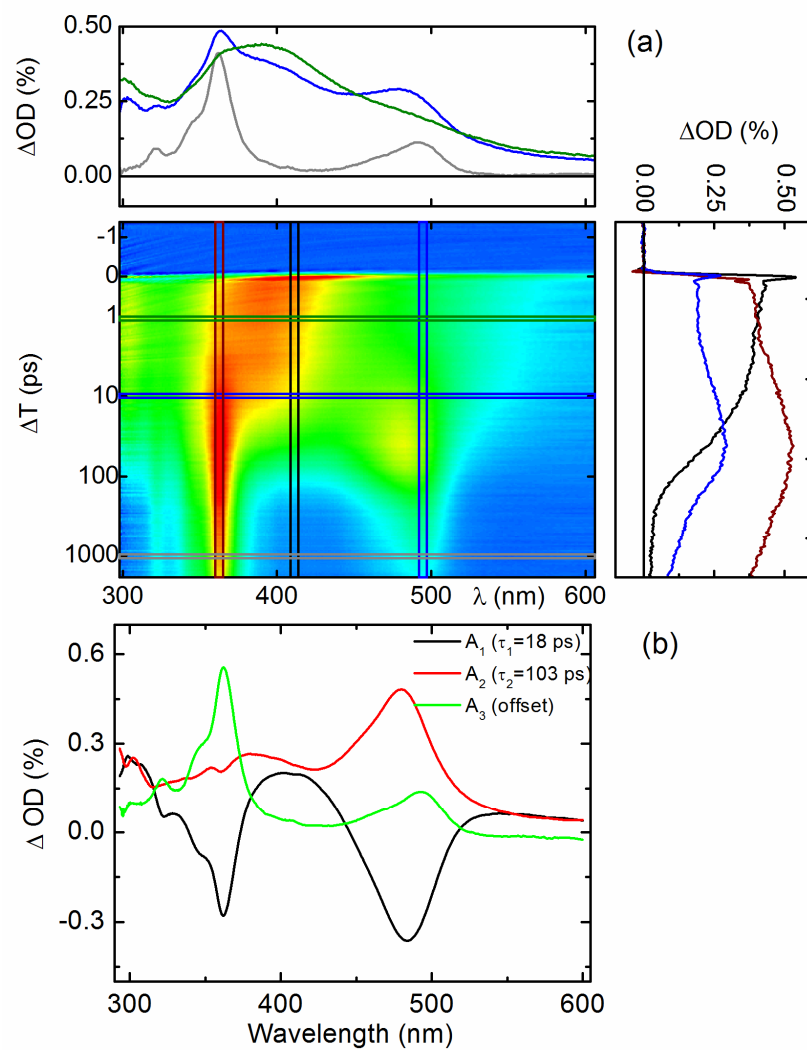
Figure S12: Transient spectra, false color representation of the transient data (a) and global fit (b) of radical and cation bands of 1(MeFF)-OAc in CH$_3$CN, fs-ps experiment (261 nm excitation).
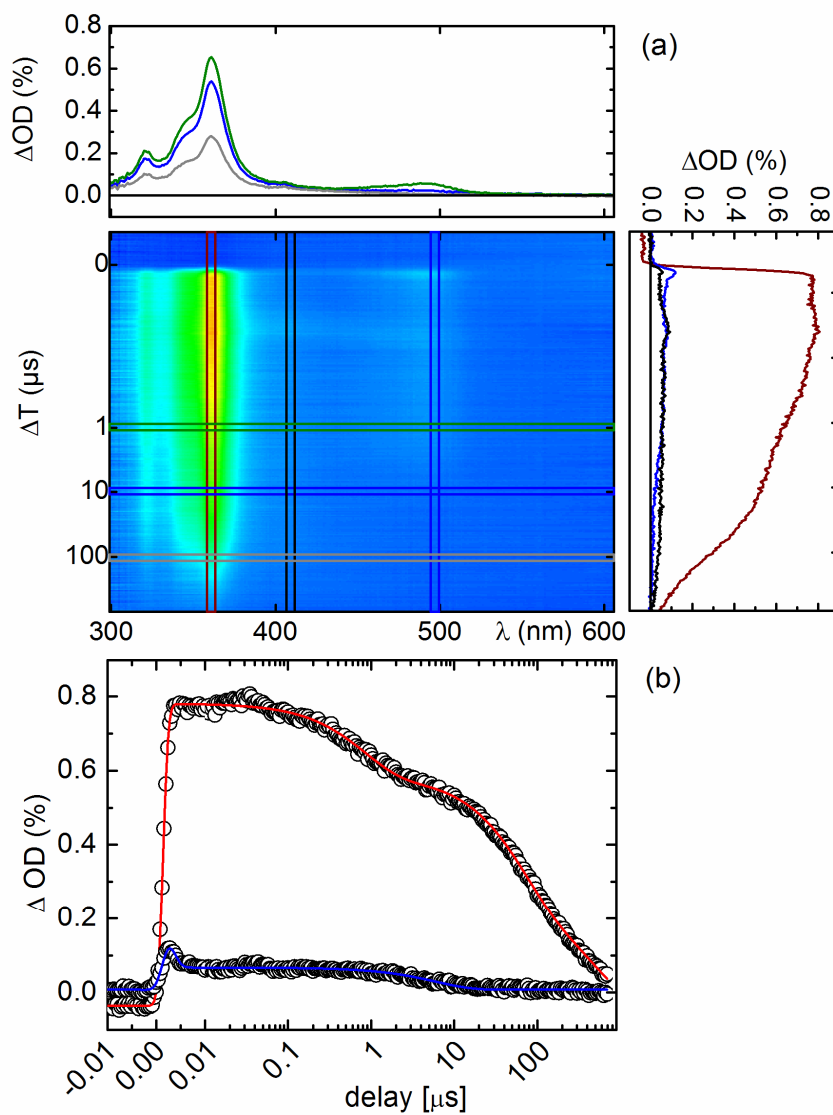
Figure S13: Transient spectra, false color representation of the transient data (a) and time traces (b) of radical (red) and cation (blue) of 1(MeFF)-OAc in CH_3CN, ns-µs experiment (261 nm excitation).
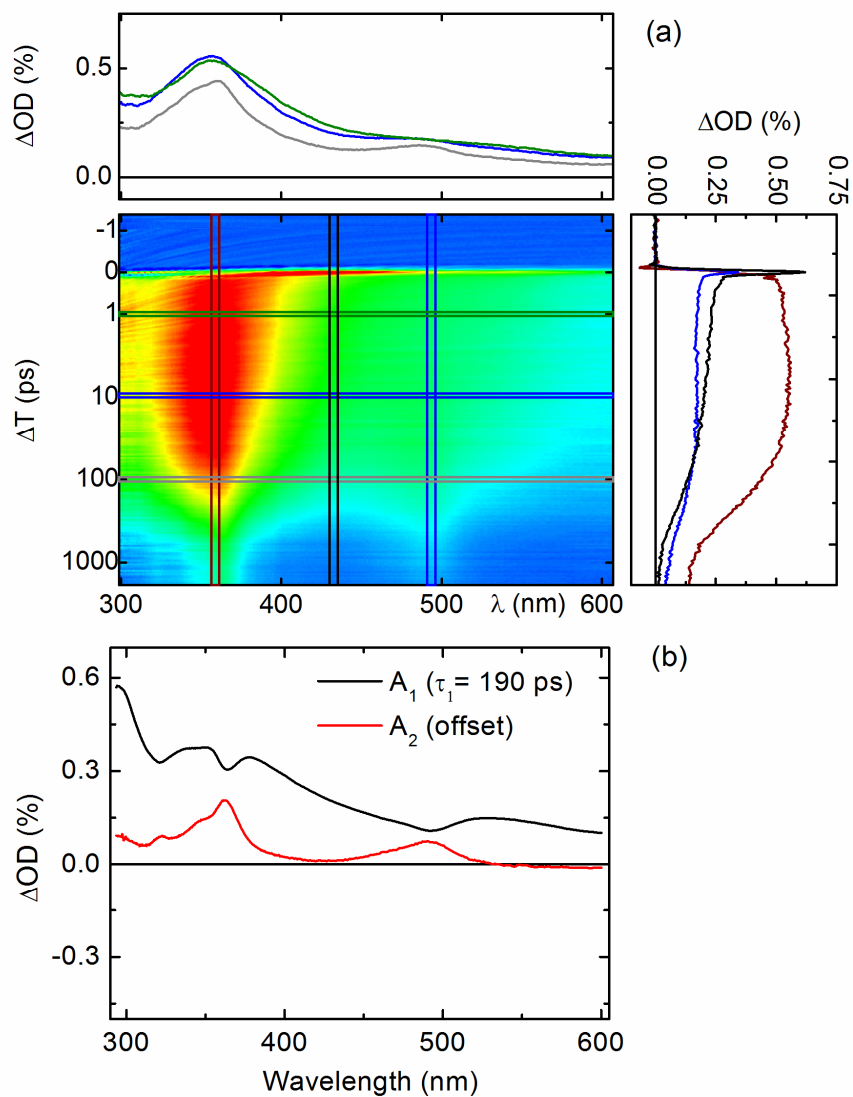
Figure S14: Transient spectra, false color representation of the transient data (a) and global fit (b) of radical and cation bands of 1(FFMe)-OAc in CH_3CN, fs-ps experiment (261 nm excitation).

Figure S15: Transient spectra, false color representation of the transient data and time traces (b) of radical (red) and cation (blue) of 1(FFMe)-OAc in CH_3CN, ns-µs experiment (261 nm excitation).
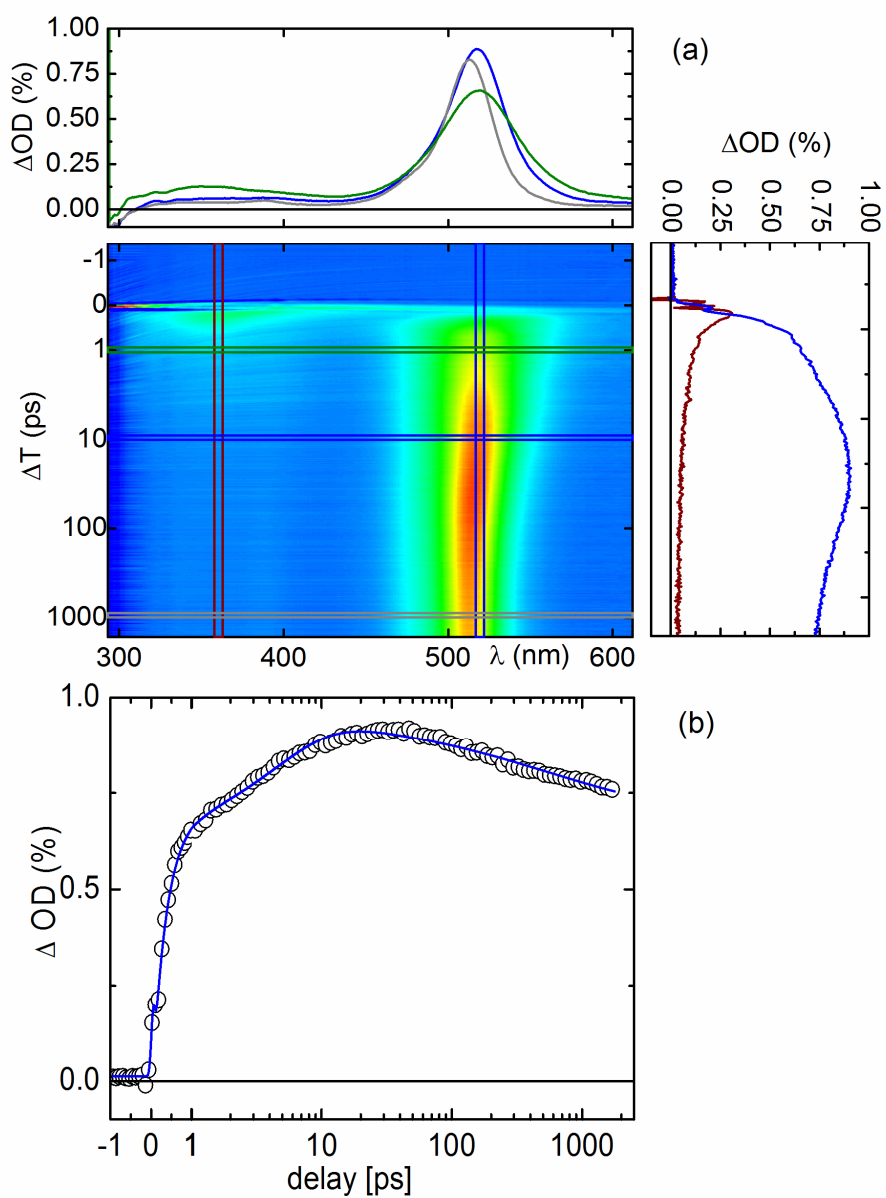
Figure S16: Transient spectra, false color representation of the transient data (a) and time trace (b) of cation band of 1(HH)-PPh$_3$BF$_4$ in CH$_3$CN, fs-ps experiment (270 nm excitation).
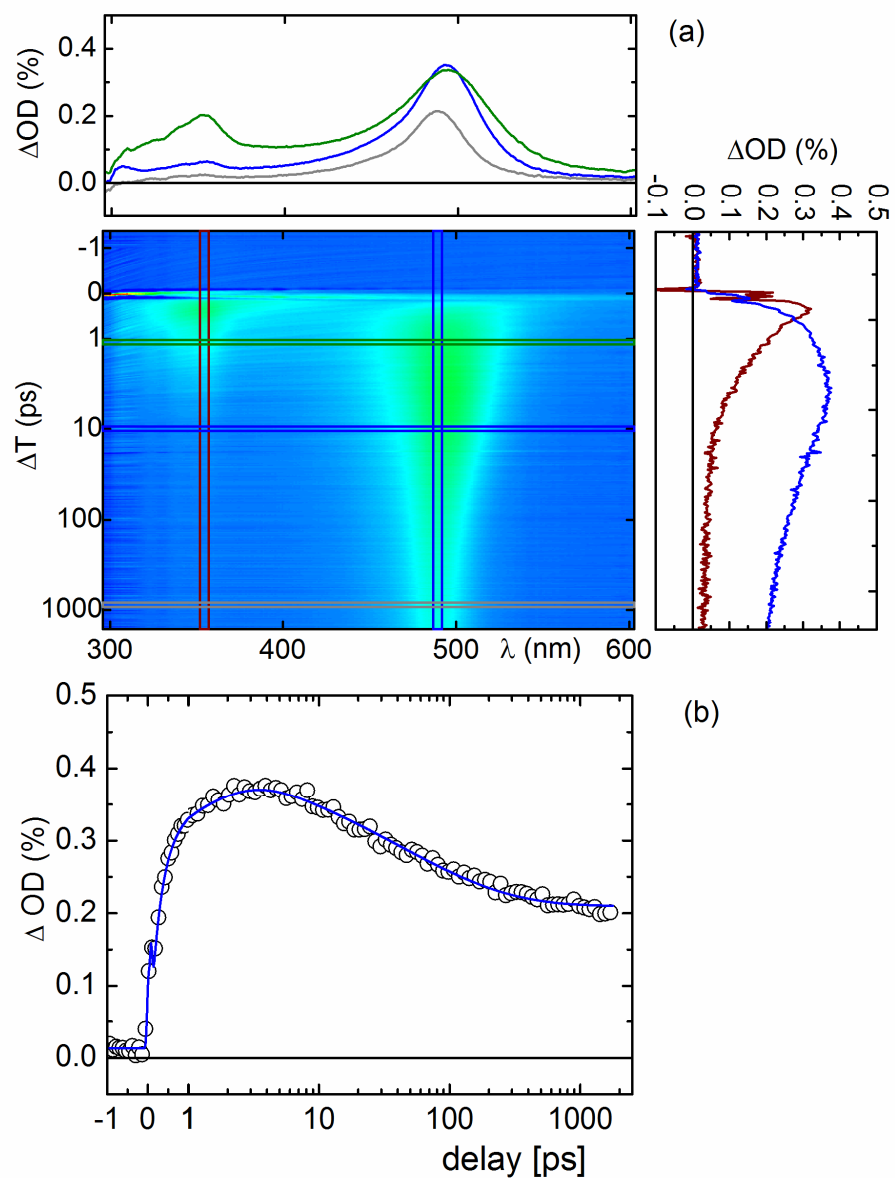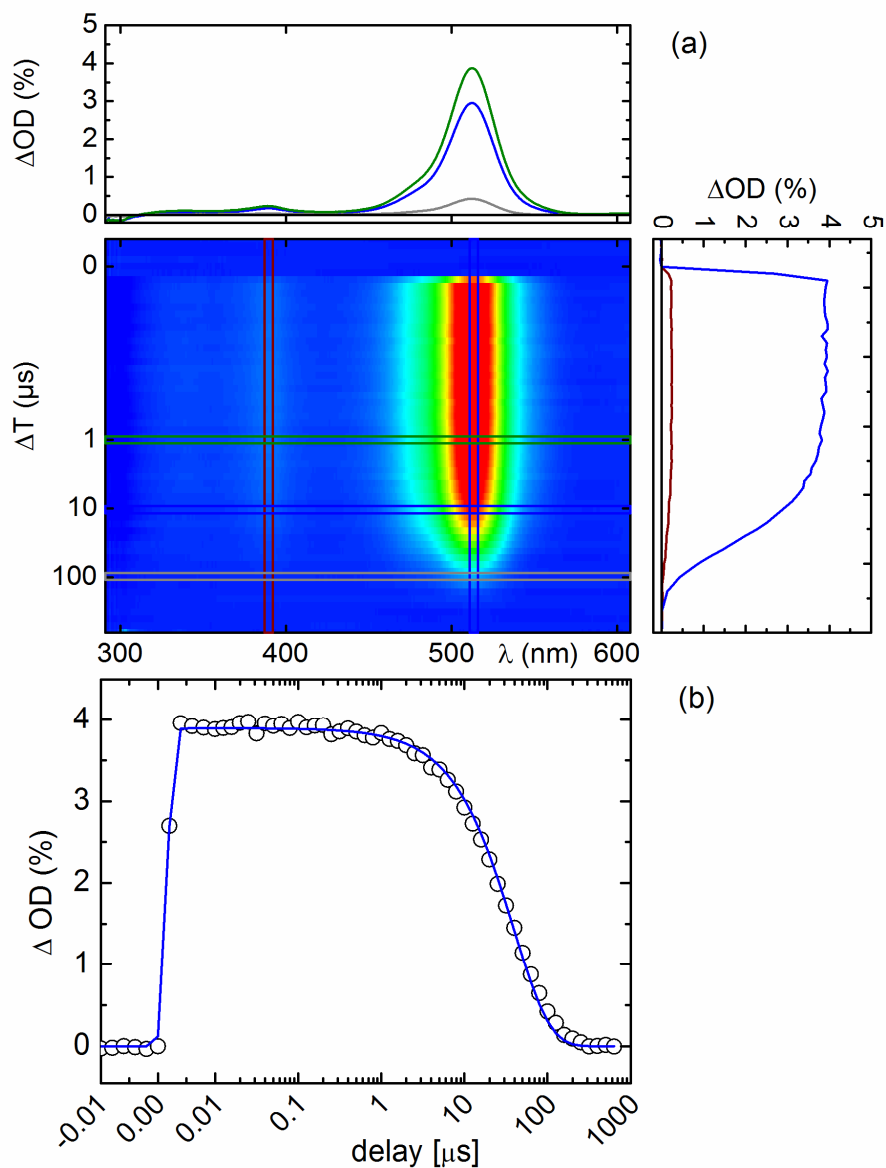
Figure S17: Transient spectra, false color representation of the transient data (a) and time trace (b) of cation band of 1-(FF)-PPh$_3$BF$_4$ in CH$_3$CN, fs-ps experiment (270 nm excitation).
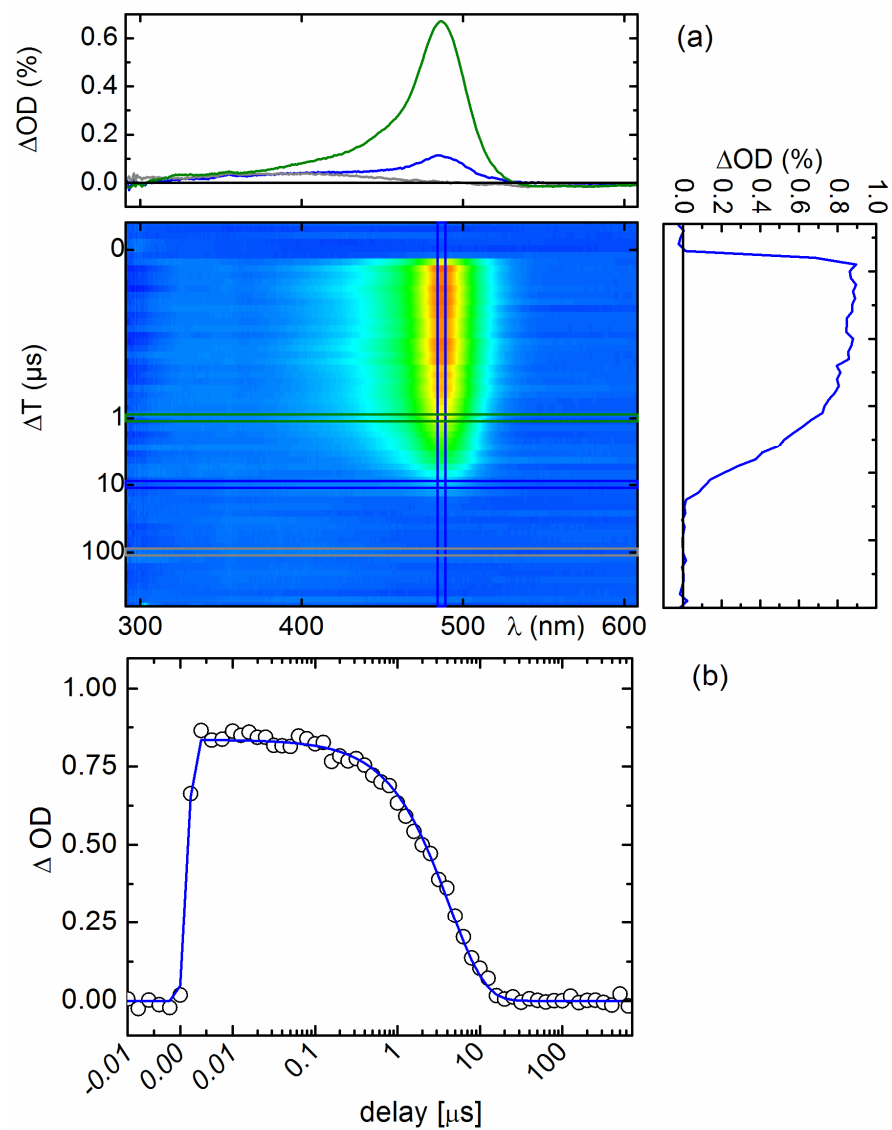
Figure S18: Transient spectra, false color representation of the transient data (a) and time trace of cation band (b) of 1(FF)-PPh$_3$BF$_4$ in CH$_3$CN, ns-µs experiment (270 nm excitation).
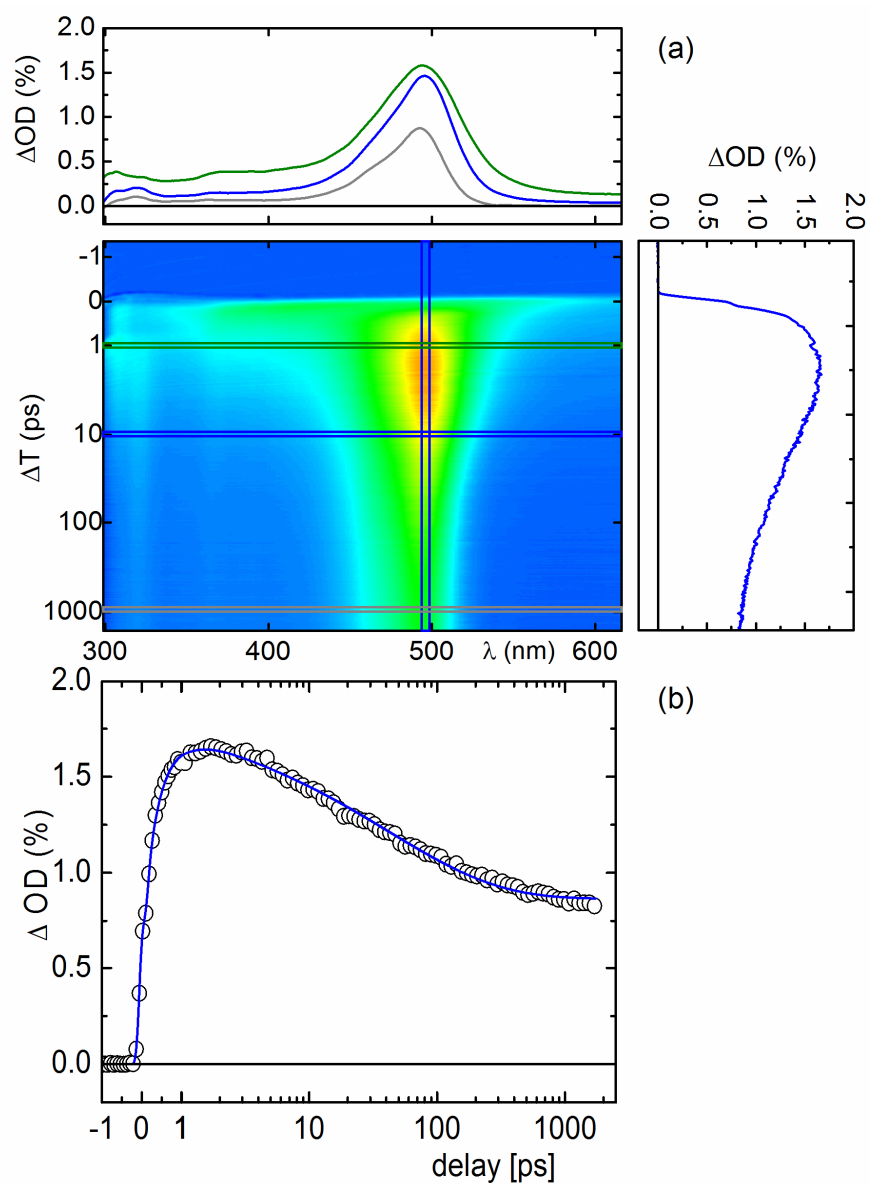
Figure S19: Transient spectra, false color representation of the transient data (a) and time trace (b) of cation band of 1(MeMe)-PPh$_3$BF$_4$ in CH$_3$CN, fs-ps experiment (270 nm excitation).
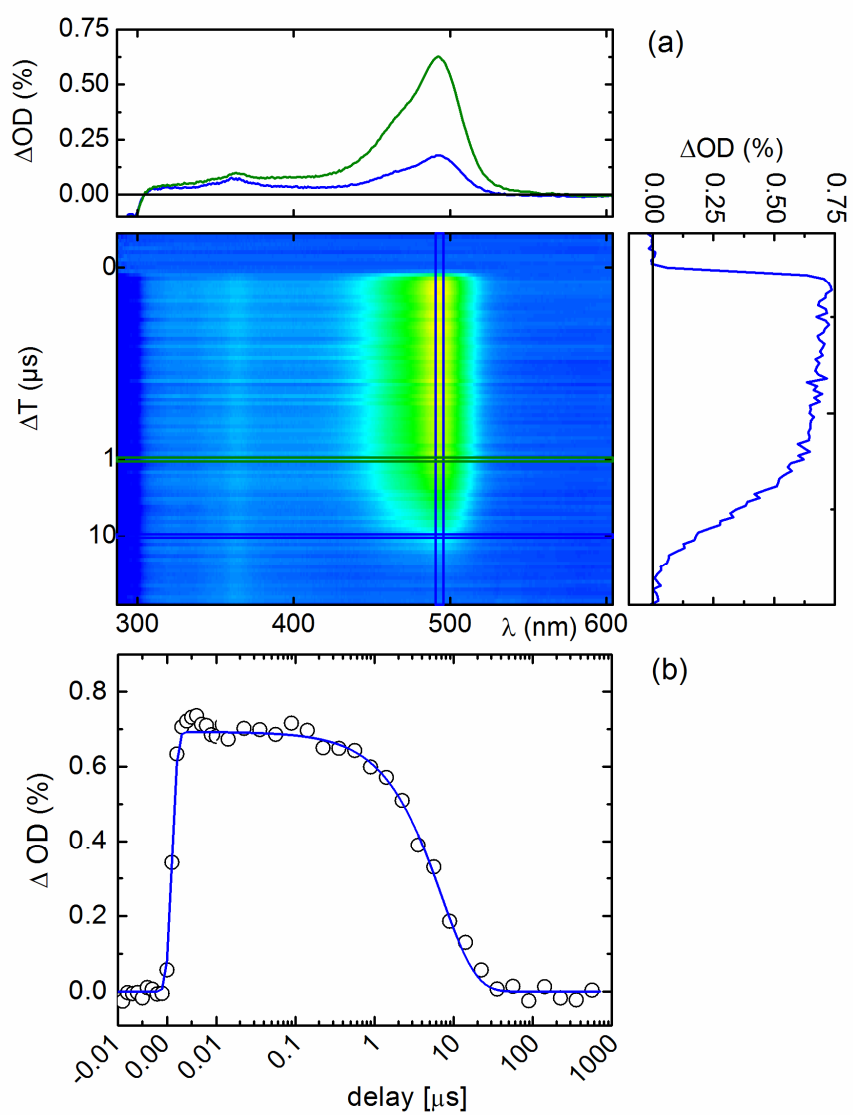
Figure S20: Transient spectra, false color representation of the transient data (a) and time trace of cation band (b) of 1(MeMe)-PPh$_3$BF$_4$ in CH$_3$CN, ns-μs experiment (270 nm excitation).

Figure S21: Transient spectra, false color representation of the transient data (a) and time trace (b) of cation band of 1(MeFF)-PPh$_2$MeBF$_4$ in CH$_3$CN, fs-ps experiment (270 nm excitation).

Figure S22: Transient spectra, false color representation of the transient data (a) and time trace of cation band (b) of 1(MeFF)-PPh$_2$MeBF$_4$ in CH$_3$CN, ns-μs experiment (270 nm excitation).
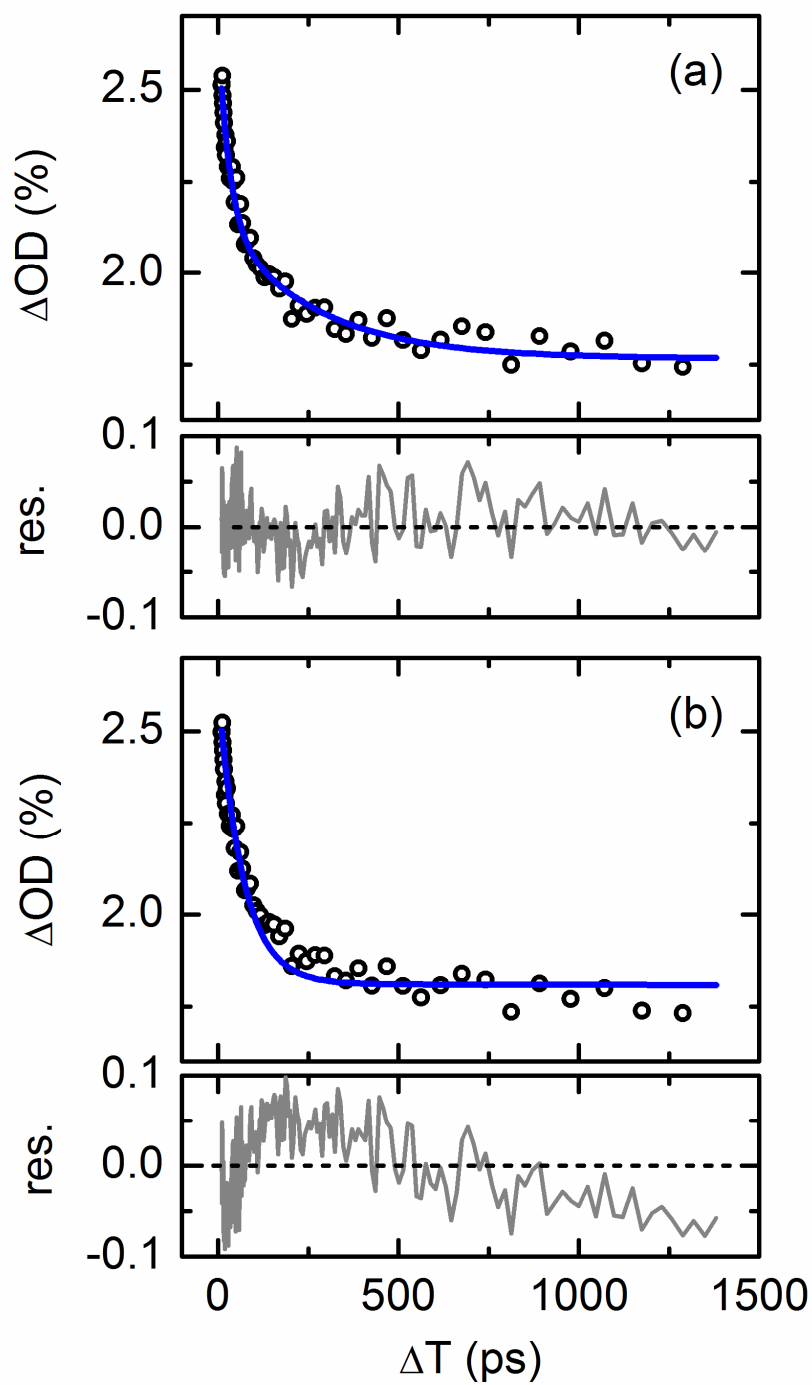
Figure S23: Comparison of the fits (blue lines) and residua (grey lines) obtained from a stretched exponential (a) and a monoexponential function (b) for the geminate recombination of the cation band of 1(HH)-PPh$_3$BF$_4$ in CH$_3$CN, fs-ps experiment (270 nm excitation).
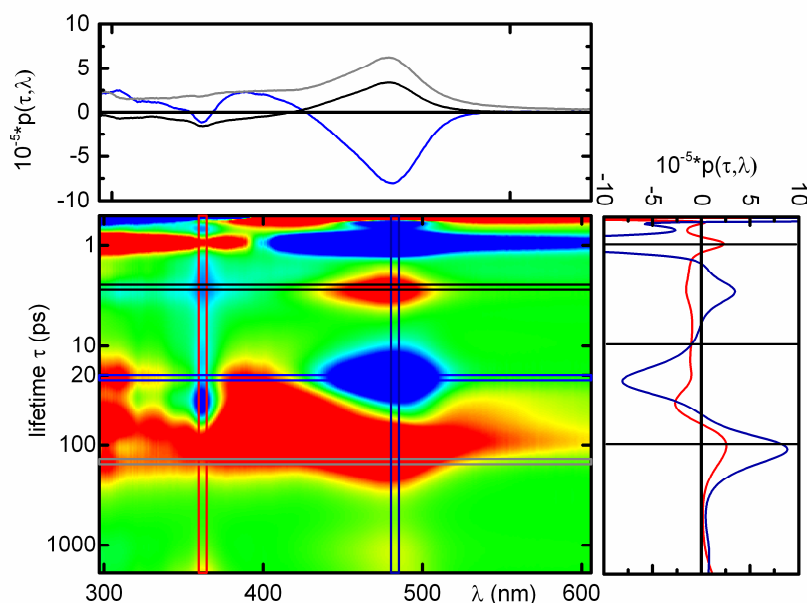
Figure S24: Results of the Maximal Entropy analysis for 1(MeFF)-OAc in CH_3CN, fs-ps experiment (261 nm excitation).

4. Synthesis and NMR characterization

1(MeFF)-OAc

The unsymmetrically substituted 1,3-diarylallyl acetate 1(MeFF)-OAc was prepared according to the procedure described in reference [Sch08] from MemFF(OH) (1.000 g, 3.842 mmol), acetyl chloride (550 μL, 605 mg, 7.70 mmol), DMAP (100 mg, 0.818 mmol) and triethylamine (1.3 mL, 0.95 g, 9.4 mmol) with a yield of 0.558 g (1.85 mmol, 48%).

^{1}H NMR (CDCl$_3$, 300 MHz): δ 2.16 (s, 3 H, CH$_3$), 2.34 (s, 3 H, CH$_3$CO), 6.20 (dd, $^3J_{HH}$ = 15.8, 7.2 Hz, 1 H, ArCHC*H*CH(OAc)Ar), 6.37 (d, $^3J_{HH}$ = 7.2 Hz, 1 H, ArCHCHC*H*(OAc)Ar), 6.65 (d, $^3J_{HH}$ = 15.8 Hz,1 H, ArC*H*CHCH(OAc)Ar), 6.70 – 6.80 (m, 1 H, H$_{Ar}$), 6.88 – 6.99 (m, 2 H, H$_{Ar}$), 7.10 – 7.17 (m, 2 H, H$_{Ar}$), 7.26 – 7.32 ppm (m, 2 H, H$_{Ar}$).

^{13}C NMR (CDCl$_3$, 75 MHz,): δ 21.16 (s, CH$_3$), 21.20 (s, CH$_3$), 75.1 (t, J_{CF} = 2.2 Hz, CH), 103.4 (t, J_{CF} = 25.3 Hz, CH), 109.7 (m, CH), 125.0 (s, CH), 126.7 (s, CH), 129.3 (s, CH), 132.9 (s, C), 133.7 (s, CH), 138.4 (s, C), 143.4 (t, J_{CF} = 8.8 Hz, C), 163.1 (dd, J_{CH} = 249, 12.6 Hz, C), 169.7 ppm (s, C).

1(FFMe)-OAc

The unsymmetrically substituted 1,3-diarylallyl acetate 1(FFMe)-OAc was prepared according to the procedure described in reference [Sch08] from mFFMe(OH) (0.906 g, 3.48 mmol), acetyl chloride (500 µL, 550 mg, 7.00 mmol), DMAP (100 mg, 0.818 mmol) and triethylamine (1.2 mL, 0.87 g, 8.6 mmol) with a yield of 0.450 g (1.49 mmol, 43%).

^{1}H NMR (CDCl$_3$, 300 MHz): δ 2.13 (s, 3 H, CH$_3$), 2.36 (s, 3 H, CH$_3$CO), 6.32 – 6.41 (m, 2 H, ArCHC*H*C*H*(OAc)Ar), 6.53 (d, J = 14.4 Hz, 1 H, ArC*H*CHCH(OAc)Ar), 6.65 – 6.72 (m, 1 H, H$_{Ar}$), 6.83 – 6.93 (m, 2 H, H$_{Ar}$), 7.16 – 7.24 (m, 2 H, H$_{Ar}$), 7.27 – 7.31 ppm (m, 2 H, H$_{Ar}$).

^{13}C NMR (CDCl$_3$, 75 MHz): δ 21.2 (CH$_3$), 21.3 (s, CH$_3$), 75.4 (s, CH), 103.1 (t, J_{CF} = 25.16 Hz, CH), 109.2 – 109.5 (m, CH), 127.1 (s, CH), 129.4 (s, CH), 130.0 (t, J_{CF} = 2.8 Hz, CH), 130.5 (t, J_{CF} ≈ 0.8 Hz, CH), 135.6 (s, C), 138.3 (s, C), 139.7 (t, J_{CF} = 9.5 Hz, C), 163.1 (dd, J_{CF} = 248, 13.0 Hz, C), 169.9 ppm (s, C).

1(MeFF)-PPh$_2$MeBF$_4$

(*E*)-(1-(3,5-difluorophenyl)-3-(4-methylphenyl)allyl)(methyl)diphenylphosphonium tetrafluoroborate 1(MeFF)-PPh2MeBF4 was synthesized using the five step procedure described below:

3-(3,5-difluorophenyl)-1-(4-methylphenyl)prop-2-enone (mFF,Me,O) was obtained from 3,5-difuorobenzaldehyde (7.17 g, 50.5 mmol) and 4-methylacetophenone (6.77 g, 50.5 mmol) using a procedure from [Tro11]. Yellow crystals (5.33 g, 20.6 mmol, 41%).

3-(3,5-difluorophenyl)-3-(diphenylphosphino)-1-(p-tolyl)propan-1-one (mFF,Me,PPh2,O). Diphenylphosphine (2.20 mL, 2.35 g, 12.6 mmol) was added dropwise to a solution of potassium tert-butoxide (1.42 g, 12.7 mmol) in dry THF (40 mL) at 0 °C under nitrogen atmosphere, and the resulting red-orange solution was stirred for 30 min at the same temperature. A solution of mFF,Me,O (3.00 g, 11.6 mmol) in THF was added dropwise to the reaction mixture leading to the fading of the red-orange color. Deoxygenated water was added to the resulting solution, and the resulting white precipitate was filtered, washed with water and

pentane and dried in vacuo. The crude product was recrystallized from CH_2Cl_2 / pentane yielding mFF,Me,PPh2,O (2.25 g, 5.07 mmol, 44%).

3-(3,5-difluorophenyl)-3-(diphenylphosphino)-1-(p-tolyl)propan-1-ol (mFF,Me,PPh2,OH). Sodium borohydride was added portionwise to a slurry of mFF,Me,PPh2,O (1.95 g, 4.40 mmol) in deoxygenated methanol at ambient temperature under nitrogen atmosphere until a homogeneous solution containing no mFF,Me,PPh2,O (TLC) was formed. The reaction mixture was freed from the solvent; the residue was dissolved in deoxygenated ethyl acetate, washed with deoxygenated water, dried with magnesium sulfate and freed from the solvent *in vacuo* yielding mFF,Me,PPh2,OH (1.90 g, 4.26 mmol, 97%) as mixture of two diastereomers containing some impurities.

(*E*)-(1-(3,5-difluorophenyl)-3-(p-tolyl)allyl)diphenylphosphine (Me,mFF,PPh2). Phosphorus pentoxide (3.00 g, 21.1 mmol) was added to a solution of mFF,Me,PPh2,OH (1.90 g, 4.26 mmol, 97%) in dry dichloromethane and the resulting mixture was stirred for 2h. The solid was filtered off, and the reaction solution was freed from the solvent and dried *in vacuo* yielding Me,mFF,PPh2 (1.30 g, 3.03 mmol, 71%) containing some impurities.

(*E*)-(1-(3,5-difluorophenyl)-3-(4-methylphenyl)allyl)(methyl)diphenylphosphonium tetrafluoroborate (Me,mFF,PPh2Me,BF4). Trimethyloxonium tetrafluoroborate (34.5 mg, 233 µmol) was added to a solution of Me,mFF,PPh2 (100 mg, 233 µmol) and the resulting solution was stirred for 30 min at rt under nitrogen atmosphere. The reaction mixture was freed from the solvent followed by drying *in vacuo* yielding Me,mFF,PPh2Me,BF4 (96.1 mg, 1.81 mmol, 78%) containing some impurities.

^{1}H NMR (CD$_2$Cl$_2$, 200 MHz) δ 2.32 (s, 3 H, CH$_3$), 2.41 (d, $^2J_{HP}$ = 13.0 Hz, 3 H, PPh$_2$CH_3), 5.70 (dd, $^2J_{HP}$ = 16.3 Hz, $^3J_{HH}$ = 9.6 Hz, 1 H, ArCHCHCH(P$^+$Ph$_2$Me)Ar), 5.82 – 6.11 ppm (ddd, 1 H, $^3J_{HH}$ = 15.6, 9.6, $^3J_{HP}$ = 6.2 Hz, ArCHCHCH(P$^+$Ph$_2$Me)Ar), 6.75 – 6.87 (m, 3 H, H$_{Ar}$), 6.94 (dd, $^3J_{HH}$ = 15.6, $^4J_{HP}$ = 4.9 Hz), 7.12 (d, $^3J_{HH}$ = 8.1 Hz, 2 H, H$_{Ar}$), 7.23 (d, $^3J_{HH}$ = 8.1 Hz, 2 H, H$_{Ar}$), 7.64 – 7.91 ppm (m, 10 H, PPh$_2$). ^{31}P NMR (CD$_2$Cl$_2$, 81 MHz) δ 24.8 ppm.

Due to the low purity of the final product, it was characterized only by ^{1}H NMR and ^{31}P spectroscopy. Further attempts to modify the synthetic procedures in order to obtain pure Me,mFF,PPh2Me,BF4 are ongoing.

Caution: working under oxygen-free atmosphere is essential to prevent the oxidation of the PPh$_2$ group during the steps 2-5.

Danksagung

Von ganzem Herzen vielen dank an:

…meinen Doktorvater **Herrn Prof. Dr. Eberhard Riedle** für die Möglichkeit, diese Arbeit durchzuführen, und für die hervorragende wissenschaftliche Betreuung.

…BMO-Lehrstuhlleiter **Herrn Prof. Dr. Wolfgang Zinth** für sehr hilfreiche technische und wissenschaftliche Ratschläge und auch für unvergessliche wissenschaftliche Gespräche.

…meinen wissenschaftlichen Betreuer **Dr. Igor Pugliesi**, der mir in allen Schritten meiner Arbeit geholfen und betreut hat.

…die internationale Max-Planck Forschungsschule IMPRS-APS – für die finanzielle Förderung (Max-Planck Stipendium) – ohne die wäre diese Arbeit nicht möglich, **Monika Wild** - für die engste Unterstützung in allen Fragen .

…**Herrn Prof. Dr. Herbert Mayr** und **Dr. Konstantin Troshin** für die erfolgreiche Zusammenarbeit zur Untersuchung der Photodynamik von Diphenylallylen, die die zentralle Rolle in meiner Dissertation spielt.

… **Herrn Prof. Dr. Dirk Trauner** für die interessanten Diskussionen.

…die nettsten und freundlichsten BMO-Kollegen (jetzigen und ehemaligen) danken, nicht nur für die wissenschaftliche Hilfe, aber auch für die wertvollen Unterhaltungen: **Anton Arsenyev, Max Bradler, Markus Breuer, Anreas Böck, Franziska Graupner, Christian Homann, Dr. Daniel Herrmann, Christian Homann, Nils Krebs, Peter Lang, Dr. Subrata Mahanta, Karin Peeper, Gerald Ryseck, Dr. Oliver Schalk, Philipp Schneider, Dr. Rupa Singh, Hamid Tejmouri, Dr. Evelyn Wendt**. Sorry, wenn ich jemanden vergessen habe!

…die BMO-Mitarbeiter **Dr. Karl-Heinz Mantel, Isabell Kalbe, Rudi Schwarz**, **Alfons Stork**, **Christian Hausmann –** für die beste EDV-chemisch-mechanische Betreuung, die überhaupt geben konnte.

…alle IMPRS-Doktoranden-KommilitonnInnen (besonders **Dr. Irina Znakovskaya** und **Dr. Jasper Werhahn**) **–** für nette Unterhaltung währen zahlreichen Seminaren.

…**Herrn Manfred Klieber** von PerkinElmer, Inc., der immer so viel Mühe gegeben hat, um unser Spektralphotometer zur Funktion zu bringen.

…meine unterstützende und motivierende Familie: **Dr. Nataly Kundeleva** (Mutter) **Dr. Yuri Mikhailov** (Vater), **Alla Mikhailova** (beste Freundin und Partnerin in allen Sachen)**.**

...alle netten und freundlichen Menschen, die mich direct und indirekt unterstützt haben.